REPUBLIC OF TÜRKİYE
ALTINBAŞ UNIVERSITY
Institute of Graduate Studies
Mechanical Engineering

HEAT TRANSFER ENHANCEMENT USING FERRO-NANOFLUID WITH MEGNATIC FIELD IN TUBE HAVING INSERTED TWISTED TUBE

Salim Abdulzahra Abboodi AL ZERKANI

Master's Thesis

Supervisor

Asst. Prof. Dr. Yaser ALAIWI

Istanbul, 2023

HEAT TRANSFER ENHANCEMENT USING FERRO-NANOFLUID WITH MEGNATIC FIELD IN TUBE HAVING INSERTED TWISTED TUBE

Salim Abdulzahra Abboodi AL ZERKANI

Mechanical Engineering

Master's Thesis

ALTINBAŞ UNIVERSITY

2023

The thesis titled HEAT TRANSFER ENHANCEMENT USING FERRO-NANOFLUID WITH MAGNETIC FIELD IN TUBE HAVING INSERTED TWISTED TUBE PREPARED by SALIM ABDULZAHRA ABBOODI AL-ZERKANI and submitted on 25/04/2023 has been **accepted unanimously** for the degree of Master of Science in Mechanical Engineering.

Asst. Prof. Dr.Yaser ALAIWI

Supervisor

Thesis Defense Committee Members:

Asst. Prof. Dr.Yaser ALAIWI	Department of Mechanical Engineering, Altınbaş University	__________
Asst. Prof. Dr. Serdar AY	Department of Mechanical Engineering, Altınbaş University	__________
Asst. Prof. Dr. Ahmed SADIK	Department of Mechanical Engineering, Hasan Kalyoncu University	__________

I hereby declare that this thesis meets all format and submission requirements of a Master's thesis.

Submission date of the thesis to Institute of Graduate Studies: ___/___/___

I hereby declare that all information/data presented in this graduation project has been obtained in full accordance with academic rules and ethical conduct. I also declare all unoriginal materials and conclusions have been cited in the text and all references mentioned in the Reference List have been cited in the text, and vice versa as required by the abovementioned rules and conduct.

Salim Abdulzahra Abboodi ALZERKANI

Signature

DEDICATION

I dedicate this work to my supervisor, Asst. Prof. Dr. Yaser ALAIWI that has been a major role in the whole work process, and my parents, who have always been there for the all thesis steps.

ABSTRACT

HEAT TRANSFER ENHANCEMENT USING FERRO-NANOFLUID WITH MEGNATIC FIELD IN TUBE HAVING INSERTED TWISTED TUBE

ALZERKANI, Salim Abdulzahra Abboodi

M.Sc., Mechanical Engineering Department, Altınbaş University,

Supervisor: Asst. Prof. Dr. Yaser ALAIWI

Date: 4 / 2023

Pages:104

Several research initiatives will investigate the application of nanofluids more fully in order to enhance its commercialisation. Over the past ten years, the usage of magnetic nanofluids for enhancing heat transfer has gradually grown as a result of its superior thermal conductivity compared to other nanofluids. Nanoparticles have a significant impact on the thermal properties of base fluids, such as thermal conductivity and viscosity. When nanofluids are used, the double-tube heat exchanger's ability to transmit heat is considerably enhanced. Other experiments showed that when the concentration of nanofluids was reduced, the heat transfer coefficient increased even more. As a result, more investigation was needed before using nanofluids in plate heat exchangers. The colloidal suspension's thermal properties essentially differ from those of the base fluid. In multi-component systems like colloidal suspensions, suspended particles interact with one another significantly. The major goals of the current work are to assess the improvement in heat transfer achieved by utilizing twisted tape and ferro-nanofluid, and to model the impact of a magnetic field on ferro-nanofluid on the rate of heat transfer. Studies in computational fluid dynamics (CFD) are conducted to have a deeper understanding of the field of the stream. The (k-ε) model is used to explain the effects of the disturbance model, which comprises the configuration of two vehicle conditions. Therefore, these Cartesian direction frameworks will be addressed by the mathematical arrangement's procedures (x, y, and z). Calculation with three layers is produced. The framework math will be created

and networked using ANSYS software, after which one case will be replicated. The mathematical results for the process of improving heat transfer utilizing twisted tape and ferro-nanofluid with the effects of several conditions: rotational cycle, magnetic field intensity, and concentration of ferro-nanofluid when using ferro-nanofluid with a magnetic field to improve heat transfer, the influence of the aforementioned conditions on pressure, temperature, and fluid velocity is also evident. The findings demonstrate that for all operating circumstances, fluid pressure decreases while velocity increases and temperature rises uniformly.
Keywords: Ferro-Nanofluid, Magnetic Field, CFD, Heat Trans.

TABLE OF CONTENTS

Pages

LIST OF TABLES

<u>Pages</u>

LIST OF FIGURES

Pages

ABBREVIATIONS

AI	:	Artificial Intelligence
FSK	:	Frequency Shift Keying
IoT	:	Internet of Things
PAN	:	Personal Area Network
OFDM	:	Orthogonal Frequency Division Multiplexing
TDMA	:	Time Division Multiple Access

1. INTRODUCTION

1.1 INTRODUCRUIN

The using of contemporary electronic devices and anything relevant to the growth that took place in the recent time has recently attracted a lot of curiosity throughout the world. We observe the fascination with heat transfer as a crucial component in several scientific implementations and as having a significant impact on many facets of life, such as (optical devices, refrigeration devices, electronics, X-rays, etc.). The miniaturization, data storage, and increased working speed of these electronic gadgets and technologies, together with their massive and quick expansion, created major issues with their heat management [1]. Over the past few decades, different approaches to improve heat transfer have been advanced. These methods are divided into three groups: I active methods, which involve introducing an external power resource into the fluid (such as electrostatic and mechanical aids domains); (ii) passive methods, which involve adding fluid additives (such as nanofluids) or turbulence promoters (such as twisted tape and coil inserts); and (iii) compound methods, which involve combining active and passive methods [2]. Twisted tapes, dimples, wire coils, fins, ribs, and micro fins have all been used to change the flow pattern. A flow channel can be modified by changing the thermal characteristics of the working fluid or the fluid flow with the aid of inserts. The working fluid, also known as nanofluid, can be made more efficient by adding nanoparticles with increased thermal conductivity [3]. Superparamagnetic nanoparticles floating in a nonmagnetic carrier fluid make up magnetic nanofluids, one type of nanofluid. Due to their distinctive properties and behaviour as intelligent or functional fluids, these fluids represent a contemporary collection of nanofluids. Under the effect of an exterior magnetic field, their conductivity and viscosity can alter, and their rheological parameters can be precisely regulated [4]. A technique for constructing heat transfer devices is to have a larger surface area to volume ratio. For instance, pipes with micro fins have gained popularity due to their capacity to increase the surface of heat transfer and create turbulence in fluid flow. This method might enhance the efficiency of heat transfer [5].

1.2 HEAT TRANSFER ENHANCEMENT USING NANOFLUIDS

In order to improve the commercialization of nanofluid, several research projects will look into its application more thoroughly. Because magnetic nanofluid has a better thermal conductivity than other nanofluids, its use for improving heat transfer has gradually increased over the past decade [6]. Base fluids' thermal characteristics, such as thermal conductivity and viscosity, are greatly impacted by nanoparticles. The performance of heat transmission is greatly improved in the double-tube heat exchanger when nanofluids are utilized. According to other studies, the heat transfer coefficient rose even more when the concentration of nanofluids decreased. Additionally, the flow pattern was connected to how well nanofluids transferred heat. Consequently, additional research was required for the use of nanofluids in plate heat exchangers [7]. A colloidal dispersion of magnetic nanoparticles with a diameter of 3 to 15 nm is called ferrofluid [8]. There are numerous types of particles with ferromagnetic characteristics, including Fe_3O_4, $CoFeO_4$, and FePt. This fluid has the property of responding with a magnetic field because of the magnetism of the particles. The fluid possesses kinetic energy and takes on a particular shape when a magnetic field is utilized [9]. In other words, there are benefits in that control is achievable with a very basic arrangement and that a flow can only be produced via a magnetic force devoid of direct contact with the fluid. Additionally, it has been demonstrated that because of the characteristics of the particles, nanofluids perform better thermally than regular fluids. [10,11].

1.3 INFLUENCE MAGNETIC FIELD ON FERRO-NANOFLUID HEAT TRANSFER

Numerous researchers have improved cooling processes using a variety of techniques, including the use of nanofluids or fluids with high heat transfer coefficients, altering the geometry of heat exchangers (HEs), generating turbulent flow, and applying magnetic fields. Their findings have been applied in several fields. The researchers used one or more widely used techniques to develop transfer of heat in HEs [12]. Clearly, the magnetic field intensity increases with the viscosity and heat conductivity of ferrofluids. In a capillary viscometer, the viscosity was assessed with the field parallel to the direction of flow. The alignment of the particles vertical to the direction of flow consequently of the magnetic field increased flow resistance [13]. Thermal characteristics of the colloidal suspension are basically different from those of the base fluid. For instance, compared to water or oil, microfluid can have a much better thermal conductivity. The interaction of suspended particles in multi-component systems like colloidal suspensions has a significant impact on them [14]. The ferrofluid's magnetic property contributes to a well-regulated current, which affects other current physical properties like heat transmission. The colloidal suspension is stabilized by the nanoparticles' stimulation of repulsion (esterification/ionization) when they are briefly subjected to magnetic fields. By using this technique, van der Waals forces and bipolar contractions that would otherwise cause nanoparticle accumulation and deposition are avoided [15]. New uses for ferrofluid and cutting-edge technologies built around magnetic nanoparticles have arisen over the past ten years. Examples contain the sensing, energy collecting, and activation of fluid micro magnets, chip-based lab equipment, and specialized medical applications like magnetic hyperthermia, magnetic drug targeting, biomolecule sorting, and magnetic resonance image contrast enhancement. Figure 1 depicted how the magnetic sources changed the nanoparticles' orientation [17].

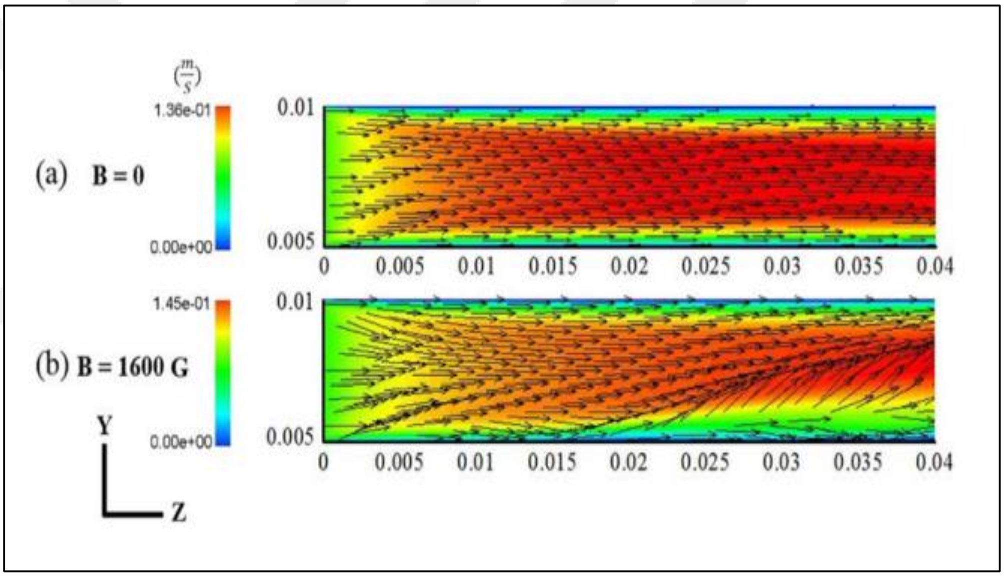

Figure 1.1 Velocity contours and vectors in the symmetry plane of the central channel alongside the direction of flow at Re = 260 in the presence and absence of a magnetic field.

1.4 TRANSFER OF HEAT IN TUBE WITH TWISTED TAPE

Techniques to improve heat transfer are frequently used in a variety of thermal systems to lower costs, reduce size and weight, and most significantly, improve performance. By disturbing the thermal boundary layer close to the walls and increasing fluid mixing, a swirl flow device can be inserted to improve heat transfer. This will improve convective heat transfer. Nevertheless, the presence of twisted tape inside the tube may result in a greater pressure drop since there is a greater surface area of contact between the fluid and the insert.

As a result, scientists have experimented with various twisted tape patterns and configurations to reduce pressure drops [18]. The velocity profile at the side wall is changed by the swirl flow created by the twisted tape tube. According to earlier studies, utilizing ribs, fins, baffles, and winglets would provide better thermal performance than using twisted-tape or wire coils [19]. In comparison to stationary twisted tape, self-rotating twisted tape has better thermal presentation. With an increasing in cut length ratio, the Nusselt number increased. The rectangular cut twisted tape creates a swirl flow that increases fluid mixing and speeds up heat transmission [20]. Transfer of heat in a circular tube is improved via utilizing a conical ring and twisted tape combination in both reverse flow and swirl flow. If 1) the conical ring is used in conjunction with the twisted tape and 2) the twisted tape ratio is low (Y=3.75) to create a larger swirl flow, heat transfer is significantly increased [21].

1.5 OBJECTIVES OF THE PRESENT WORK

Due to its direct connection to the longevity and security of electronic devices, heat dissipation is particularly significant. As a result, numerous studies were being done to manage heat in electrical gadgets. The present work is interested in an experimental investigation of improving heat transfer by employing ferro-nanofluid with magnetic field in tube with inserted twisted tape. This study was one of many that intended to do so.

The main objectives of present work are:

a. Evaluate the enhancement in heat transfer by using ferro-nanofluid and twisted tape
b. Study the effect of increasing the nanofluid concentration and Reynolds number on Nusselt number
c. Simulated the effect of magnetic field on ferro-nanofluid to enhance heat transfer rate.

2. LITERATURE REVIEW

2.1 INTRODUCTION

Nanofluids are mixtures of base fluid and typically sub-100 nm-sized nanoparticles. When compared to base fluids, nanofluids have considerable benefits over them in terms of superior thermophysical characteristics and greater values of the base numbers (Nusselt, Prandtl, and Darcy). Nanofluids are useful in many technical applications, including the automobile industry, medical technology, and electronic gadgets, because of their excellent thermal conductivity. Due to its direct connection to the longevity and security of electronic devices, heat dissipation is particularly significant. As a result, numerous studies are being carried out to manage heat in electrical gadgets. Using ferrofluid as one of them, this study intended to enhance heat transfer performance. A colloidal dispersion of magnetic nanoparticles with a diameter of 3 to 15 nm is called ferrofluid. There are numerous types of particles with ferromagnetic characteristics, including Fe_3O_4, $CoFeO_4$, and FePt. This fluid has the property of responding with a magnetic field because of the magnetism of the particles. The fluid acquires kinetic energy and takes on a certain shape in the presence of a magnetic field. The fact that control is feasible with a comparatively simple setup and that a flow can only be produced by a magnetic force without direct contact with the fluid are advantages. Additionally, it has been demonstrated that because of the characteristics of the particles, nanofluids perform better thermally than ordinary fluids. By increasing Re or altering the frequency when an electromagnet was carried out, mathematical data were compared and analysed. This confirmed that the high temperature ferrofluid and the low temperature wall behave differently in terms of heat transfer. Finally yet importantly, when Re = 100 and magnetic flux density (B) = 1 T were used, the heat transfer improved by 17.410% as compared to the scenario where no electromagnet was used.

2.2. ENHANCEMENT OF HEAT TRANSFER WITH NANOFLUIDS

The improvement of heat transmission using twisted tape and nanofluid has been studied. For laminar and turbulent flow of various twisted tape with varied twist ratios and nanofluid with varying concentrations, review paper has taken into consideration heat transfer, pressure drop, and thermal performance investigation. Utilizing fine-grained nanoparticles increases surface area, which increases the rate of heat transmission. In comparison to flat twisted tape, the flow during the swirl of fluid is more turbulent when the geometry of the twisted tape has been adjusted [22].

Titanium dioxide (TiO_2) has been used in water as a nanofluid in conjunction with overlapped dual twisted tapes (O-DTs) in order to improve heat transfer. According to the mathematical and experimental results, ODTs with a smaller overlapped twisted ratio supplied a stronger swirl intensity and more turbulent kinetic energy (TKE). As opposed to using O-DTs alone, the usage of O-DTs with twist ratios of 1.5 and a nanofluid with a volume concentration of 0.21% TiO_2 resulted in heat transfer enhancements of 9.9–11.2% and a 4.5% improvement in thermal performance [23].s

The performance of the water/iron oxide nanofluid has been examined in a turbulent flow regime in a double pipe heat exchanger with perforated twisted tapes. Iron oxide nanoparticles having a diameter of 15 nm and a concentration of 0.12 to 0.2% by volume is employed as a nanofluid. The findings demonstrated that the Nusselt number and heat transmission are both increased by the inclusion of nanoparticles. Additionally, increasing this value by 130% by utilizing a nanofluid with a concentration of 0.2% v/v and reducing the twist ratio of perforated twisted tape (H/D=2.5). Also, Reynolds number has a significant impact on heat transmission, regardless of whether it involves water or nanofluids and with or without twisted tape [24**]**.

An experimental investigation has been presented of how three different forms of twisted tape typical twisted tape, twisted tape with a V-cut, and clockwise-counter clockwise twisted tape with twist ratios (TR = 4, 6, 8) would improve heat transmission in a horizontal circular tube. The concentrations of nanofluids under fully developed turbulent flow and uniform heat flux conditions are (0, 0.01, 0.05, 0.1, 0.5, 1, 2, 3) % by volume. The experimental findings unequivocally demonstrate that heat transmission is improved by nanoparticles dispersed in water. The local Nusselt numbers along the tube were taken into account for determining the total Nusselt number of the tube, as mentioned above [25].

The passive 17 approaches have been employed to improve heat transmission and, consequently, the thermal efficiency of the solar water heater includes twisted tape inserts and Al_2O_3 nanofluids. A tube with or devoid of a twisted tape that is filled with water or 20 nanofluids effectively serves as the collector 19 in the solar water heating system that was the subject of this investigation. The heat transfer enhancement for a Reynolds number of 21 13000 for a 0.3% volume concentration of nanofluid is 21% for 22 the plain tube, and it is further enhanced to 49.75% when a twisted tape of H/D = 5 is put 23 in the tube, according to the results of the heat transfer experiments [26].

An experimental examination has been provided of twisted tape inserts with different cut radii in hairpin heat exchangers by using Fe_3O_4 water-based nanofluid. Data from experiments is produced at mass flow rates between 0.05 kg/s and 0.25 kg/s and at Reynolds numbers between 3000 and 25000. The investigation's findings indicate that as the volume concentration of the nanofluid rises, the heat exchanger's performance parameter the heat transfer coefficient friction factor improves. It has been observed that when the Reynolds number and nanoparticle volume concentration rise, so do the average Nusselt numbers [27].

Stable study TiO_2-H_2O nanofluids and their stabilities have been prepared. The construction of an experimental configuration prepared for analysing nanofluids' heat transfer and flow characteristics. The results show that heat transfer is greatly enhanced by rotating built-in twisted tape and TiO_2-H_2O 16 nanofluids, increasing it by 101.6% in comparison to that of a circular tube. On the heat transfer and flow characteristics of TiO_2-H_2O nanofluids, the effects of Reynolds numbers (Re=600-7000) and nanoparticle mass fractions (= 0.1%, 0.3%, and 0.5%) are investigated [28].

The heat transfer characteristics of Fe_3O_4 and its hybrid combination of Fe_3O_4 and SiC nanoparticles have been established in the volume ratio of 50:50 in 20:80 Ethylene Glycol (EG)-Water in order to compare the experimental results to those of the base fluid. The results indicate that the hybrid nanofluid has a thermal conductivity that is 16.19% higher and a viscosity that is 11.6% lower than the Fe_3O_4 /20:80 EG-Water nanofluid at an operating temperature of 45°C. Hybrid nanofluid outperforms Fe_3O_4/20:80 EG-Water nanofluid overall by a margin of 27.75% [29].

The continuous turbulent flow of copper oxide nanofluid has been simulated using the K-E model. The results indicated the variation of the Reynolds number and the height of the turbulator (b), which was selected from a variety of geometric parameters. A greater height can be used to achieve enhanced thermal management. Lower b disrupts and mixes fluids, weakening the boundary layer. To have the smallest energy loss, Re and b should both have the lowest values [30].

The heat transfer and pressure drop of a multiwall carbon nanotube (MWCNT)/water nanofluid heat exchanger has been investigated. The pressure drop of nanofluids with a concentration of 0.1%, 0.3%, and 0.5% is found to be 16%, 30%, and 42% advanced than water, respectively. Even 45 days after preparation, the MWCNT/water nanofluids are still found to be stable, and there has been no appreciable build-up of nanotubes on the tube's inner wall. Research has also revealed that there are not many immediate risks associated with handling MWCNT, and that even after several test runs, there isn't any visible erosion of the coiled tube's inner wall surface [31].

Passive solutions like twisted tape insert and nanofluid turbulent flow has been studied to improve heat transmission in the curved tube. Copper is used to create the twisted tape and curved tube. The impact of flow rate, nanoparticle concentration, and twisted tape insert on the convective heat transfer coefficient, Nusselt number, and Darcy friction factor is examined. The results show that the curved tube and twisted tape insert improve convective heat transfer coefficient by up to 31%. The twisted tape and the addition of the nanoparticle, on the other hand, affect the Darcy friction factor, and it is higher than it would be without the twisted tape and base fluid [32].

A thorough analysis of the published research on the advantages of nanofluids for heat transfer has been presented in macro- and micro-channels. There are both experimental and computational results provided for a number of significant performance characteristics, such as pressure drop, critical heat flux, and single-phase and two-phase heat transfer coefficients (CHF). The main findings of this review can be summed up as follows: The general opinion is that nanofluids are successful at increasing single-phase heat transfer coefficient near the entrance region due to a reduction in thermal boundary layer thickness, but the improvement declines downstream despite variances in research [33].

An experimental and numerical analysis have been explained to examine how the use of a metal oxide [Al_2O_3 (20 nm)]/distilled water nanofluid as a coolant can improve heat transfer in a circular finned tube with V-Cut twisted tape having a twist ratio (TR=1.85). Under conditions of turbulent flow, the studied concentrations of nanofluids are (0, 3, 5) % by volume. The key conclusions are summarized as follows: By incorporating nanoparticles into the base fluid, heat transmission is improved, and the rate of heat transfer rises as the concentration of the nanoparticles rises. Using the nanofluid and the V-Cut twisted tape together greatly improved the heat transmission [34].

The volume fraction of the nanoparticles, the Reynolds number, and the different types and configurations of inserts has been evaluated for their effects on improvement of heat transfer of nanofluid flowing within the tube with inserts. Conclusions drawn from the review are as follows: In the future, more thorough experiments and simulations including a wide range of geometrical parameters will be required to arrive at the ideal modification for twisted tape. In order to understand how nanoparticle dispersion and random movement caused by swirl flow created by twisted tape affect the overall enhancement ratio, further research is required [35].

The convective heat transfer (HT), pressure drop (PD), irreversibility, energy efficiency, and thermal performance has been investigated for turbulent flow inside a circular, evenly heated channel fitted with a new hybrid tape shape. The analysis's findings can easily be utilized to the design of very effective tube-type heat exchangers. Based on the aforementioned findings, it can be said that using hybrid grooved tape is a proven method for improving the thermal energy transmission coefficient [36].

ANSYS FLUENT software has been used to research the thermal and rheological properties of a power-law non-Newtonian CMC-based CuO nanofluid in a tube. There are two fully developed and uniform flow inlet velocity distributions used. It was demonstrated that the volume fractions under 1.5% slightly affect local heat transfer. It turns out that the average Nusselt number and the local heat transfer both decline as the Reynolds number rises. In contrast to earlier studies, the current findings demonstrate that lowering the average Nu requires raising the volume fraction of nanoparticles [37].

Mathematical research on characteristics of heat transfer and flow for two pipes fitted with two distinct dimpled spiral centre plates has been presented by using Al_2O_3, CuO, and TiO_2 nanofluids as cooling fluids. Results show that geometry with an in-line arrangement behaves better than geometry with a staggered layout. When compared to a smooth spiral central plate with base flow, the in-line configuration maximizes convection heat transfer by

47.3%. The distribution of wall temperatures was improved by utilizing nanofluids, which also resulted in significant rises in thermal conductivity and dynamic viscosity [38].

The impacts of the twisted tape truncation %, pitch value, position, and Reynolds number on the convective heat transfer in a heat exchanger equipped with twisted tape elements has been studied by using 3D numerical simulation. The obtained results showed that, due to the creation of an effective secondary and mixing flow, employing the twisted tape and decreasing its pitch value enhances the Nusselt number, friction coefficient, and PEC number. In the case of fully fitted twisted tape with a pitch value of L/4, the average Nusselt number increased by approximately 151.42 for a Reynolds number of 1000 [39].

The flow of nanofluid comprising nickel-zinc ferrite and ethylene glycol over a curved surface has been studied. Nonlinear thermal radiation and heat generation/absorption effects are included in the heat equation by using heat transfer analysis. The slip and thermal stratification boundary conditions support the suggested mathematical model. The following standout characteristics define the current attempt: The increase in the slip parameter causes a decrease in the velocity distribution. For increasing values of the curvature parameter, the fluid velocity is increased; nevertheless, the temperature profile shows a contrary tendency [40].

A numerical simulation has been carried out on the thermal properties and second law analysis of turbulent Cu-H_2O nanofluid flow inside heat exchangers fitted with transverse-cut twisted tapes (TCTTs) with alternate axis with nanoparticle volume percentage of 0 to 1.5%. The following are the key findings of the current work: In comparison to modified TTs with thin margins (b/w=0.9), transverse-cut twisted tapes with broader cut edges (b/c=0.7) can produce higher swirl flow and flow disturbance. Near the alternate axis intersection, the rate of TKE also significantly rises [41].

The MHD flow of water-based ferro-nanofluid has been analysed in the presence of heat generation, thermal radiation, and the shape effect of nanoparticles. The findings showed that both temperature and velocity Felds are significantly influenced by the fractional parameter. With stepped heating, the fractional parameter increases while the temperature and velocity fields decrease. For the fractional parameter, this pattern in the isothermal case reverses near the plate and gradually ramps up and isothermal heating becomes similar farther from the plate [42].

the heat transfer rate and flow of a non-Newtonian water-Carboxyl methyl cellulose based Al_2O_3 nanofluid in a helical heat exchanger fitted with conventional and unique turbulators has been examined by using a two-phase model. The results showed that using a novel heat exchanger in place of a basic smooth system increased the thermal properties (as measured by the Nusselt number) by about 210%, the hydraulic performance (as measured by the friction factor) by about 28%, the performance evaluation criteria index by about 57%, and the material consumption by about 31% [43].

The two-phase flow of nanofluids and their thermal energy transport coefficients have been investigated in three-dimensional diamond-shaped cavities with reducing-dimensional square barriers. While the hot side is kept at 400 or 500 K, materials with two emissivity values, = 0.3 and 0.9, have been taken into consideration to study the impact of the radiation thermal energy transmission coefficient. The rate of the thermal energy transmission coefficient is further enhanced by raising Ra. The optimal NP volume fraction for each model in each circumstance produces the maximum Nusselt number [44].

The use of nanofluids (NFs) in heat exchangers (HExs) of various geometries has been discussed. A persistent research focus throughout the years, the search for heat instruments with quick reaction for the industrialized sector remains a significant problem. It has been determined through a thorough examination of the available literature that the use of NFs greatly raises the thermal efficiency of HExs. It was determined that the use of NF and various shapes had significantly improved heat transmission efficiency on both an individual and a group level [45].

The significance of heat transfer and the techniques have been determined to develop heat transfer. Heat transfer was developed using fins, porous materials, and nanomaterials. When using the original materials without using these ingredients, there is a noticeable difference because there is less heat transfer and it takes longer. The less efficient heat transmission and longer processing times are evident when using the original materials alone. Researchers should concentrate on enhancing heat transmission because it is crucial for numerous applications that directly affect human existence [46].

A mathematical analysis has been studied of the influence of a helical baffle on the hydrothermal characteristics and irreversibility behaviour of a turbulent forced convection flow of water CuO nanofluid (NF) inside a hairpin heat exchanger with a 10 mm inner tube internal diameter, a 100 mm length, and a 15 mm outer tube internal diameter. The results showed that increasing Re and causes pressure to rise, whereas increasing B causes pressure to fall. Furthermore, it was determined that the case with B= 33.3 mm, = 2%, and Re= 10,000 has the best thermal performance of NF, which is equivalent to 1.067 [47].

The laminar convective heat transfer of a water-based ferrofluid flowing through a pipe both with and without an external magnetic field has been investigated. The working fluid is Fe_3O_4-Water. Use of Ans. 2019 R3 was made for simulation and analysis. Simulated was a single-tube configuration. The findings imply that increasing the amount of hidden nanoparticles in the base fluid may boost the heat exchangers' heat transfer coefficient (HTC). By also raising the volume proportion of nanoparticles, the HTC could potentially increase [48].

2.3 IMPROVEMENT OF HEAT TRANSFER IN THE PRESENCE OF MAGNETIC FIELD

A microfluidic system has been constructed to explain the magnetic control of heat transfer in a circular chamber experimentally and numerically. Three instances were looked at and contrasted: ferrofluid in a magnetic field, diluted ferrofluid, and DI-water. According to experimental evidence, heat trapping occurs when a magnetic field is present at a relatively modest flow rate. Paramagnetic nanoparticles gravitate toward a magnet with a magnetic field. As a result, at larger flow rates, convective heat transfer and Nu number are enhanced. The observed behaviour is clearly depicted by simulation findings, which are in good agreement with the experimental data [49].

An experimental study has been presented on improving heat transmission in a shell and tube heat exchanger by inserting helical coiled wires into the tube bundle. The pitch sizes employed were 4.8, 6.4, 8.0, and 9.6 mm. Water served as the exchanger's operating fluid on both the shell and tube sides. With a Reynolds number for the tube inside ranging from

1, the flow arrangement employed was parallel and laminar on both sides (100-920). The introduction of 9.6 mm pitched inserts increased the heat transfer coefficient on the tube side by 54%, according to the study's findings [50].

A ferrofluid material characterization and measurement of heat transfer rates for single-phase ferrofluid forced convective flow in microchannels analysed and demonstrated that the use of ferrofluids improves the flow's heat transfer properties and that these properties are influenced by the ferrofluid's material composition. The findings demonstrate that, in general, greater magnetic nanoparticle solid volume concentrations improve heat transfer rates. Additionally, it was noted that viscosity does, if barely, rise as magnetic flux rises [51].

The effects of a non-uniform magnetic field on ferrofluid heat transport have been investigated inside a 90° elbow channel using numerical calculations. The finite volume method and the SIMPLEC algorithm are used to simulate the flow inside the domain in order to show how a non-uniform magnetic field affects ferrofluid's thermal and friction properties. The obtained results showed that as a magnetic field with strength of Mn 9.32 x 106 is applied close to the elbow, the average Nusselt number of ferrofluid increases by more than 28.6% [52].

The impact of a non-uniform magnetic field on the hydrodynamic and thermal behaviour of ferrofluid flow in a wavy channel has been demonstrated by using a 3D numerical simulation. Heat fluxes that are constant heat up the channel's undulating surfaces at the top and bottom. The findings show that the wavy wall increases the rate of heat transfer on the channel's bottom compared to the plain wall, but it has no discernible impact on the top wall, where natural convection is weak. [53].

The effects of a consistent external magnetic field and porous fins on the pressure drop and convective heat transfer of a magnetite (Fe_3O_4/water) nanofluid have been examined numerically in a heat sink. As a result, heat transmission is shown to increase at large volume fractions, fin porosities, and magnetic field intensities while decreasing with Reynolds number. For the heat sink with solid fins, utilizing ferrofluid results in a 13% increase in heat transfer when compared to pure water flow. By applying a magnetic field to the heat sink and utilizing porous fins, this value increases by up to 35% [54].

The effect of an axial magnetic field on heat transfer and nanofluid flow between two horizontal coaxial tubes has been studied in the presence of thermal radiation. Viscous dissipation's effects were also taken into account. The findings show that the velocity and temperature boundary layer thicknesses decrease as the radiation parameters and Hartmann number increase. The thickness of the velocity and temperature boundary layers, however, may rise if the Eckert number and Reynolds number are improved [55].

The influence of a magnetic field on ferrofluid heat and fluid flow has been investigated in a helical tube. The boundary condition for the helical tube is constant wall temperature. According to the results, the magnetic field causes the Nusselt number to increase by around 40%. While Nusselt number and friction factor only minimally increase at high magnetic gradient values, Nusselt number increases significantly at low magnetic gradient values. Additionally, for high magnetic gradient values, the development of wall shear stress on tube walls leads to decreased thermal-hydraulic performance [56].

The impact of an external magnetic field on the mixed convection flow of Fe_3O_4 and water ferrofluid in a horizontal porous channel has been investigated numerically. The Darcy-Brinkman-Forchheimer formulation's governing equations were solved using the finite volume method. By increasing Mn, Re, the volume fraction of nanoparticles, and Da, the friction factor lowers. By raising the magnetic field intensity and nanoparticle volume percentage, Nu increases significantly. The influence of magnetic field on heat transmission is made more efficient by increasing the permeability of the porous material [57].

The effects of utilizing nanoparticles with and without the use of a magnetic field have been investigated experimentally on flow behaviour properties and the rate of forced convection heat transfer of Fe_3O_4-water nanofluid with a laminar flow regime in a horizontal tube under constant heat flux conditions. The experiment presented that an increase in the heat flux and nanofluid concentration led to a rise in the Nusselt number. It was also discovered that the usage of magnetic intensity improved heat transmission considerably more [58].

The water-based ferrofluid's convective heat transfer has been examined as it passed through a conduit. Convective heat transfer of a water-based ferrofluid flowing through a pipe was explored and studied in relation to the effects of an externally provided magnetic field and twisted tape insert. Fe_3O_4 in water is the working fluid. Analyses and simulations were conducted using Ansys 2019. It has been discovered that ferrofluid reacts to an external magnetic field. Heat transfer rate was seen to rise under the application of a continuous magnetic field by 12–14% for systems without twisted tape arrangements and 18.7–21.4% for systems with twisted tape arrangements for all Re ranges [59].

A magnetic field affects the forced convective heat transfer characteristics of Fe_3O_4 nanofluids has been described based on water and ethylene glycol (EG) as well as Fe_3O_4-MWCNT hybrids. The results demonstrated that the convective heat transfer coefficient of magnetic nanofluids increased with the strength of the magnetic field. When the magnetic field intensity was increased from 0 to 750 G, the largest convective heat transfer coefficients were seen for the 0.2 wt. % Fe_3O_4 and 0.1 wt. % Fe_3O_4-MWNCT nanofluids; the improvements were around 2.78% and 3.23%, respectively [60].

The presentation of a fin-tube heat exchanger in terms of heat transfer has been studied by using ferrofluid as a coolant while external magnetic fields were applied. The thermal boundary layer was seen to alter as the magnetic fields were applied. Additionally, it generated vortexes, which had an impact on how flow patterns developed. This procedure made use of the ferrofluid's ability to flow when magnetic fields are present. The reference model started to circulate around tubes when a permanent magnet was used. The impact of equal cooling between tubes, however, was not realized [61].

The effects of converting the heating fluid to a unique type of magnetic nanofluid on efficiency improvement have been studied. In the current work, case studies involving ferrofluid (Fe_3O_4) are compiled, and similar findings are examined. The following list includes some of the most significant findings: The magnetic field effect can increase the effectiveness of heat transmission. The findings of numerical simulations show that the magnetic number increases and the opening ratio decreases, although this improvement was dependent on the magnetic field intensity and the geometry of the flowing channel [62].

The impact of subjecting different magnetic field strengths of 15.1, 30.3, and 45.5 mT has been investigated on the improvement of heat transfer in a horizontal pipe heated with a constant heating flux of 420W. Results demonstrated that regardless of whether a magnetic field is present or absent, the Nusselt number (Nu) for water and nanofluids increases as Re increases. Additionally, higher values than water were attained. When the magnetic field is not present, the average rise in Nusselt number for Fe_3O_4-nanofluids is 16.7% compared to water [63].

Experiments, simulations, and optimization have been carried out to assess ferrofluids' ability to transport heat. Colloidal suspensions of magnetic nanoparticles with a diameter of 5 to 15 nm are known as ferrofluids, and they can be found in base fluids like water or oil. Setting the temperature range from TC_1 to TC_3 and imposing limits on the design variables D_1 and D_2 allowed the maximum temperature of TC_4 to be determined. The average relative error of TC1–TC_4 in the experiment findings was roughly 0.6% in comparison to the projected value, indicating that the NPR model's prediction of the ideal value was accurate [64].

The creation of nanofluids and their thermal properties, including viscosity and thermal conductivity, have been presented. The study compiles the several theoretical models of thermal conductivity and viscosity of nanofluids. Additionally, studies are done to determine how variations in heated walls impact heat transfer. It is found that the pressure drop can be reduced by about 10% and the presentation of heat transfer of a Fe_3O_4-water nanofluid is enhanced when a magnetic field is applied to corrugated plate heat exchangers [65].

The joint impact of a magnetic baffle and a dimple turbulator has been examined computationally on the heat transport and pressure decrease in a small channel. The numerical simulations were conducted using the finite-volume based commercial computational fluid dynamics solver ANSYS-Fluent 18.1. The study's observations allowed us to draw the following conclusions: The employment of a virtual baffle created by the magnetic field and an artificially created rough surface (dimple turbulator) increases heat transfer by fostering turbulence and flow mixing zones [66].

3. METHODOLOGY

3.1 INTRODUCTION

In this chapter, all the basic equations through which the results were obtained from within the numerical aspect, the programs and settings required to obtain accurate and reliable results will be reviewed.

3.2 COMPUTATIONAL ANALYSIS USING ANSYS SOFTWARE

3.2.1 Introduction

Computational Fluid Dynamics (CFD) studies are performed to grow a more profound knowledge into the field of the stream. To explain the impact of the disturbance model which includes the arrangement of two vehicle condition, (k-ε) model is utilized. Accordingly, the methods of the mathematical arrangement will address these Cartesian direction frameworks (x, y, and z). Three-layered calculation is created. ANSYS variant (20.1) will be utilized to make and network the framework math and afterward to reproduce one case.

3.2.2 Assumptions

In the current study, water and Fe3o4 is considered as the running nanofluid and the characteristics of flow are assumed (Steady flow, three dimensional, Newtonian, Incompressible, Turbulent).

3.2.3 Governing Equations

3.2.3.1 Magnetic induction method

In the principal approach, the attractive acceptance condition is gotten from Ohm regulation and Maxwell condition. The condition gives the coupling between the stream field and the attractive field. By and large, Ohm regulation that characterizes this thickness is given by:

$$\vec{J} = \sigma\vec{E} \tag{3.1}$$

Where σ: is the electrical conductivity of the media. For liquid speed field $\vec{U}$ in an attractive field $\vec{B}$, Ohm regulation takes the structure:

$$\vec{j} = \sigma(\vec{E} + \vec{U} \times \vec{B}) \tag{3.2}$$

From Ohm regulation and Maxwell condition, the enlistment condition can be inferred as:

$$\frac{\partial \vec{B}}{\partial t} + (\vec{U} \cdot \nabla)\vec{B} = \frac{1}{\mu\sigma}\nabla^2\vec{B} + (\vec{B} \cdot \nabla)\vec{U} \tag{3.3}$$

From the tackled attractive field $\vec{B}$, the present thickness $\vec{U}$ can be determined involving Ampere's connection as:

$$\vec{j} = \frac{1}{\mu}\nabla \times \vec{B} \tag{3.4}$$

By and large, the attractive field $\vec{B}$ in a MHD issue can be deteriorated into the remotely forced field ($\vec{B}_0$) and the prompted field $\vec{b}$ because of smooth movement. Just the actuated field $\vec{b}$ should be addressed.

From Maxwell situations, the forced field $\vec{B}_0$ fulfills the accompanying condition:

$$\nabla^2\vec{B}_0 - \mu\sigma'\frac{\partial \vec{B}_0}{\partial t} = 0 \tag{3.5}$$

Where σ': is the electrical conductivity of the media wherein field $\vec{B}_0$ is produced. Two cases should be thought of.

3.2.3.2 Standard k- ε model

The standard k-e model is a model for the disturbance dynamic energy (k) and its dispersal rate based on model viscose circumstances. The model viscose condition for k is derived from the particular condition, whereas the model vehicle condition for was obtained via real thought and resembles its numerically correct counterpart. In the k-model inference, the assumption is that the stream is totally fierce, and the effects of subatomic thickness are insignificant. As a result, the typical k-model is only significant for totally turbulent streams.

As the benefits and drawbacks of the traditional k-ε model have been revealed. The choppiness dynamic energy, k, and its scattering rate, are derived from the following vehicle conditions:

$$\frac{\partial}{\partial t}(\rho k) + \frac{\partial}{\partial x_i}(\rho k u_i) = \frac{\partial}{\partial x_j}\left[\left(\mu + \frac{\mu_t}{\sigma_k}\right)\frac{\partial k}{\partial x_j}\right] + G_k + G_b - \rho\varepsilon - Y_M + S_k \quad (3.6)$$

And

$$\frac{\partial}{\partial t}(\rho\varepsilon) + \frac{\partial}{\partial x_i}(\rho\varepsilon u_i) = \frac{\partial}{\partial x_j}\left[\left(\mu + \frac{\mu_t}{\sigma_\varepsilon}\right)\frac{\partial \varepsilon}{\partial x_j}\right] + C_{1\varepsilon}\frac{\varepsilon}{k}(G_k + C_{3\varepsilon}G_b) - C_{2\varepsilon}\rho\frac{\varepsilon^2}{k} + S_\varepsilon \quad (3.7)$$

In these cases, G_k addresses the age of choppiness active energy due to mean speed slopes, as shown in Modeling Turbulent Production in the k-ε Models. G_b is the age of the disturbance dynamic energy due to lightness, as shown in Effects of Buoyancy on Turbulence in the k-ε Models. Y M is concerned with the commitment of the fluctuating dilatation in compressible disturbance to the overall scattering rate, as depicted in Effects of Compressibility on Turbulence in the k-ε and are the violent Prandtl numbers for k and, respectively. S k and S_ε are client-defined source words. Displaying the Turbulent Viscosity, the violent (or whirlpool) consistency μ_t is figured by joining k and ε as follows:

$$\mu_t = \rho C_\mu \frac{k^2}{\varepsilon} \quad (3.8)$$

Where C_μ : is a constant.

Model Constants The model constants $C_{1\varepsilon}, C_{2\varepsilon}, C_\mu, \sigma_k$, and σ_ε have the following default values:

$$C_{1\varepsilon} = 1.44, C_{2\varepsilon} = 1.92, C_\mu = 0.09, \sigma_k = 1.0, \sigma_\varepsilon = 1.3$$

These default values not entirely settled from tests for crucial tempestuous streams including habitually experienced shear streams like limit layers, blending layers and planes as well as Standard, RNG, and Realizable k-ε Models for rotting isotropic matrix disturbance. They have been found to function admirably for a wide scope of divider limited and free shear streams. Albeit the default upsides of the model constants are the standard ones generally broadly acknowledged, you can transform them (if necessary) in the Viscous Model Dialog Box.

3.2.3.3 The Energy equation

Ansys Fluent solves the energy equation in the following form:

$$\frac{\partial}{\partial t}\left(\rho\left(e+\frac{v^2}{2}\right)\right)+\nabla\cdot\left(\rho v\left(h+\frac{v^2}{2}\right)\right)=\nabla\cdot\left(k_{eff}\nabla T-\sum_j\ h_j\vec{J}_j+\dot{\tau}_{eff}\cdot\vec{v}\right)+S_h \qquad (3.9)$$

Where k_{eff} is the forceful conductivity (k + k_t, where k t is the turbulent warm conductivity, as defined by the choppiness model used), and $\vec{J}_j$ is the species j dispersion transition. The first three terms on the right-hand side address energy movement as a result of conduction, species dispersion, and sloppy scattering, in that order. S h combines the volumetric hotness sources you've identified as well as the hotness aging rate from synthetic replies. Nonetheless, this response source has no effect on the total enthalpy condition (see Energy Sources Due to Reaction for subtleties).

The enthalpy h is characterized for ideal gases as

$$h=\sum_j\ Y_jh_j \qquad (3.10)$$

And for incompressible materials includes the contribution form pressure work

$$h=\sum_j\ Y_jh_j+\frac{p}{\rho} \qquad (3.11)$$

Y_j: is the mass fraction of species j and the sensible heat of species h_j is the part of enthalpy that includes only changes in the enthalpy due to specific heat

$$h_j=\int_{T_{ref}}^{T}\ c_{p,j}dT \qquad (3.12)$$

The value used for T_{ref} in the reasonable enthalpy computation is determined by the solver and models employed. T_{ref} is 298.15 K for the tension-based solver, except for PDF models, where T "ref " is a client input for the species. T "ref" is 0 for the thickness-based solver, unless when illustrating species movement with responses, in which case T ref is a client input for the species. The internal energy e is uniformly defined for compressible and incompressible materials as:

$$e=h-\frac{p_{op}+p}{\rho} \qquad (3.13)$$

In the above equations p and p_{op} are check and working strain individually. Such definitions of enthalpy and inward energy oblige an incompressible ideal gas in like manner formulation:

$$h = c_v T + \frac{p_{abs}}{\rho} = c_v T + R_g T + \frac{p}{\rho} = c_p T + \frac{p}{\rho} \quad (3.14)$$

3.2.3.4 The mass conservation equation

The mass conservation equation, often known as the continuity equation, is written as follows:

$$\frac{\partial \rho}{\partial t} + \nabla \cdot (\rho \vec{v}) = S_m \quad (3.15)$$

This is the most general sort of mass protection condition, and it applies to both incompressible and compressible streams. The mass contributed to the persistent stage from the scattered second stage (for example, due to evaporation of fluid droplets) and any client-defined sources is called S m. For 2D axisymmetric calculations, the progression condition is given by:

$$\frac{\partial \rho}{\partial t} + \frac{\partial}{\partial x}(\rho v_x) + \frac{\partial}{\partial r}(\rho v_r) + \frac{\rho v_r}{r} = S_m \quad (3.16)$$

Where x: the axial is coordinate, r is the radial coordinate, v_X is the axial velocity, and v_r is the radial velocity.

3.2.3.5 Momentum conservation equations

In an inertial (non-accelerating) reference frame, momentum is conserved.

$$\frac{\partial}{\partial t}(\rho \vec{v}) + \nabla \cdot (\rho \vec{v} \vec{v}) = -\nabla p + \nabla \cdot (\bar{\bar{\tau}}) + \rho \vec{g} + \vec{F} \quad (3.17)$$

Where p denotes the static strain, tensor denotes the pressure tensor (shown below), and g and F denote the gravitational and outer body powers, respectively (for example, those arising from interaction with the scattering stage). Other model-subordinate source terminology, such as permeable media and client described sources, are also included in F. The pressure tensor $\tau^{-\bar{}}$ is given by:

$$\bar{\bar{\tau}} = \mu\left[(\nabla\vec{v} + \nabla\vec{v}^T) - \frac{2}{3}\nabla\cdot\vec{v}I\right] \quad (3.18)$$

Where is the subatomic thickness, I is the unit tensor, and the influence of volume widening is the second component on the right-hand side. The pivotal and spiral force protection criteria for 2D axisymmetric computations are given by

$$\frac{\partial}{\partial t}(\rho v_x) + \frac{1}{r}\frac{\partial}{\partial x}(r\rho v_x v_x) + \frac{1}{r}\frac{\partial}{\partial r}(r\rho v_r v_x) = -\frac{\partial p}{\partial x} + \frac{1}{r}\frac{\partial}{\partial x}\left[r\mu\left(2\frac{\partial v_x}{\partial x} - \frac{2}{3}(\nabla\cdot\vec{v})\right)\right] + \frac{1}{r}\frac{\partial}{\partial r}\left[r\mu\left(\frac{\partial v_x}{\partial r} + \frac{\partial v_r}{\partial x}\right)\right] + F_x \quad (3.19)$$

And

$$\frac{\partial}{\partial t}(\rho v_r) + \frac{1}{r}\frac{\partial}{\partial x}(r\rho v_x v_r) + \frac{1}{r}\frac{\partial}{\partial r}(r\rho v_r v_r) = -\frac{\partial p}{\partial r} + \frac{1}{r}\frac{\partial}{\partial x}\left[r\mu\left(\frac{\partial v_r}{\partial x} + \frac{\partial v_x}{\partial r}\right)\right] + \frac{1}{r}\frac{\partial}{\partial r}\left[r\mu\left(2\frac{\partial v_r}{\partial r} - \frac{2}{3}(\nabla\cdot\vec{v})\right)\right] - 2\mu\frac{v_r}{r^2} + \frac{2}{3}\frac{\mu}{r}(\nabla\cdot\vec{v}) + \rho\frac{v_z^2}{r} + F_r \quad (3.20)$$

Where

$$\nabla\cdot\vec{v} = \frac{\partial v_x}{\partial x} + \frac{\partial v_r}{\partial r} + \frac{v_r}{r} \quad (3.21)$$

And v_z is the swirl velocity.

3.2.4 Turbulence Model

The average (k-ε) model is efficient with consistent exactness for wide violent streams reach and it is by and large utilized in the reproduction of hotness move. In the (k-ε) model, two extra vehicle conditions for the tempestuous motor energy (k) and violent dispersal rate (ε) are addressed and the whirlpool consistency (μ_t) is figured as an element of k and ε.

3.2.5 ANSYS Package

The stream conditions are addressed by utilizing two modules:

i. The essential module is pre-processor module; a program structure that makes the calculation and matrix as in the following:

a. Modeling of calculation.
b. Mesh age.
c. Boundary condition.

ii. The second module is the Solution module, for settling Navier-Stokes conditions (which incorporates progression, force and energy conditions), as well as the violent stream model.

3.2.6 System Geometry

The system engineering system is shown in Figure (3.1), where the model was designed with an internal diameter of 25.4 mm for flow and a total length of the tube 500 mm and contains within it a twisted bar with a thickness of 2 mm and a length of 20 mm, where three values of the torsion rotation are taken once two, four and six turns, and it will also be shed Magnetic field with different tolerances, where the length of the magnetic field was taken once 30 mm, 50 mm and 70 mm.

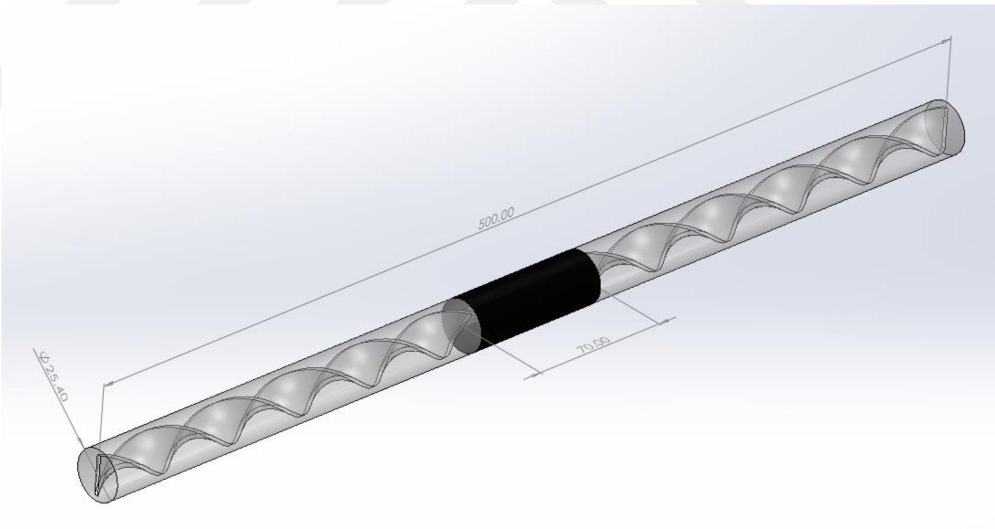

Figure 3.1: Geometry Shape**.**

3.2.7 Mesh Generation

Generally, because unstructured grids work well for complicated geometries, the unstructured tetrahedron grids were chosen in the current investigation. ANSYS support solid geometry mesh generation and three-dimensional models with minimum input from a single phase from the user. The number of cells taken, in this study was (2223270), see Figure (3.2).

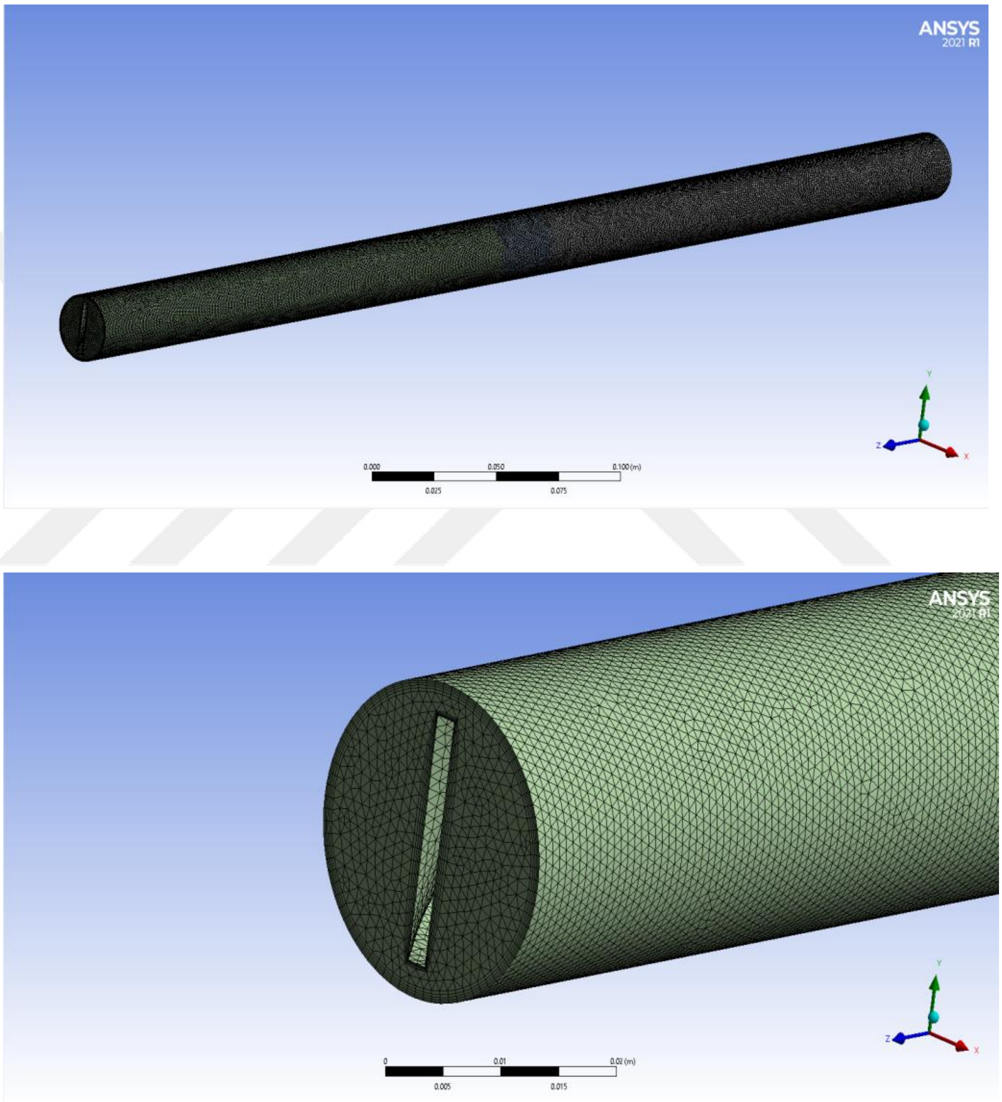

Figure 3.2: Mesh Generated.

In order to obtain accurate and reliable results, a Mesh independency must be made to see the clear change when changing the number of the element and the output results, as it stops when the stability of the output results is reached, where the element size is used 0.001m.

Table 3.1: Mesh Independency.

Case	Node	Element	Max temperature (k)	outlet temperature (k)	pressure difference (pa)
1	252360	1253477	335.812	305.363	47.42
2	326252	1532207	331.493	302.976	49.21
3	483412	1744345	329.081	302.881	49.47
4	597355	2223270	329.074	302.879	49.48

3.2.8 Conditions of the Boundary

Figure (3.3) shows the limits that were used, where three variable entry velocities were taken at the entry area (0.1, 0.3, and 0.5) m/s representing the entry of the nanomaterial at a temperature of 25C. In the exit area, an exit pressure of 0pa was applied to the surfaces of Heat A constant temperature of 40 C was shed, where three cases of the magnet were taken when the magnet have length 30,50,70 mm, then the twisted tape have 2 turns ,4 turns and 6 turns. Three forces of magnetic flux were taken (2, 4 and 6) tesla.

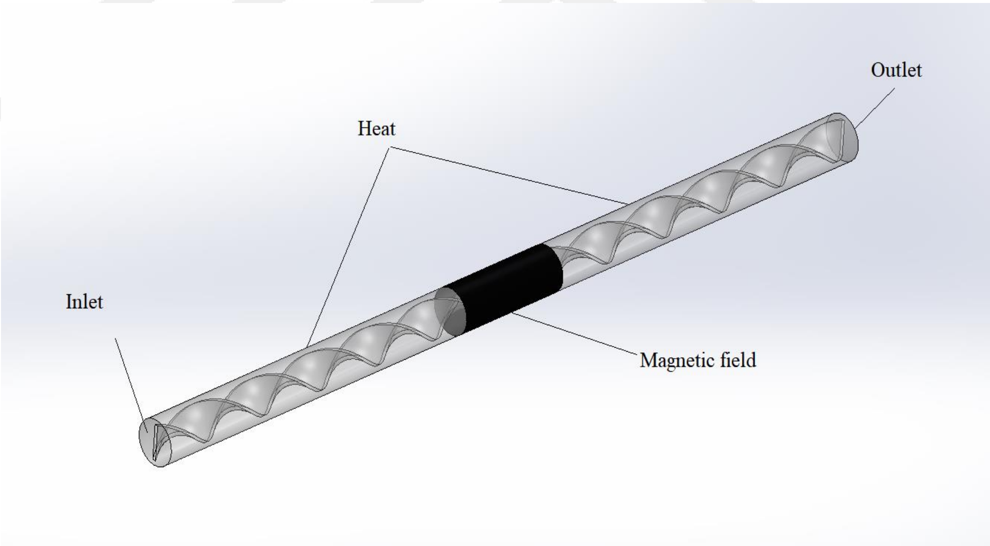

Figure 3.3: Boundary of Conditions.

3.2.9 Problem Solution

A volume of the control depended technique that comprises of the accompanying advances, which can be utilized for arrangement:

a. A network is created on the field.

b. Sets of conditions like speed, pressure, and preserved scalars, mathematical are built by the combination on each control volume of the administering conditions.

c. The Discretized Equations are linearized and tackled iteratively.

ANSYS is the arrangement calculation utilized by FLUENT and is embraced in the current work. The overseeing conditions are settled consecutively (i.e., isolated from each other). Since the administering conditions are non-straight (and coupled), numerous cycles might be done before a joined arrangement is gotten.

3.2.10 Solution Parameters

The solution parameters include the following:

a. Precision Solver Type

Ordinarily, accuracy solvers in are found by single and double as it were. A PC with limitless accuracy, residuals would go to zero as the arrangement combines. A genuine PC, the residuals rot to some little worth ("adjust") and afterward end changing ("level out").

b. Iterations Number

This is the highest digit of iterations done before the solver terminates.

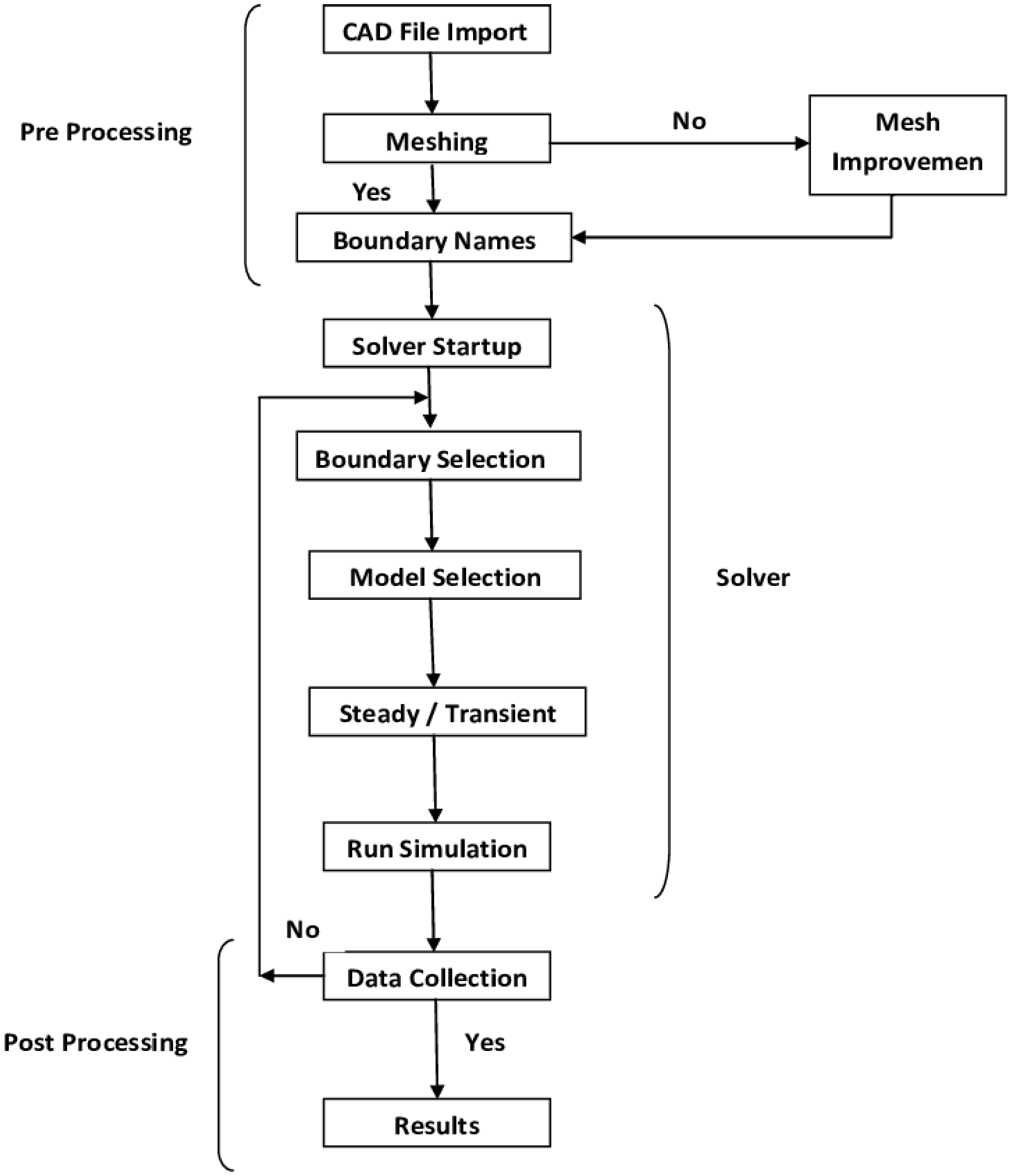

Figure 3.4: Flow Chart of CFD.

3.2.11 Convergence Criteria

The CFD method requires emphasizing the arrangement of the liquid stream conditions till it is met. The emphases are halted when the arrangement continues as before inside the exactness of the chose intermingling models. The most generally utilized strategy to check arrangement combination is the mistake residuals, which is the contrast between the upsides of a variable in two continuous emphases standardized by the biggest outright leftover for the initial five cycles. The arrangement is supposed to be united when the residuals are under a resilience breaking point of 10-6 for all the liquid stream conditions introduced previously.

4. RESULTS AND DISCUSSION

4.1 GENERAL VIEW

This chapter shows the mathematical results obtained for the process of the enhancement in heat transfer by using ferro-nanofluid and twisted tape with effect of different conditions: cycles of rotation, intensity of magnetic field, and concentration of ferro-nanofluid. It is also present the influence of the mentioned conditions on pressure, temperature, and velocity of fluid during the process of improving heat transfer by employing ferro-nanofluid with magnetic field.

4.2 FACTORS AFFECTED ON THE ENHANCEMENT HEAT TRANSFER RATE

4.2.1 Effect of Cycles of Rotation

Cycles of rotation are one of the influential factors in enhancement in heat transfer which play an important role. Figures (4.1 to 4.27) explain the effect of cycles of rotation on the enhance heat transfer rate. From these figures it has been noticed that when cycle of rotation is 2 cycles, intensity of magnetic field is 6 Tesla, and concentration 0.5 wt.%, the effect of cycles on the pressure of fluid decreased from 351.782 to -13.5 Pa at 30 width of magnetic field, at 50 width of magnetic field, the pressure still decreased from 414.584 to -11.627 Pa. The same results have been obtained at 70 width of magnetic field, the pressure of fluid decreased from 352.222 to -21.005 Pa.

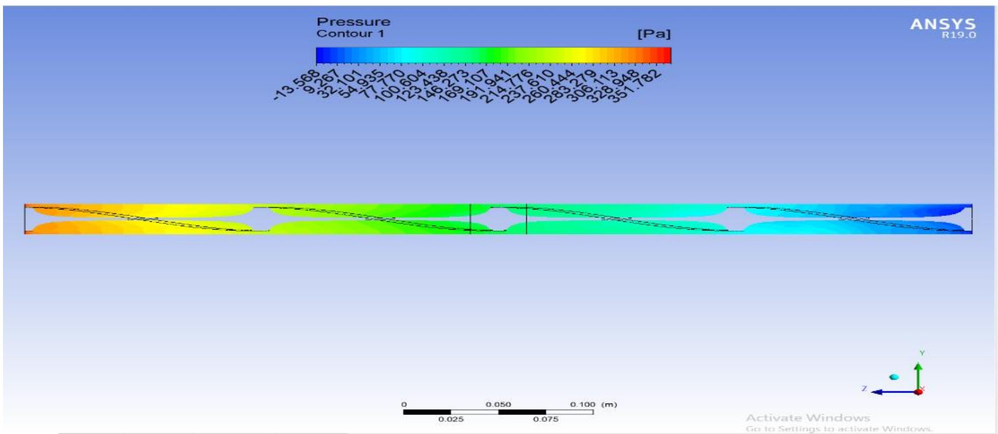

Figure 4.1: Effect Of Cycles Of Rotation On Pressure Of Fluid At 2 Cycles, 0.5 Wt% Concentration Of Ferro-Nanofluid, And 6 Tesla Intensity Of Magnetic Field With 30 Width Of Magnetic Field.

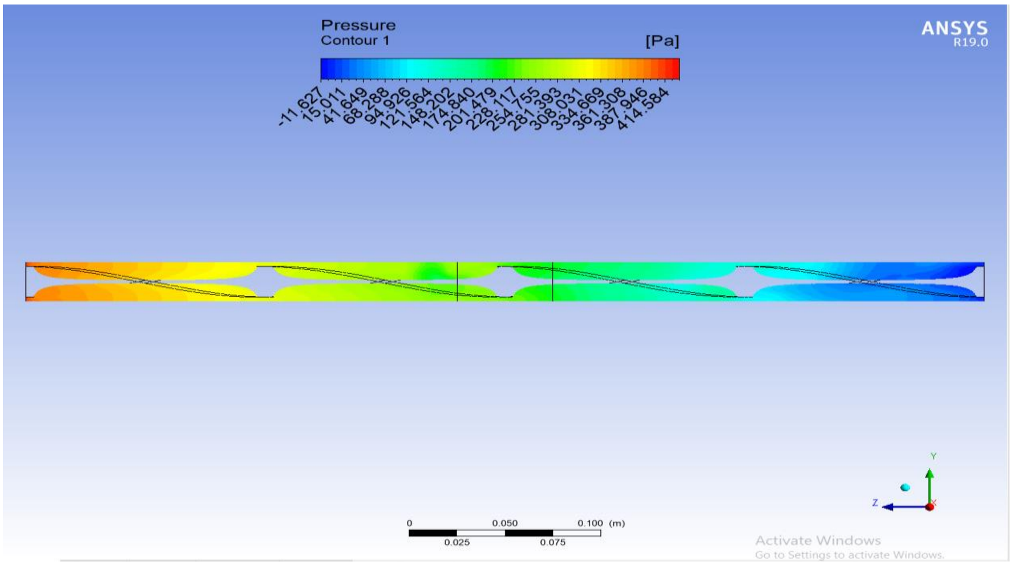

Figure 4.2: Effect Of Cycles Of Rotation On Pressure Of Fluid At 2 Cycles, 0.5 Wt% Concentration Of Ferro-Nanofluid, And 6 Tesla Intensity Of Magnetic Field With 50 Width Of Magnetic Field.

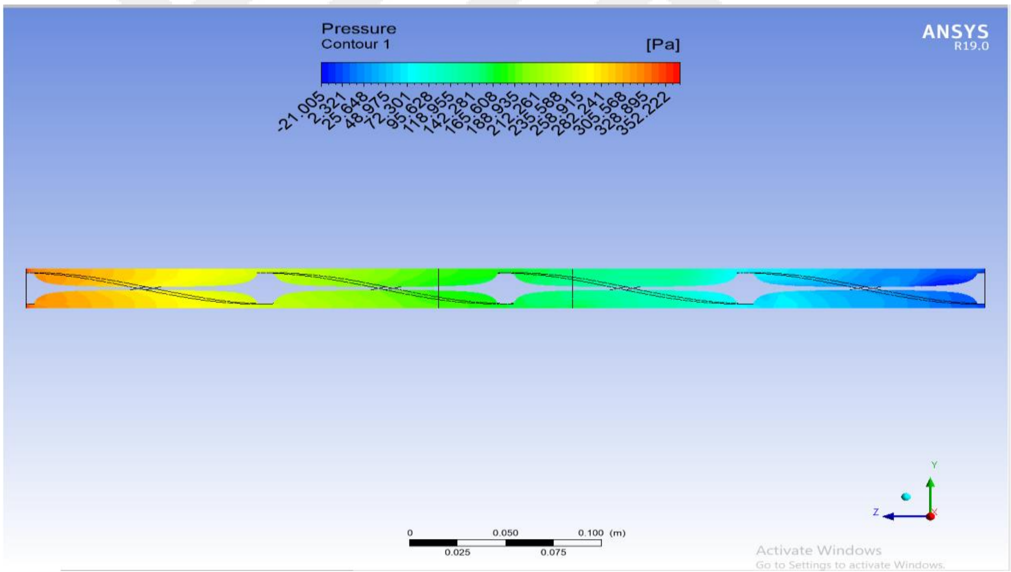

Figure 4.3: Effect Of Cycles Of Rotation On Pressure Of Fluid At 2 Cycles, 0.5 Wt% Concentration Of Ferro-Nanofluid, And 6 Tesla Intensity Of Magnetic Field With 70 Width Of Magnetic Field.

The effect of cycles on the temperature of fluid have been displayed in Figures from (4.4 to 4.6), it can be concluded that the temperature increased from 25.0 to 39.4 ºC at 2 cycles, 6 Tesla intensity of magnetic field, and 0.5 wt% concentration of ferro-nanofluid with 30 width of magnetic field. At 50 and 70 width of magnetic field, the temperature of fluid raised from 25.0 to 39.4 ºC at 2, 6, and 0.5 of cycles of rotation, intensity of magnetic field, and concentration of ferro-nanofluid respectively.

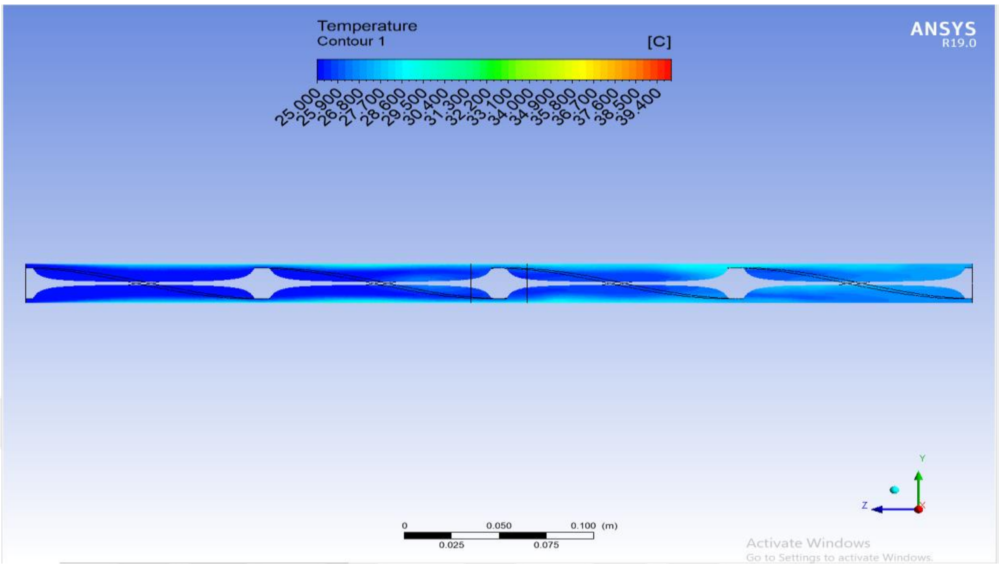

Figure 4.4: Effect Of Cycles Of Rotation On Temperature Of Fluid At 2 Cycles, 0.5 Wt% Concentration Of Ferro-Nanofluid, And 6 Tesla Intensity Of Magnetic Field With 30 Width Of Magnetic Field.

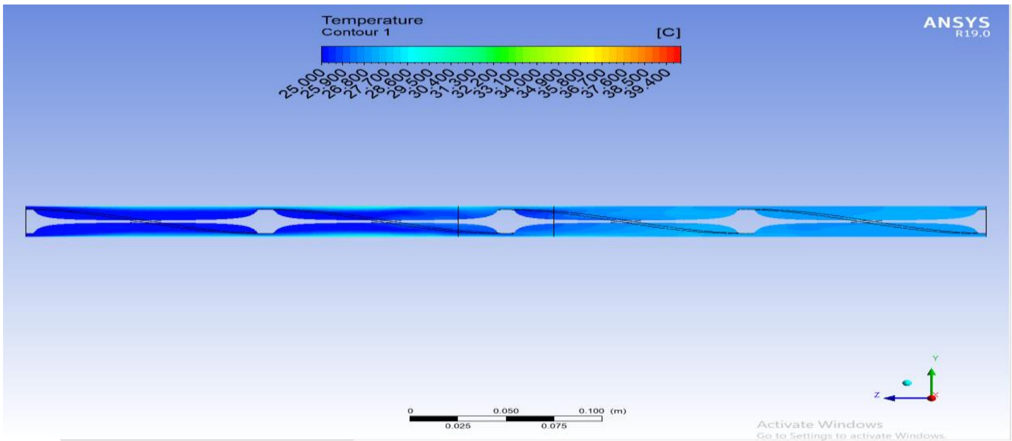

Figure 4.5: Effect Of Cycles Of Rotation On Temperature Of Fluid At 2 Cycles, 0.5 Wt% Concentration Of Ferro-Nanofluid, And 6 Tesla Intensity Of Magnetic Field With 50 Width Of Magnetic Field.

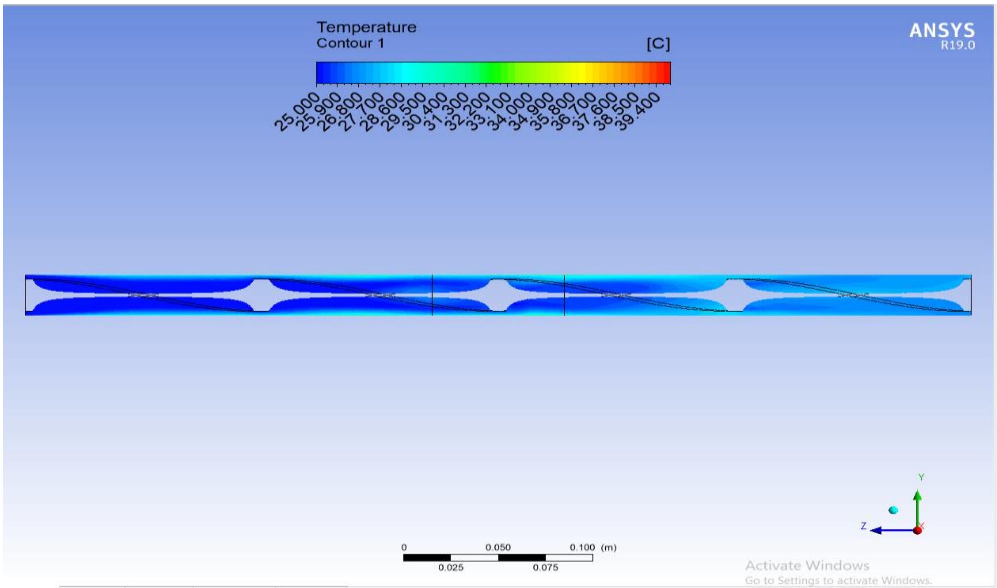

Figure 4.6: Effect Of Cycles Of Rotation On Temperature Of Fluid At 2 Cycles, 0.5 Wt% Concentration Of Ferro-Nanofluid, And 6 Tesla Intensity Of Magnetic Field With 70 Width Of Magnetic Field.

Figures from (4.7 to 4.9) show the effect of cycles of rotation on the velocity of fluid. The velocity of fluid tends to grow from 0.0 to 0.725 m/s at condition of 2 cycles, intensity of magnetic field 6 Tesla, and concentration of ferro-nanofluid is 0.5 wt% with 30 width of magnetic field. The similar outcomes of velocity of fluid appeared at the same conditions with 50 width of magnetic field whereas velocity increased from 0.0 to 0.723 m/s, while it is at high rising from 0.0 to 0.819 m/s at 2 cycles, intensity of magnetic field 6 Tesla, and concentration of ferro-nanofluid 0.5 wt% with 70 width of magnetic field.

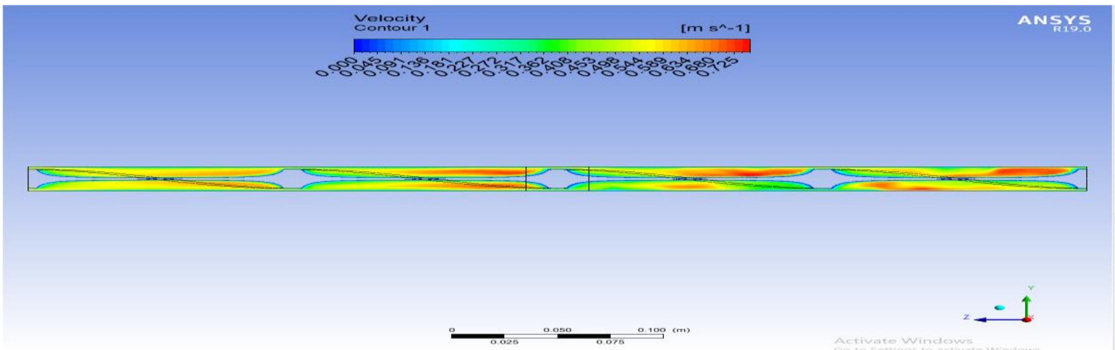

Figure 4.7: Effect Of Cycles Of Rotation On Velocity Of Fluid At 2 Cycles, 0.5 Wt% Concentration Of Ferro-Nanofluid, And 6 Tesla Intensity Of Magnetic Field With 30 Width Of Magnetic Field.

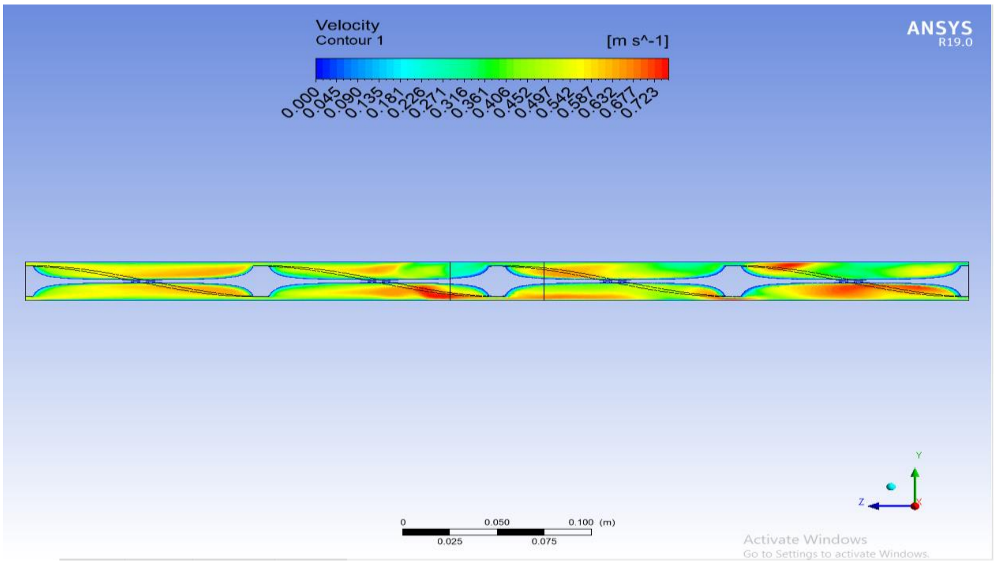

Figure 4.8: Effect Of Cycles Of Rotation On Velocity Of Fluid At 2 Cycles, 0.5 Wt% Concentration Of Ferro-Nanofluid, And 6 Tesla Intensity Of Magnetic Field With 50 Width Of Magnetic Field.

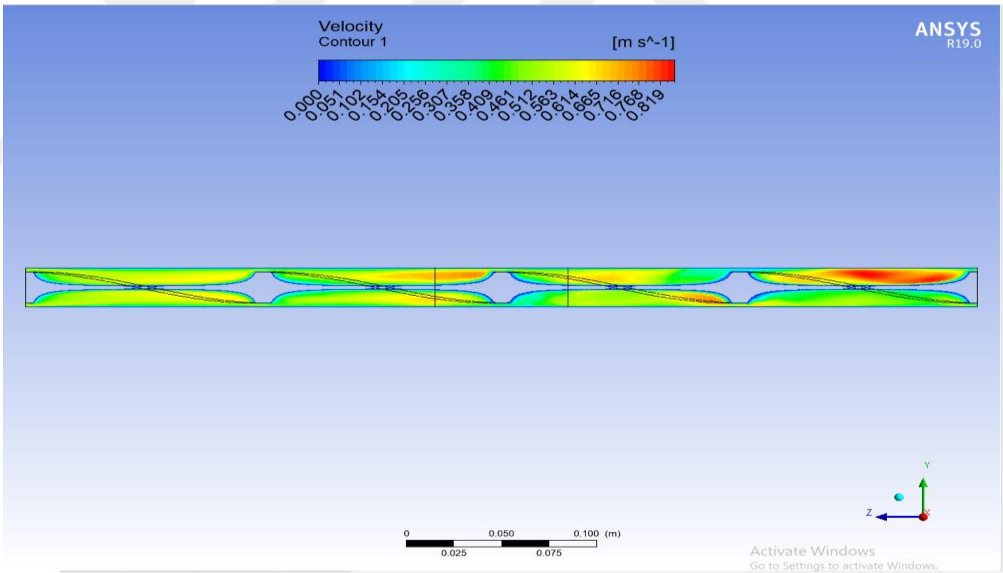

Figure 4.9: Effect Of Cycles Of Rotation On Velocity Of Fluid At 2 Cycles, 0.5 Wt% Concentration Of Ferro-Nanofluid, And 6 Tesla Intensity Of Magnetic Field With 70 Width Of Magnetic Field.

The pressure drop increases when velocity of fluid rises from 0.1 to 0.5 m/s. At thickness of magnetic 30 mm, 2 cycles of rotation, and intensity of magnetic 2 Tesla, the pressure drop reach to 35 Pa with 0.1 m/s. While at 0.3 and 0.5 m/s, pressure drop record 154.8 Pa, and

339.2 respectively with the same other operating conditions. See Figures from (4-10 to 4-12).

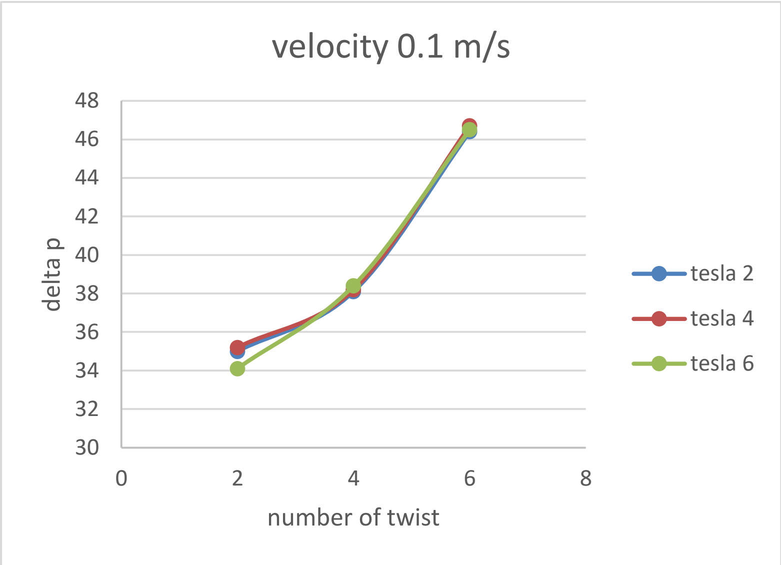

Figure 4.10: Effect Of Cycles Of Rotation And Intensity Of Magnetic Field On Pressure Drop At Velocity 0.1 M/S And Thickness Of Magnetic 30 Mm.

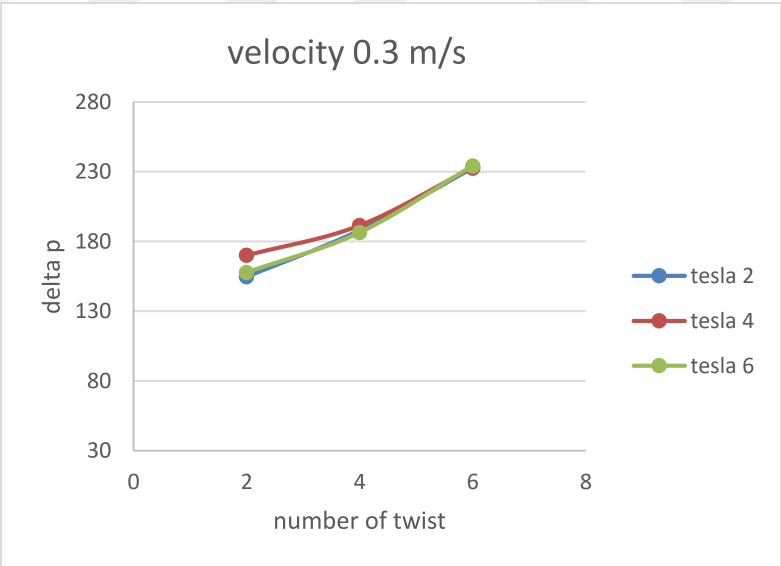

Figure 4.11: Effect Of Cycles Of Rotation And Intensity Of Magnetic Field On Pressure Drop At Velocity 0.3 M/S And Thickness Of Magnetic 30 Mm.

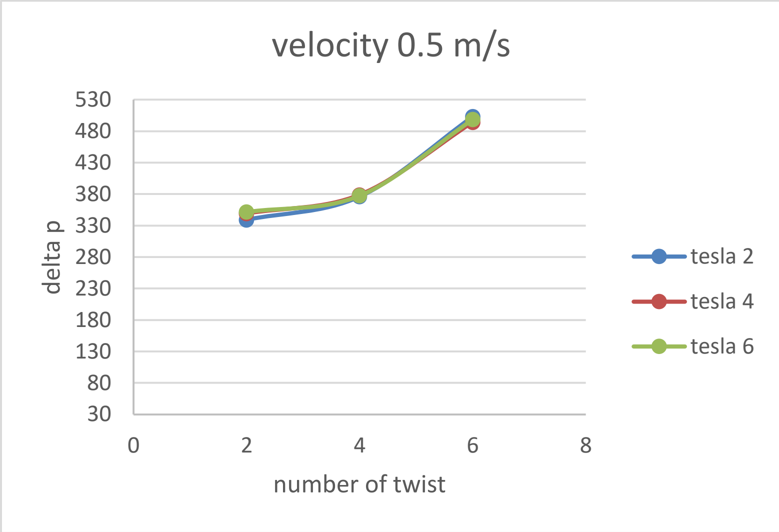

Figure 4.12: Effect Of Cycles Of Rotation And Intensity Of Magnetic Field On Pressure Drop At Velocity 0.5 M/S And Thickness Of Magnetic 30 Mm.

Again, the effect of cycles of rotation on pressure of fluid has been studied with 4 cycles. Figures (4-13 to 4-15) present this effect, it is obvious from Figure (4.10), the pressure decreased from 377.693 to -52.075 Pa at intensity of magnetic field 6 Tesla and 0.5 wt% concentration of fluid with 30 width of magnetic field. The pressure continues to reduce, it record the decreasing 16445.937 to -55.535 Pa at the same conditions with 50 width of magnetic field. Finally, the pressure dropped from 387.443 to -42.121 Pa with 70 width of magnetic field. It can be noticed that the more dropping of pressure is at 50 width of magnetic field.

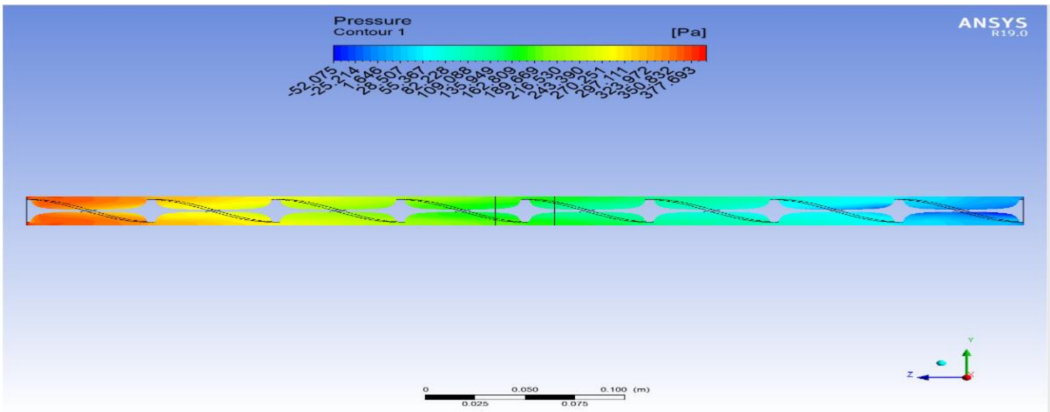

Figure 4.13: Effect Of Cycles Of Rotation On Pressure Of Fluid At 4 Cycles, 0.5 Wt% Concentration Of Ferro-Nanofluid, And 6 Tesla Intensity Of Magnetic Field With 30 Width Of Magnetic Field.

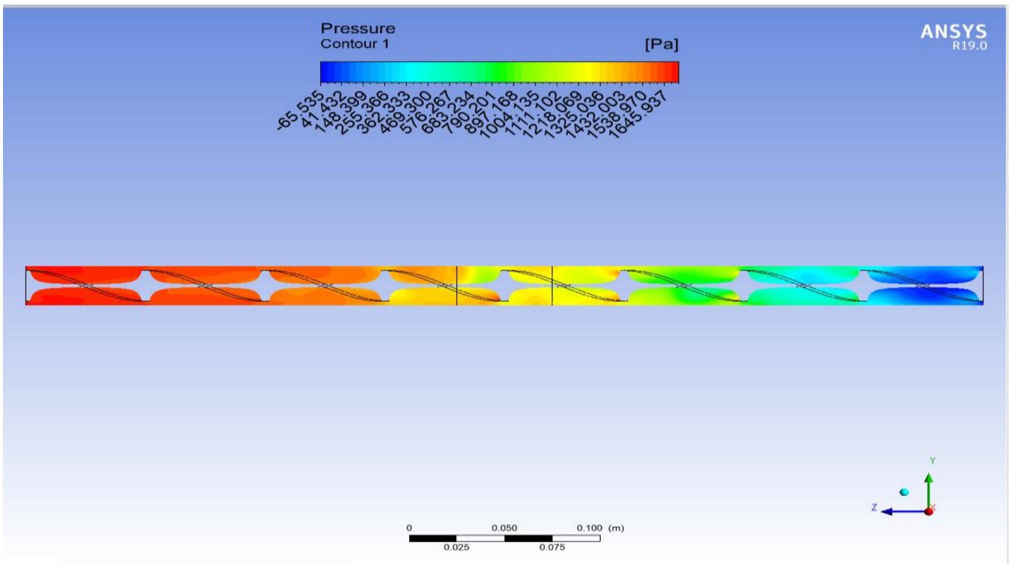

Figure 4.14: Effect Of Cycles Of Rotation On Pressure Of Fluid At 4 Cycles, 0.5 Wt% Concentration Of Ferro-Nanofluid, And 6 Tesla Intensity Of Magnetic Field With 50 Width Of Magnetic Field.

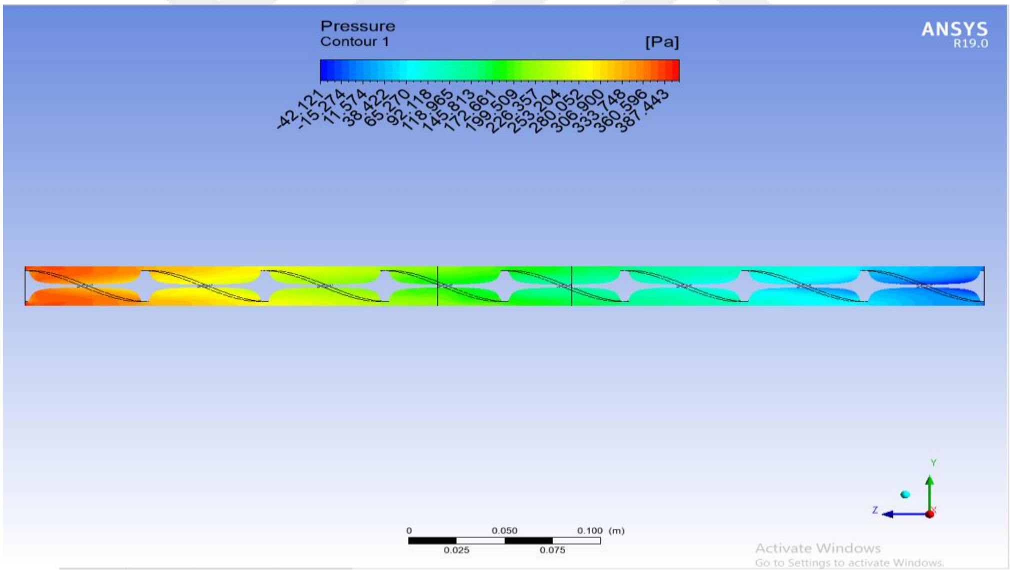

Figure 4.15: Effect Of Cycles Of Rotation On Pressure Of Fluid At 4 Cycles, 0.5 Wt% Concentration Of Ferro-Nanofluid, And 6 Tesla Intensity Of Magnetic Field With 70 Width Of Magnetic Field.

Now, the effect of cycles of rotation on temperature of fluid is repeated at condition of process, 4 cycles, 6 Tesla intensity of magnetic field, 0.5 wt% concentration of ferro-nanofluid. From Figures (4.16 to 4.18), we can conclude that the temperature of fluid increase at the same level with 30, 50, and 70 width of magnetic field at the above mentioned operating conditions. Temperature increase from 25 to 39.4 ºC.

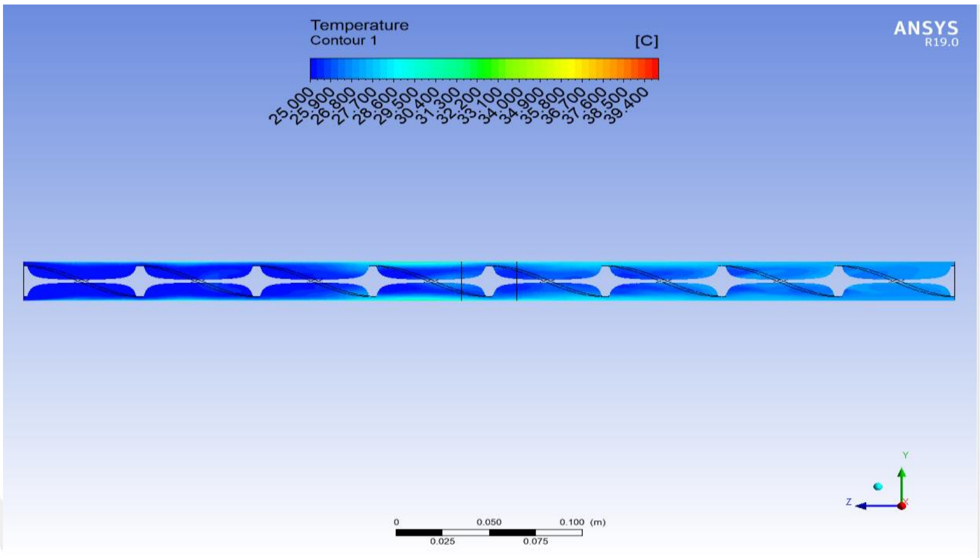

Figure 4.16: Effect Of Cycles Of Rotation On Temperature Of Fluid At 4 Cycles, 0.5 Wt% Concentration Of Ferro-Nanofluid, And 6 Tesla Intensity Of Magnetic Field With 30 Width Of Magnetic Field.

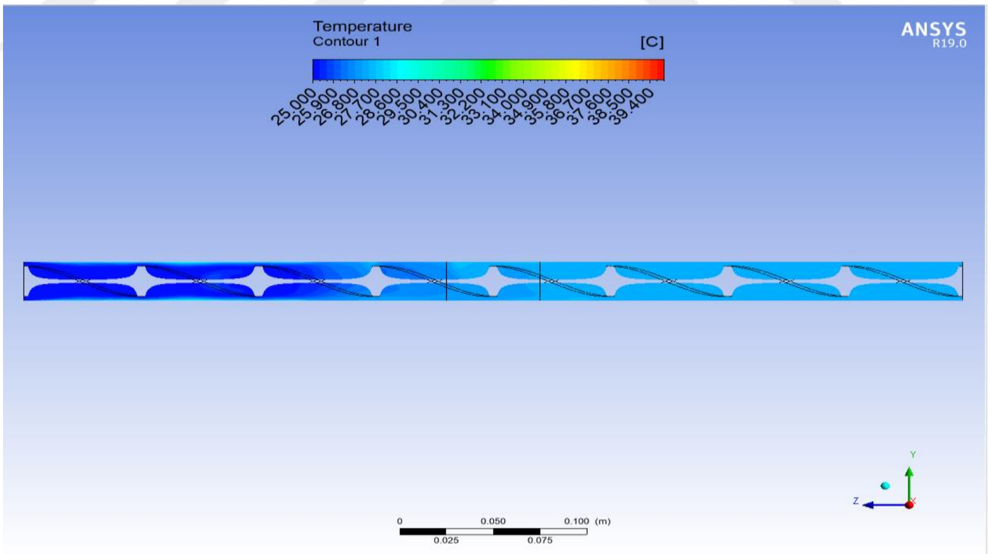

Figure 4.17: Effect Of Cycles Of Rotation On Temperature Of Fluid At 4 Cycles, 0.5 Wt% Concentration Of Ferro-Nanofluid, And 6 Tesla Intensity Of Magnetic Field With 50 Width Of Magnetic Field.

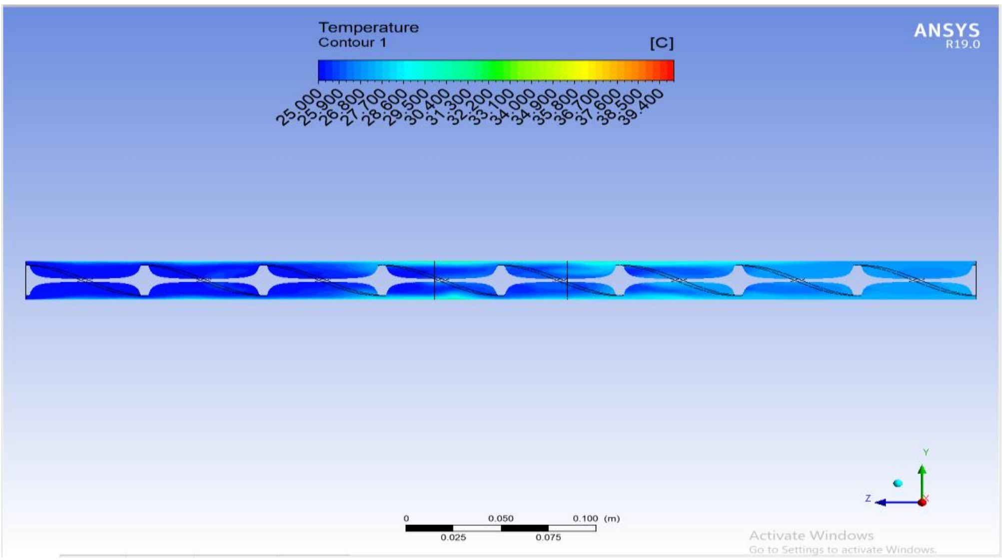

Figure 4.18: Effect Of Cycles Of Rotation On Temperature Of Fluid At 4 Cycles, 0.5 Wt% Concentration Of Ferro-Nanofluid, And 6 Tesla Intensity Of Magnetic Field With 70 Width Of Magnetic Field.

The effect of cycles of rotation on velocity of fluid has been studied with 4 cycles, 6 Tesla intensity of magnetic field, 0.5 wt % concentration of ferro-nanofluid. Velocity of fluid increase from 0 to 0.75 m/s at 30 width of magnetic field. Then continue to raise with 50 width of magnetic field from 0 to 1.065 m/s. Eventually, velocity of fluid with 70 width of magnetic field increase as the same level of rising in the first case 30. See Figures from (4.19 to 4.21).

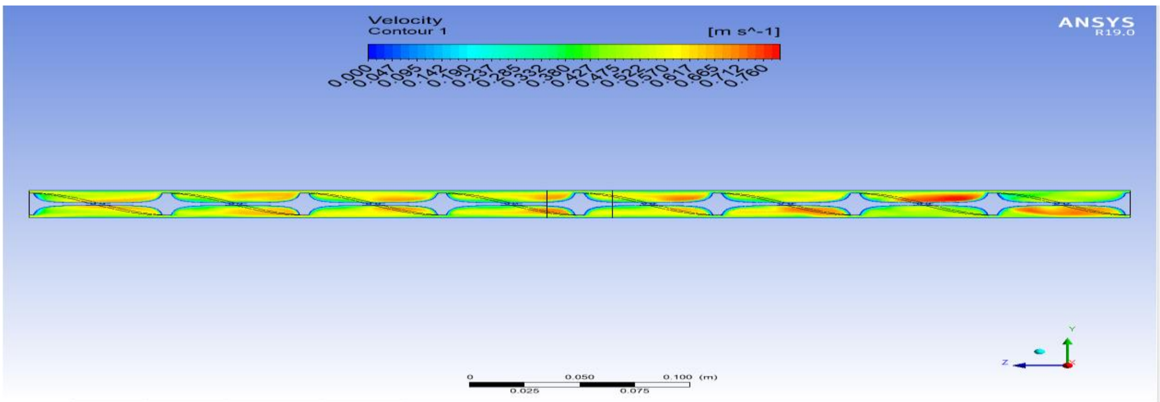

Figure 4.19: Effect Of Cycles Of Rotation On Velocity Of Fluid At 4 Cycles, 0.5 Wt% Concentration Of Ferro-Nanofluid, And 6 Tesla Intensity Of Magnetic Field With 30 Width Of Magnetic Field.

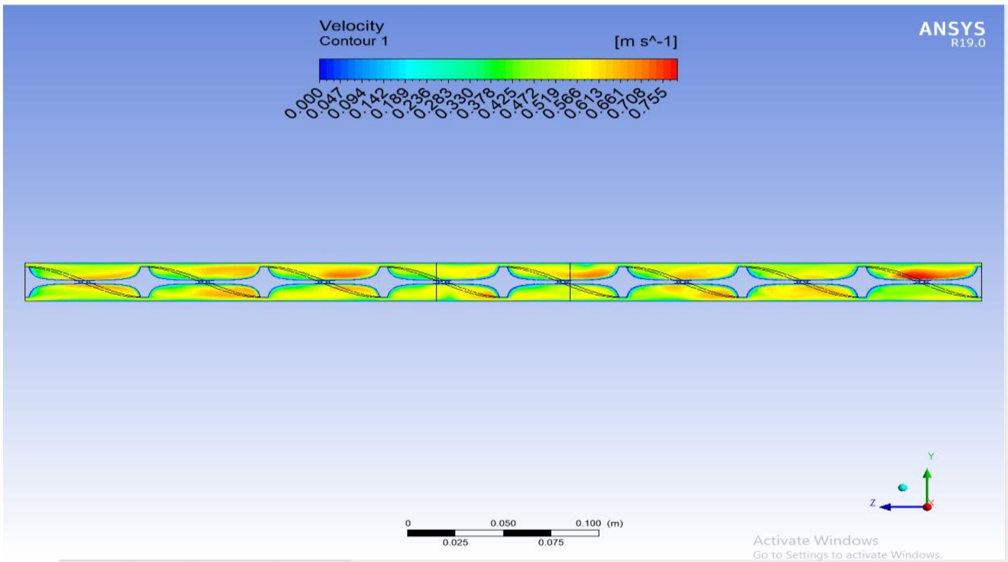

Figure 4.20: Effect Of Cycles Of Rotation On Velocity Of Fluid At 4 Cycles, 0.5 Wt% Concentration Of Ferro-Nanofluid, And 6 Tesla Intensity Of Magnetic Field With 50 Width Of Magnetic Field.

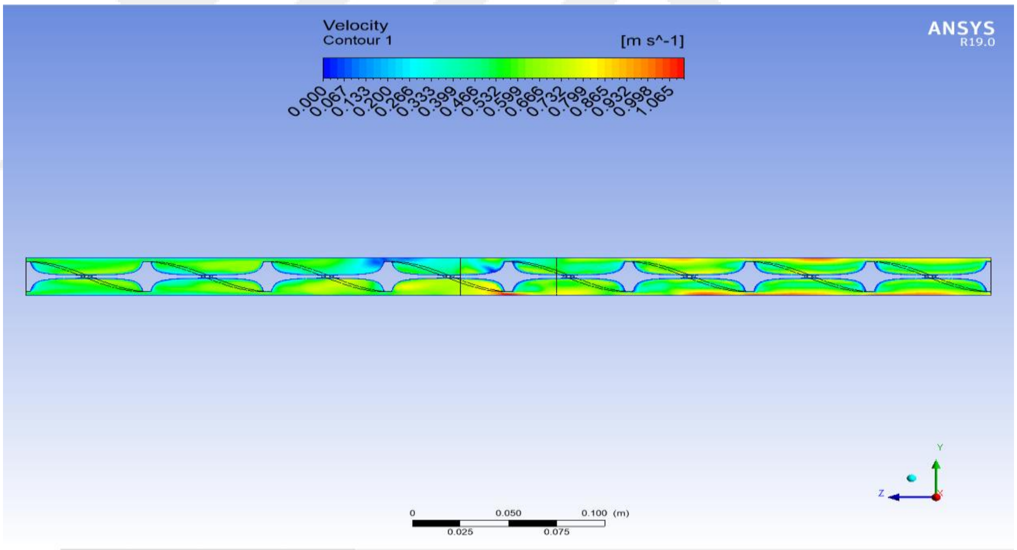

Figure 4.21: Effect Of Cycles Of Rotation On Velocity Of Fluid At 4 Cycles, 0.5 Wt% Concentration Of Ferro-Nanofluid, And 6 Tesla Intensity Of Magnetic Field With 70 Width Of Magnetic Field.

6 cycles of rotation is the last value which has been taken in consideration to present the effect of cycles on pressure, temperature, and velocity of fluid. It is clear as the pervious results, from Figure (4.22), pressure of fluid decrease from 498.53 to -85.628 Pa with 0.5 wt% concentration of ferro-nanofluid, 30 width of magnetic field, and 6 Tesla intensity of

magnetic field. The pressure of fluid suffer more dropping at the same conditions at 50 width of magnetic field as in Figure (4.23), then at 70 width of magnetic field, pressure reducing as at 30, and 50. See Figure (4.24).

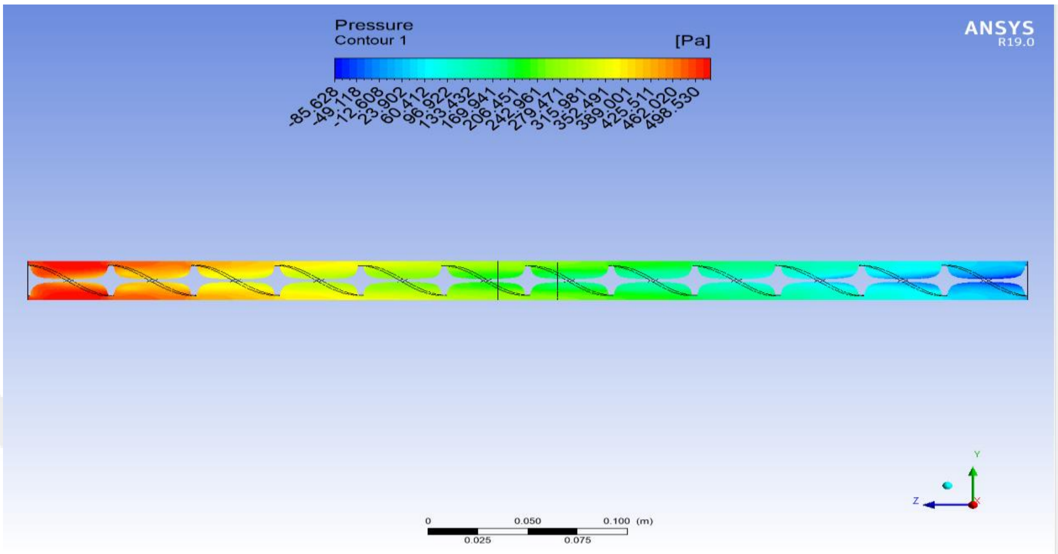

Figure 4.22: Effect Of Cycles Of Rotation On Pressure Of Fluid At 6 Cycles, 0.5 Wt% Concentration Of Ferro-Nanofluid, And 6 Tesla Intensity Of Magnetic Field With 30 Width Of Magnetic Field.

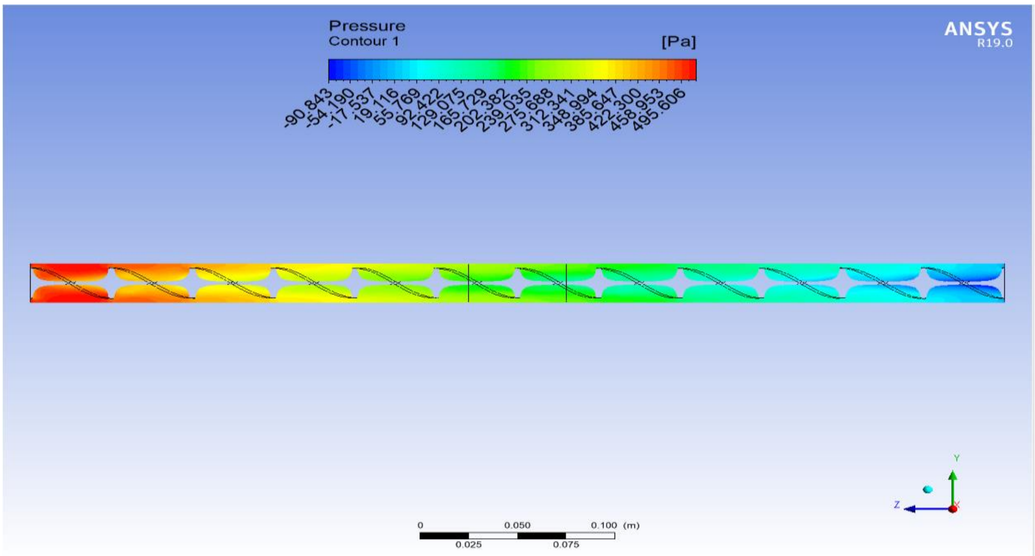

Figure 4.23: Effect Of Cycles Of Rotation On Pressure Of Fluid At 6 Cycles, 0.5 Wt% Concentration Of Ferro-Nanofluid, And 6 Tesla Intensity Of Magnetic Field With 50 Width Of Magnetic Field.

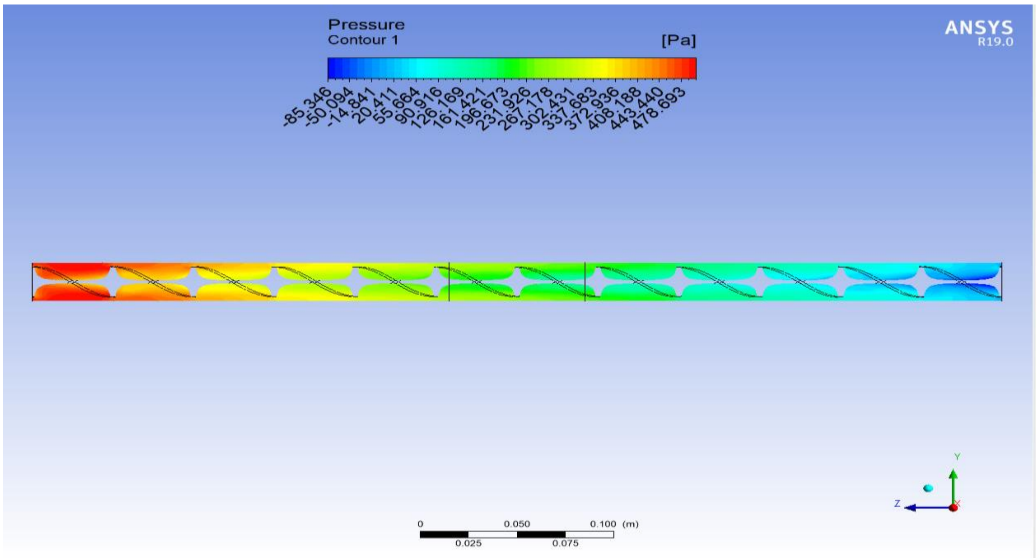

Figure 4.24: Effect Of Cycles Of Rotation On Pressure Of Fluid At 6 Cycles, 0.5 Wt% Concentration Of Ferro-Nanofluid, And 6 Tesla Intensity Of Magnetic Field With 70 Width Of Magnetic Field.

Figures (4.25 to 4.27) display the effect of 6 cycles of rotation on temperature of fluid. The other operating conditions were 6 Tesla intensity of magnetic field, 0.5 wt% concentration of ferro-nanofluid and 30, 50, and 70 width of magnetic field, respectively. It is clear that the temperature of fluid grow at the same level for all magnetic fields, whereas temperature increases from 25 to 39.4 ºC at 30, 50, and 70.

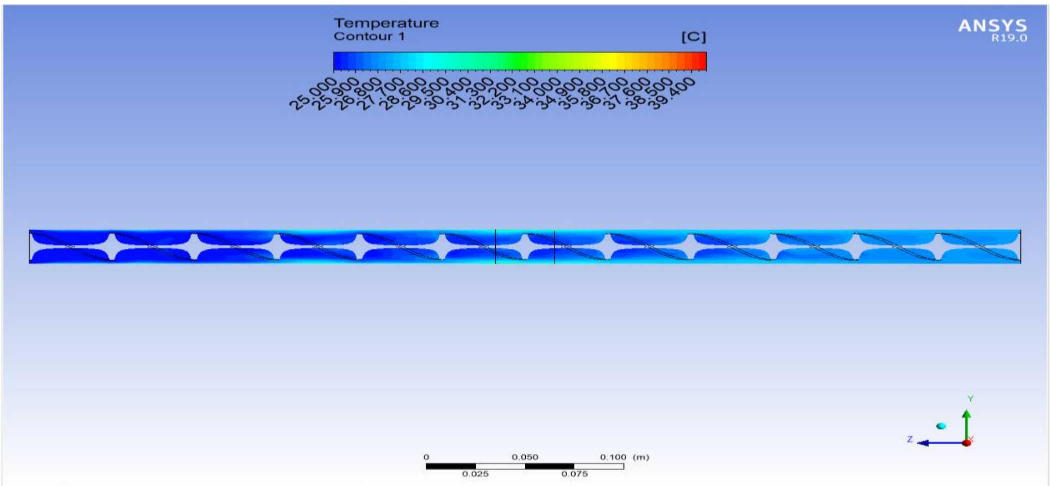

Figure 4.25: Effect Of Cycles Of Rotation On Temperature Of Fluid At 6 Cycles, 0.5 Wt% Concentration Of Ferro-Nanofluid, And 6 Tesla Intensity Of Magnetic Field With 30 Width Of Magnetic Field.

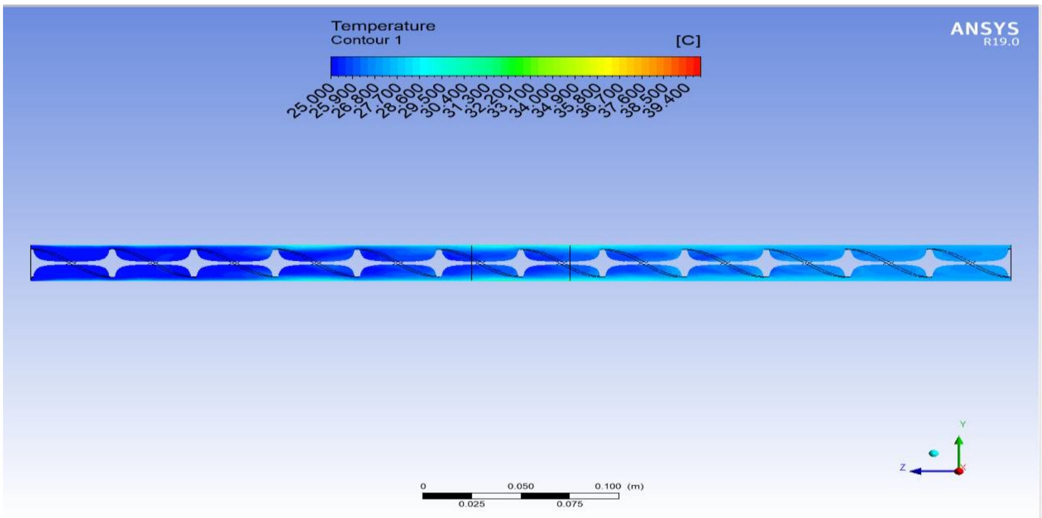

Figure 4.26: Effect Of Cycles Of Rotation On Temperature Of Fluid At 6 Cycles, 0.5 Wt% Concentration Of Ferro-Nanofluid, And 6 Tesla Intensity Of Magnetic Field With 50 Width Of Magnetic Field.

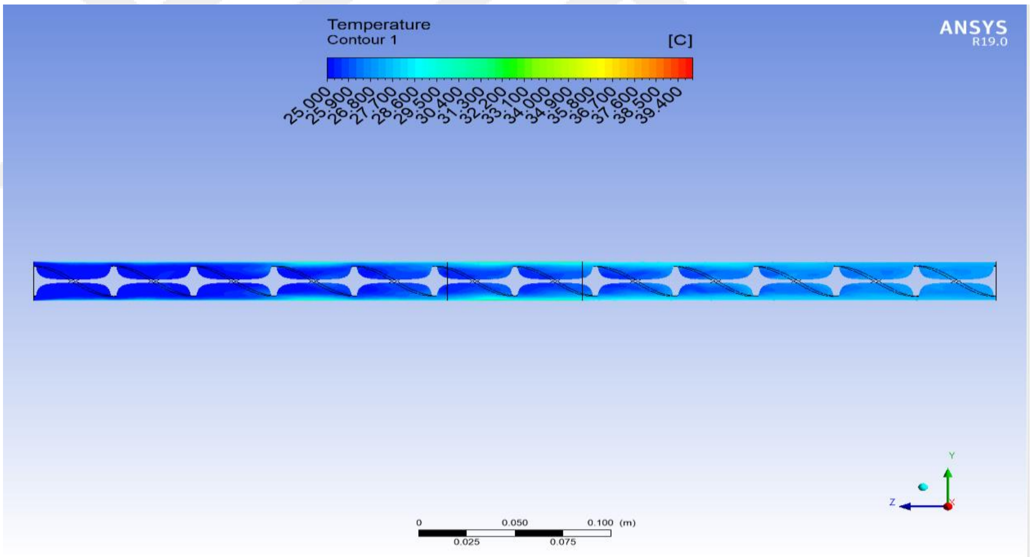

Figure 4.27: Effect Of Cycles Of Rotation On Temperature Of Fluid At 6 Cycles, 0.5 Wt% Concentration Of Ferro-Nanofluid, And 6 Tesla Intensity Of Magnetic Field With 70 Width Of Magnetic Field.

The fluid velocity isn't affected by an increase in width of magnetic field, it recorded the same rising from 0 to 0.749 m/s at 30, 50, and 70 width of magnetic field respectively, and the other operating conditions are 6 Tesla intensity of magnetic field, 0.5 wt% concentration of ferro-nanofluid, and 6 cycles of rotation. See Figures (4.28 to 4.30).

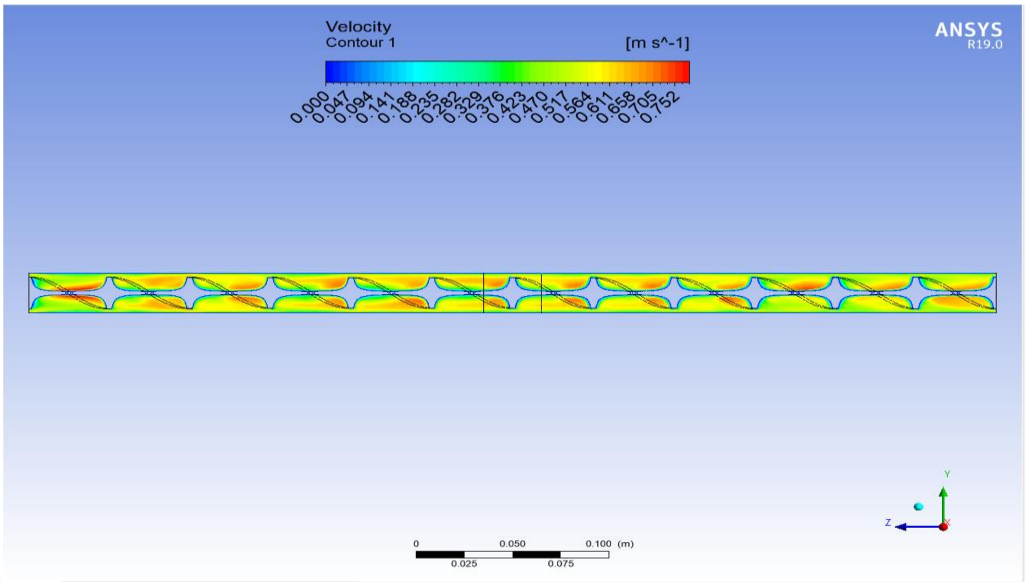

Figure 4.28: Effect Of Cycles Of Rotation On Velocity Of Fluid At 6 Cycles, 0.5 Wt% Concentration Of Ferro-Nanofluid, And 6 Tesla Intensity Of Magnetic Field With 30 Width Of Magnetic Field.

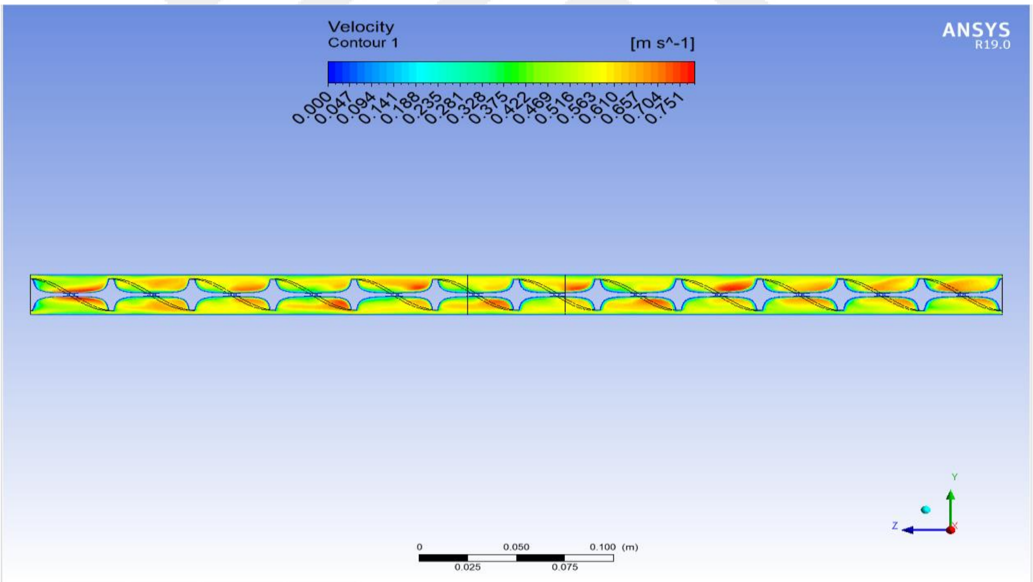

Figure 4.29: Effect Of Cycles Of Rotation On Velocity Of Fluid At 6 Cycles, 0.5 Wt% Concentration Of Ferro-Nanofluid, And 6 Tesla Intensity Of Magnetic Field With 50 Width Of Magnetic Field.

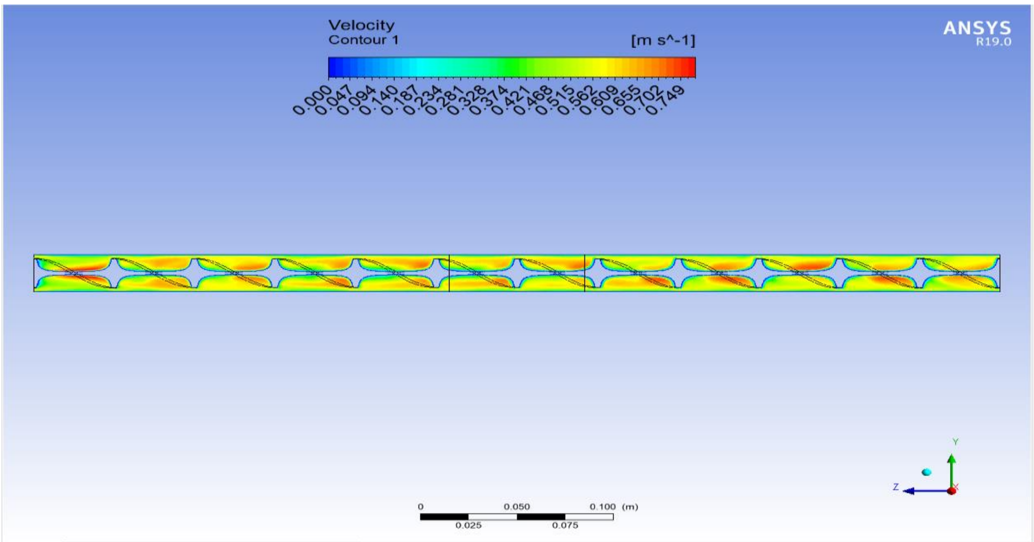

Figure 4.30: Effect Of Cycles Of Rotation On Velocity Of Fluid At 6 Cycles, 0.5 Wt% Concentration Of Ferro-Nanofluid, And 6 Tesla Intensity Of Magnetic Field With 70 Width Of Magnetic Field.

The twisted tape inserts act as passive turbulence promoters in an effort to increase heat transfer rates. The inclusion of these inserts causes the flow to experience the following benefits: I higher local velocities due to the reduced flow area, which is accompanied by secondary flow recirculation; (ii) improved mixing and turbulence by the helically twisted fluid flow; and (iii) improved heat transfer in the flow because the inserts act as fins. The heat transfer rate rises as a result of these interrelated factors. The implants' only real drawback is the little increase in pumping force needed to compensate for the pressure decrease they create. Additionally, it can be seen that the magnetic field has very little influence on the pressure drop. When an external force is present, pressure drops rise. The fundamental reason viscosity increases in the presence of an external magnetic field is pressure decrease. Additionally, the development of vortices that serve as barriers in the flow field may also be a factor in the second explanation for the rise in pressure drop. When a magnetic dipole source is used to create the magnetic field, this is what happens. The recent findings, however, were based on the supposition that viscosity is solely a product of temperature and concentration. Additionally, the heated ferrofluid tends to be removed off the surface by the upward magnetic force without the development of a vortex. Therefore, there has not been a significant change in the pressure decrease as a result of the magnetic field.

4.2.2 Effect of Concentration of Ferro-nanofluid

Concentration of ferro-nanofluid is one of the most important parameters which has effect on the pressure, temperature, and velocity of fluid. Figures (4.31 to 4.33) show the effect of concentration on pressure of fluid. As mentioned in the previous sections, pressure of fluid decrease from 38.276 to -0.629 Pa, 36.647 to -0.645 Pa, and 37.219 to -0.43 Pa for 30, 50, and 70 width of magnetic field respectively with 4cycles of rotation, 4 Tesla intensity of magnetic field, and 0.1 wt% concentration of ferro-nanofluid.

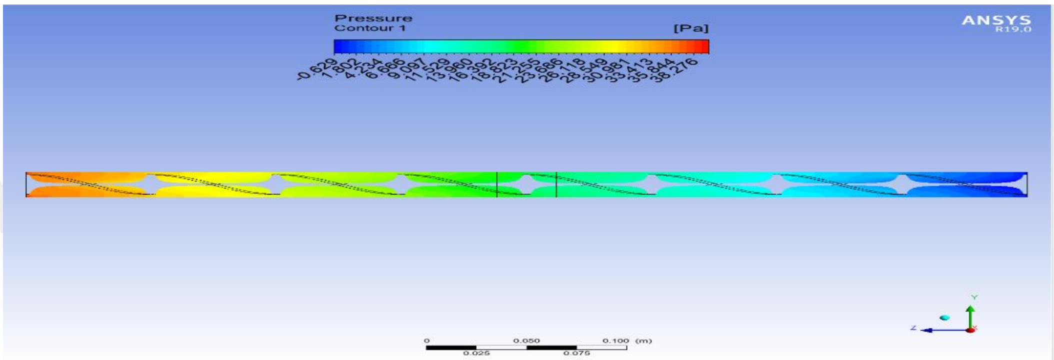

Figure 4.31: Effect Of Concentration Of Ferro-Nanofluid On Pressure Of Fluid At 4 Cycles, 0.1 Wt% Concentration Of Ferro-Nanofluid, And 4 Tesla Intensity Of Magnetic Field With 30 Width Of Magnetic Field.

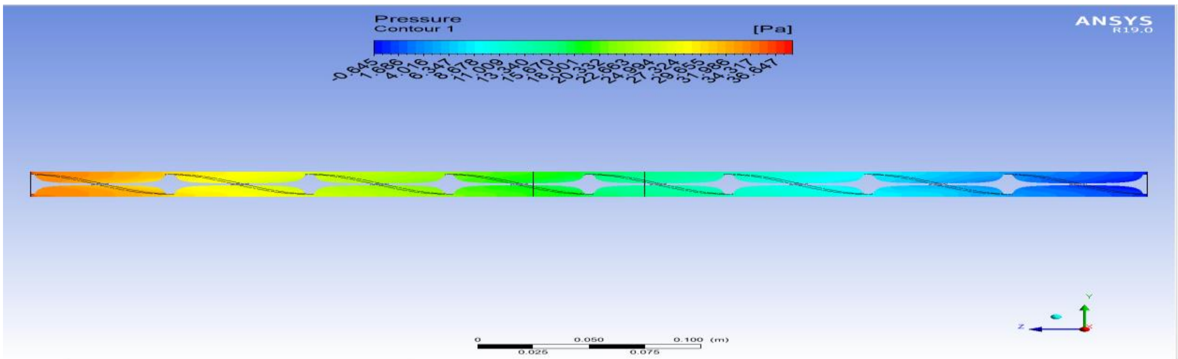

Figure 4.32: Effect Of Concentration Of Ferro-Nanofluid On Pressure Of Fluid At 4 Cycles, 0.1 Wt% Concentration Of Ferro-Nanofluid, And 4 Tesla Intensity Of Magnetic Field With 50 Width Of Magnetic Field.

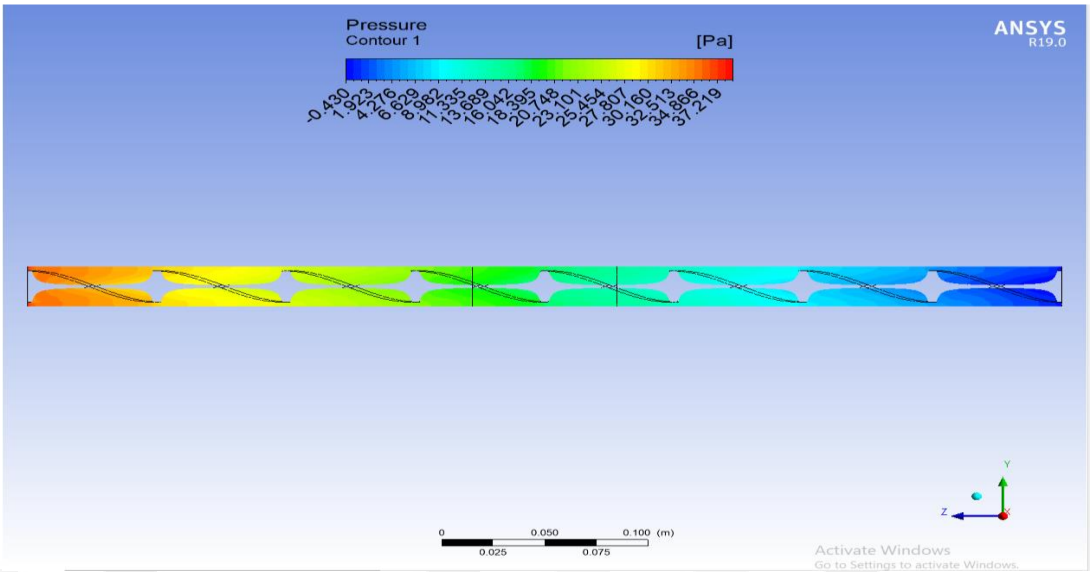

Figure 4.33: Effect Of Concentration Of Ferro-Nanofluid On Pressure Of Fluid At 4 Cycles, 0.1 Wt% Concentration Of Ferro-Nanofluid, And 4 Tesla Intensity Of Magnetic Field With 70 Width Of Magnetic Field.

Temperature of fluid rise at the similar level from 25 to 39. 4 ºC with 30, 50, and 70 width of magnetic field at 0.1 wt% concentration of ferro-nanofluid , 4 cycles of rotation, and 4 Tesla intensity of magnetic field as shown in Figures (4.34 to 4.36).

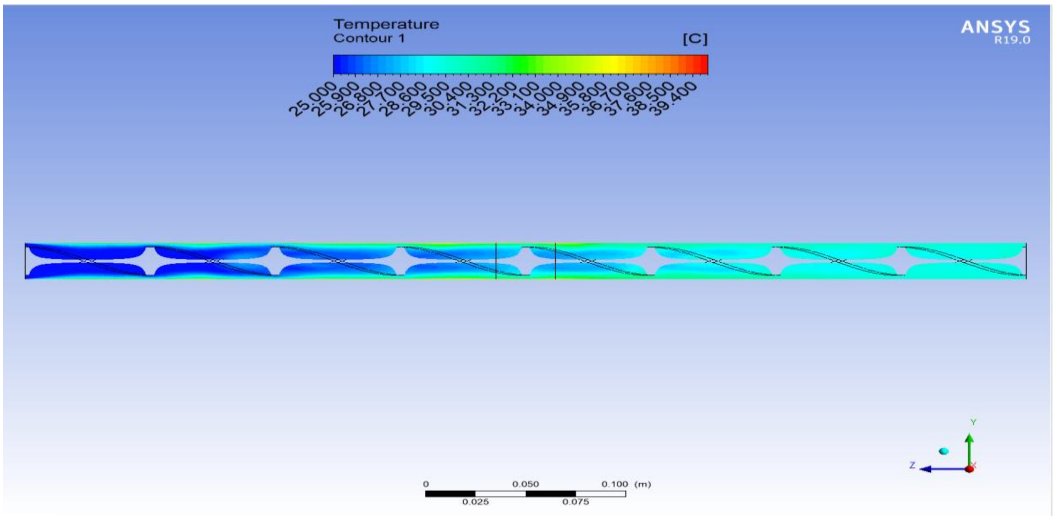

Figure 4.34: Effect Of Concentration Of Ferro-Nanofluid On Temperature Of Fluid At 4 Cycles, 0.1 Wt% Concentration Of Ferro-Nanofluid, And 4 Tesla Intensity Of Magnetic Field With 30 Width Of Magnetic Field.

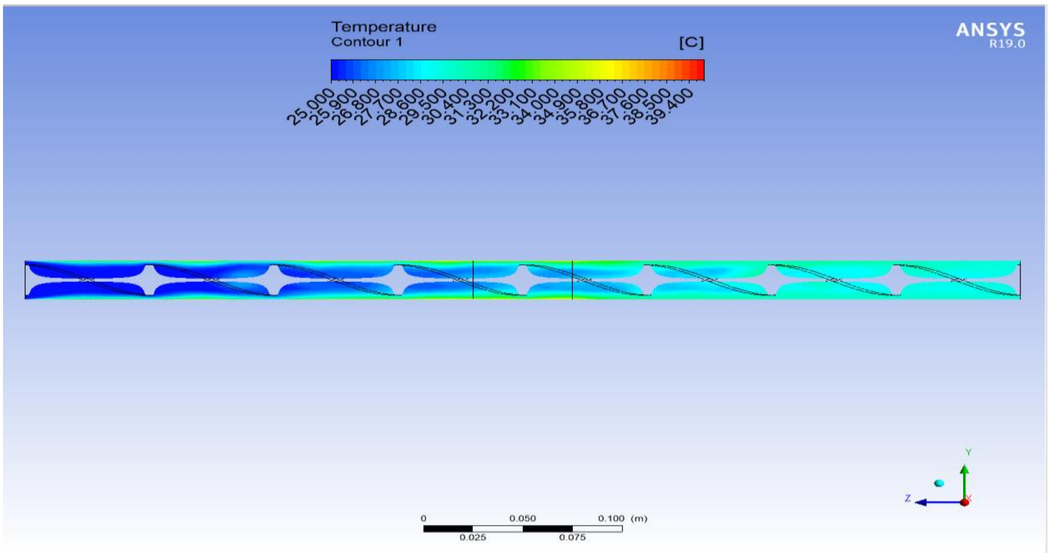

Figure 4.35: Effect Of Concentration Of Ferro-Nanofluid On Temperature Of Fluid At 4 Cycles, 0.1 Wt% Concentration Of Ferro-Nanofluid, And 4 Tesla Intensity Of Magnetic Field With 50 Width Of Magnetic Field.

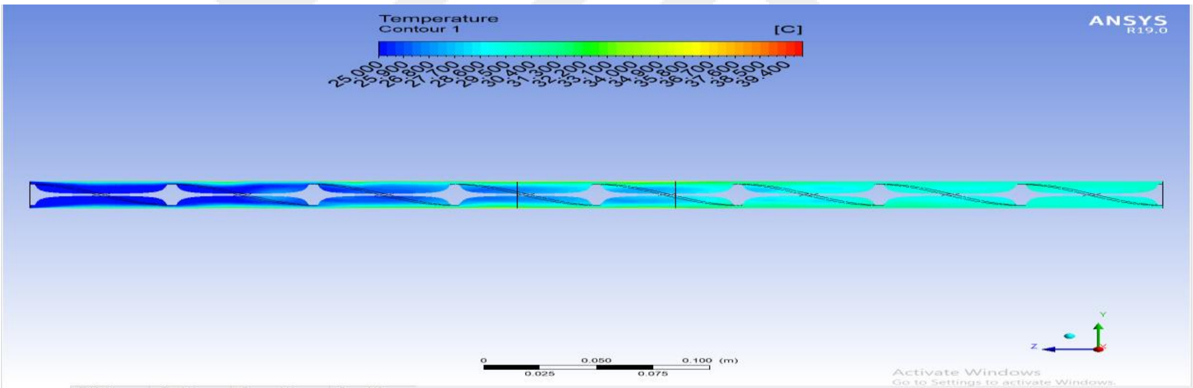

Figure 4.36: Effect Of Concentration Of Ferro-Nanofluid On Temperature Of Fluid At 4 Cycles, 0.1 Wt% Concentration Of Ferro-Nanofluid, And 4 Tesla Intensity Of Magnetic Field With 70 Width Of Magnetic Field.

While the velocity of fluid increase from 0.009 to 0.146 m/s, from 0.01 to 0.155 m/s, and from 0.01 to 0.164 m/s at 30, 50, and 70 width of magnetic field respectively, with 0.1 wt% concentration of ferro-nanofluid , 4 cycles of rotation, and 4 Tesla intensity of magnetic field. See Figures (4.37 to 4.39).

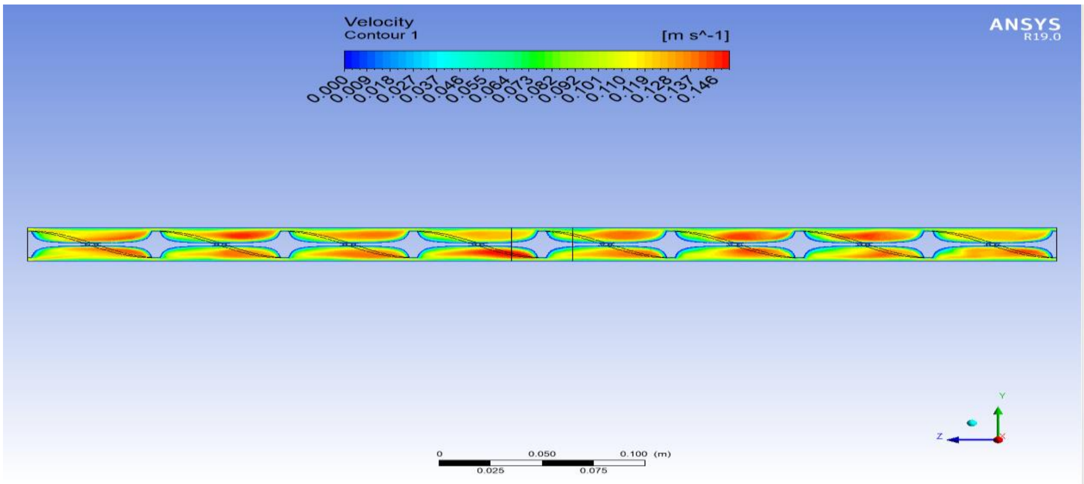

Figure 4.37: Effect Of Concentration Of Ferro-Nanofluid On Velocity Of Fluid At 4 Cycles, 0.1 Wt% Concentration Of Ferro-Nanofluid, And 4 Tesla Intensity Of Magnetic Field With 30 Width Of Magnetic Field.

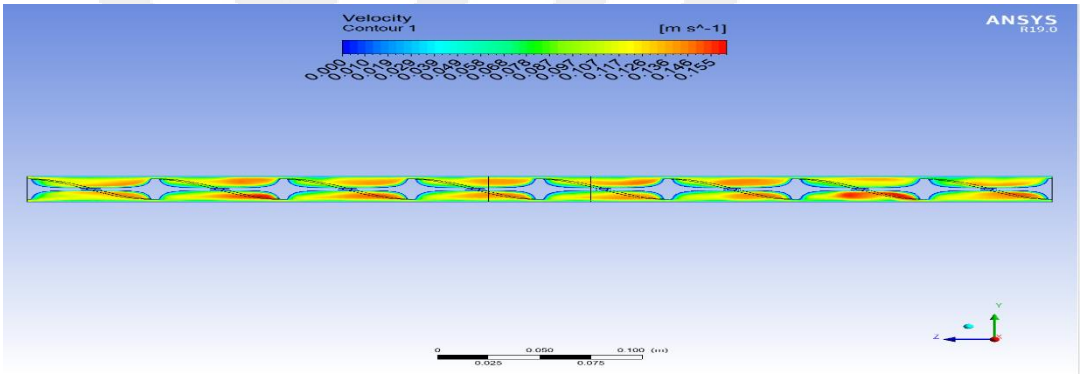

Figure 4.38: Effect Of Concentration Of Ferro-Nanofluid On Velocity Of Fluid At 4 Cycles, 0.1 Wt% Concentration Of Ferro-Nanofluid, And 4 Tesla Intensity Of Magnetic Field With 50 Width Of Magnetic Field.

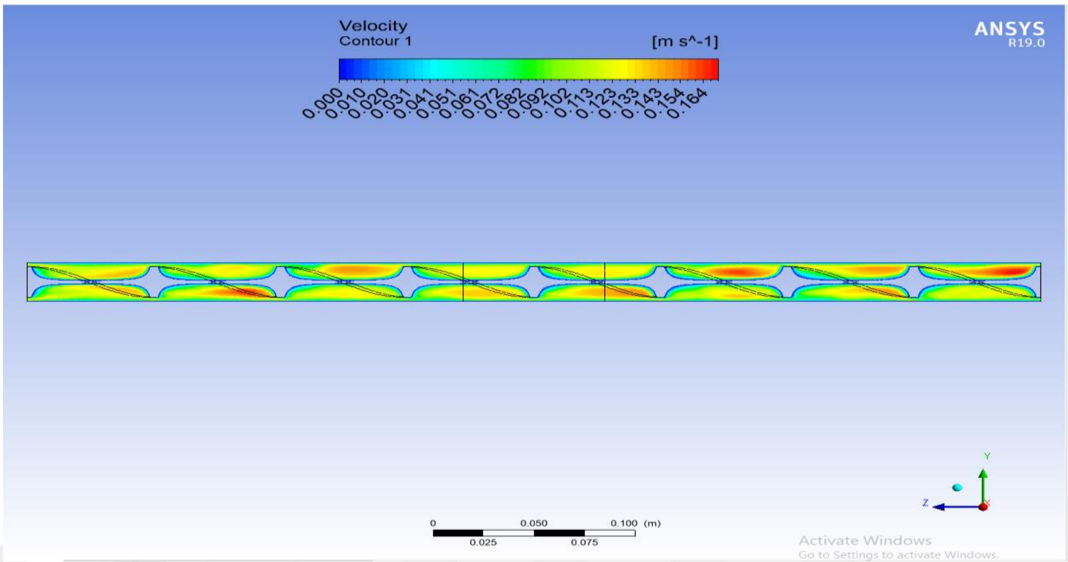

Figure 4.39: Effect Of Concentration Of Ferro-Nanofluid On Velocity Of Fluid At 4 Cycles, 0.1 Wt% Concentration Of Ferro-Nanofluid, And 4 Tesla Intensity Of Magnetic Field With 70 Width Of Magnetic Field.

The pressure drop reach to 37.5, 36.6, and 37.8 Pa at intensity of magnetic field 2, 4, and 6 Tesla, and 4 cycles of rotation respectively, with 50 mm thickness of magnetic, and 0.1 m/s. Figures (4-40 to 4.42) show the behavior of pressure drop.

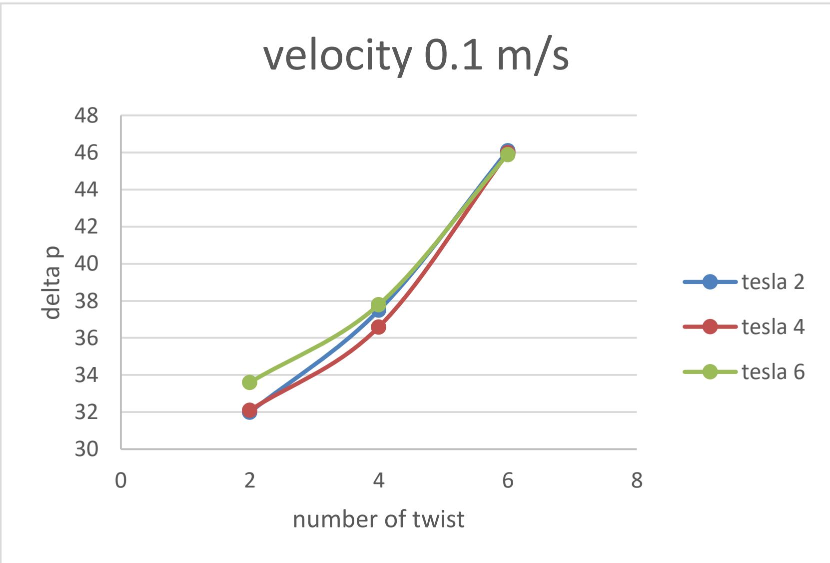

Figure 4.40: Effect Of Cycles Of Rotation And Intensity Of Magnetic Field On Pressure Drop At Velocity 0.1 M/S And Thickness Of Magnetic 50 Mm.

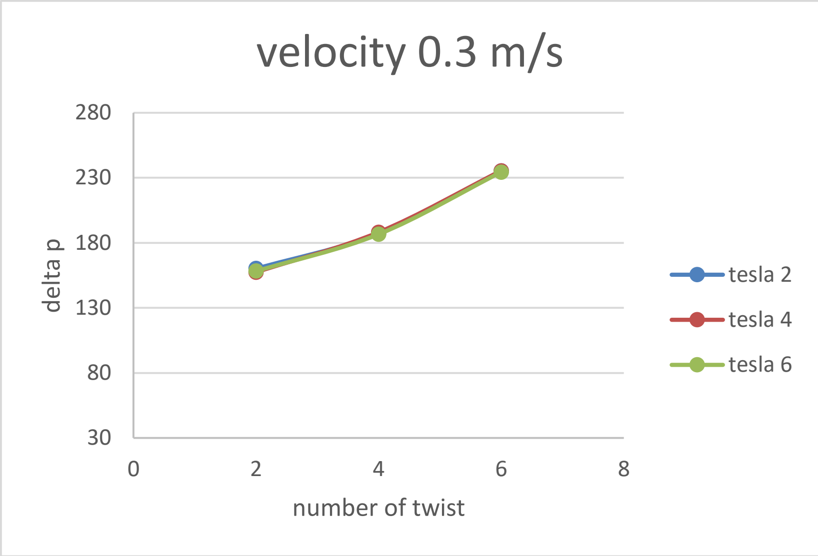

Figure 4.41: Effect Of Cycles Of Rotation And Intensity Of Magnetic Field On Pressure Drop At Velocity 0.3 M/S And Thickness Of Magnetic 50 Mm.

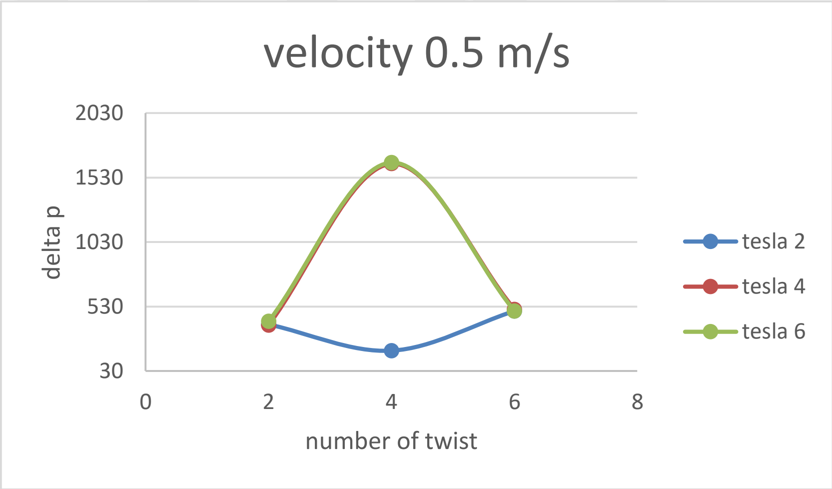

Figure 4.42: Effect Of Cycles Of Rotation And Intensity Of Magnetic Field On Pressure Drop At Velocity 0.5 M/S And Thickness Of Magnetic 50 Mm.

Now, the concentration of ferro-nanofluid is 0.3 wt%, the pressure of fluid tends to decrease at 4 Tesla intensity of magnetic field, and 4 cycles of rotation. Pressure dropped from 191.513 to -15.404 Pa, from 188.065 to -13.078 Pa, and from 179.652 to -10.979 Pa, at 30, 50, and 70 width of magnetic field respectively, as displayed in Figures below.

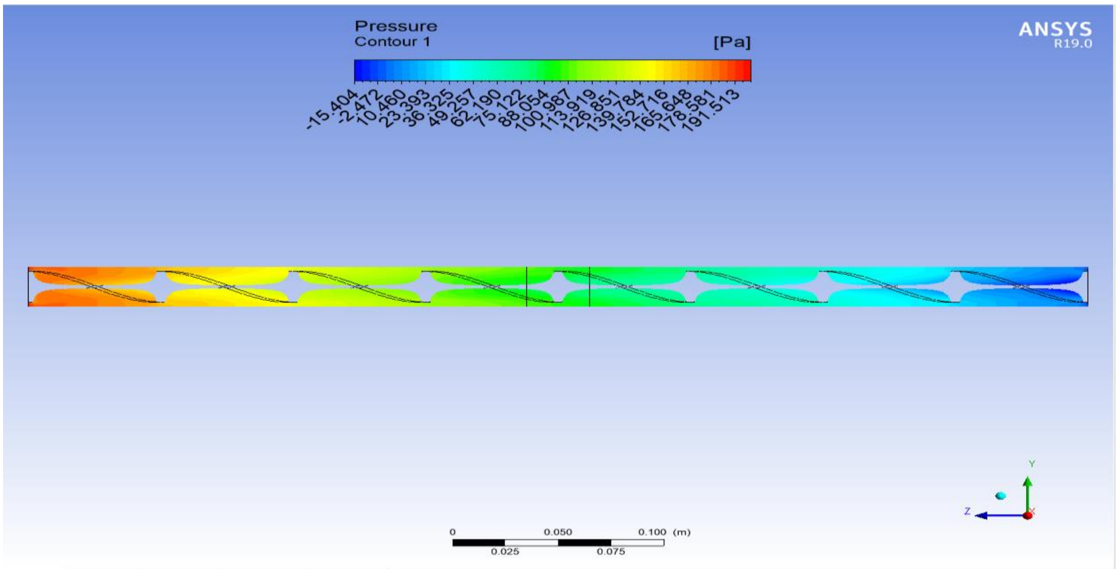

Figure 4.43: Effect Of Concentration Of Ferro-Nanofluid On Pressure Of Fluid At 4 Cycles, 0.3 Wt% Concentration Of Ferro-Nanofluid, And 4 Tesla Intensity Of Magnetic Field With 30 Width Of Magnetic Field.

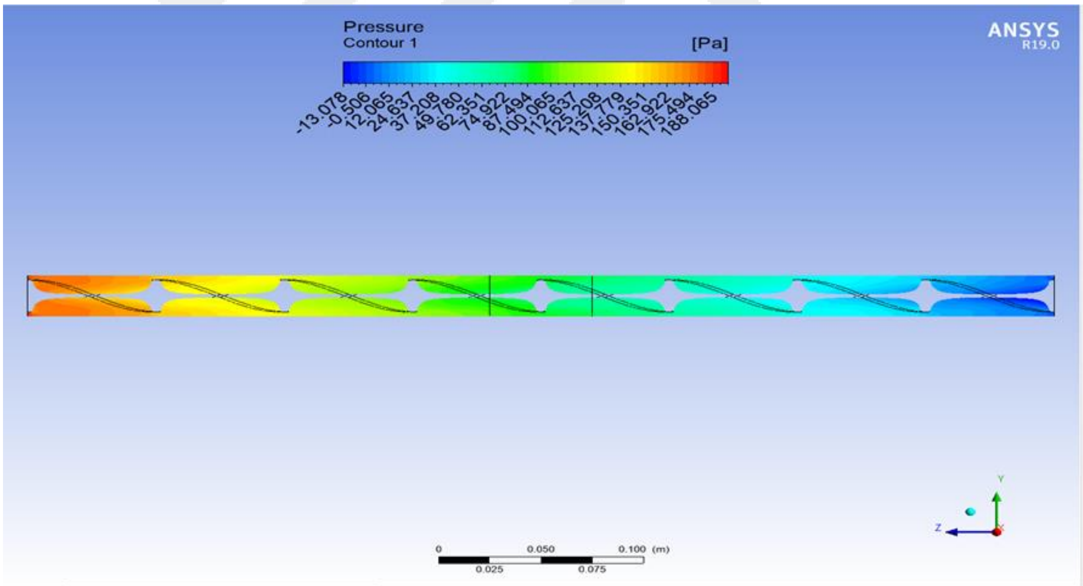

Figure 4.44: Effect Of Concentration Of Ferro-Nanofluid On Pressure Of Fluid At 4 Cycles, 0.3 Wt% Concentration Of Ferro-Nanofluid, And 4 Tesla Intensity Of Magnetic Field With 50 Width Of Magnetic Field.

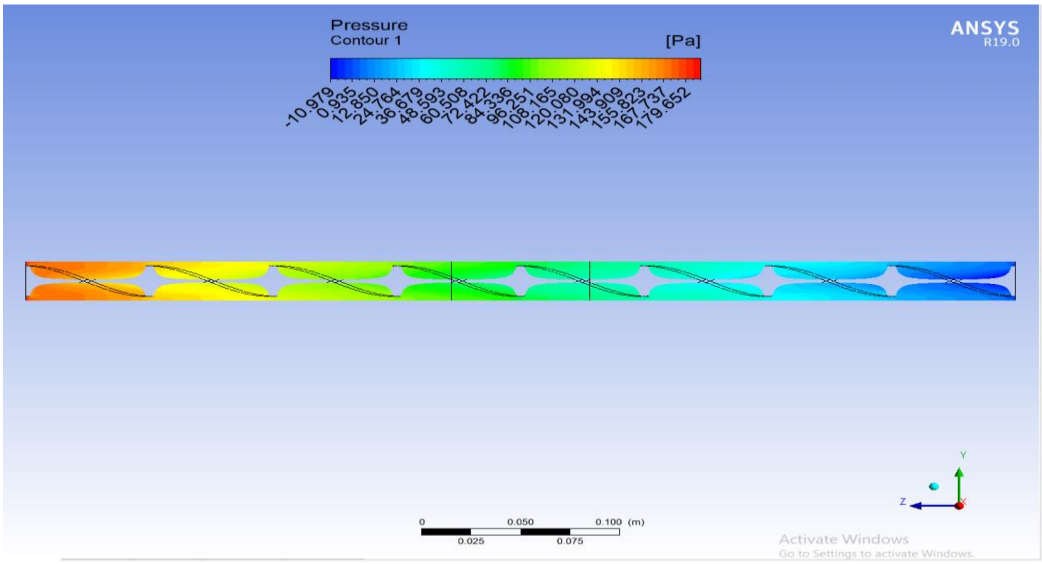

Figure 4.45: Effect Of Concentration Of Ferro-Nanofluid On Pressure Of Fluid At 4 Cycles, 0.3 Wt% Concentration Of Ferro-Nanofluid, And 4 Tesla Intensity Of Magnetic Field With 70 Width Of Magnetic Field.

Temperature of fluid behaves the same as when the concentration of ferro-nanofluid is 1 wt%. It can be notice rising in temperature from 25 to 39.4 °C at 4 cycles of rotation, 4 Tesla intensity of magnetic field, and 0.3 wt% concentration of ferro-nanofluid with 30, 50, and 70 width of magnetic field.

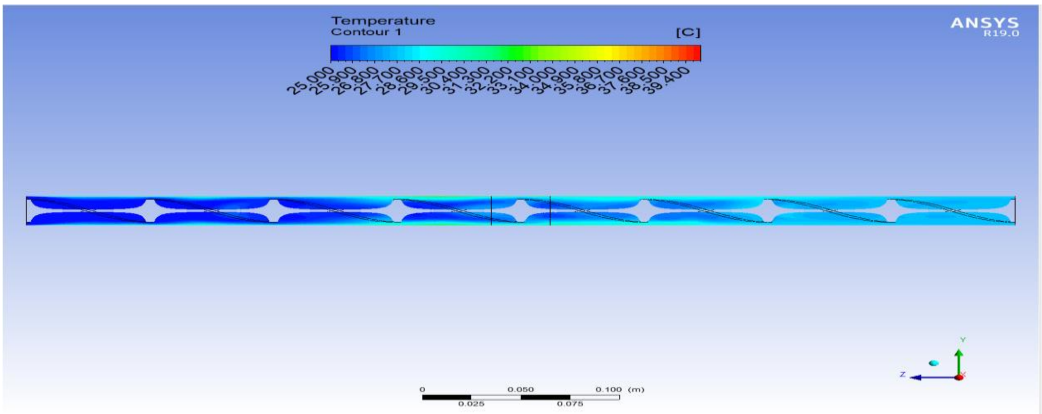

Figure 4.46: Effect Of Concentration Of Ferro-Nanofluid On Temperature Of Fluid At 4 Cycles, 0.3 Wt% Concentration Of Ferro-Nanofluid, And 4 Tesla Intensity Of Magnetic Field With 30 Width Of Magnetic Field.

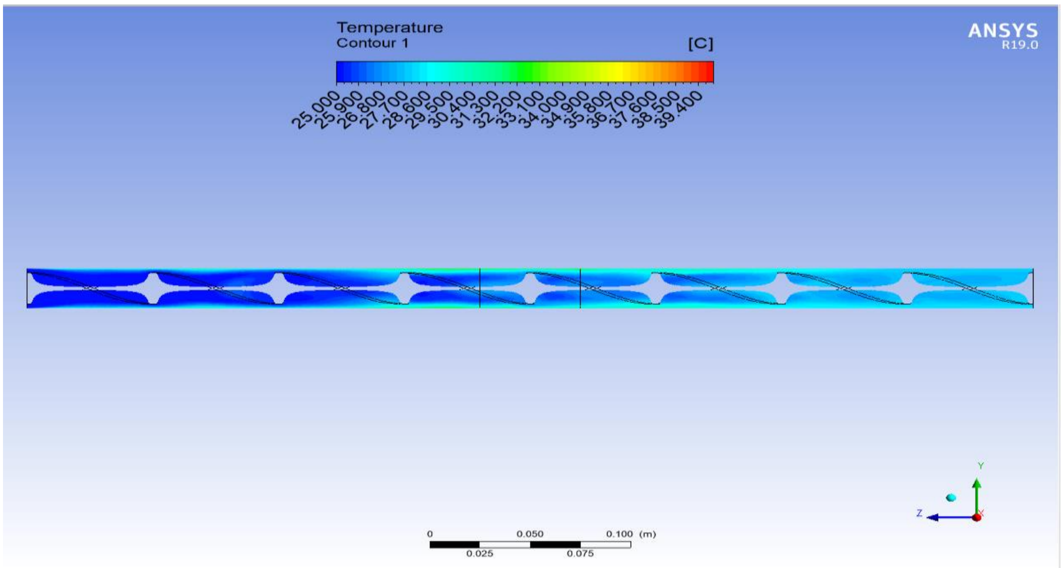

Figure 4.47: Effect Of Concentration Of Ferro-Nanofluid On Temperature Of Fluid At 4 Cycles, 0.3 Wt% Concentration Of Ferro-Nanofluid, And 4 Tesla Intensity Of Magnetic Field With 50 Width Of Magnetic Field.

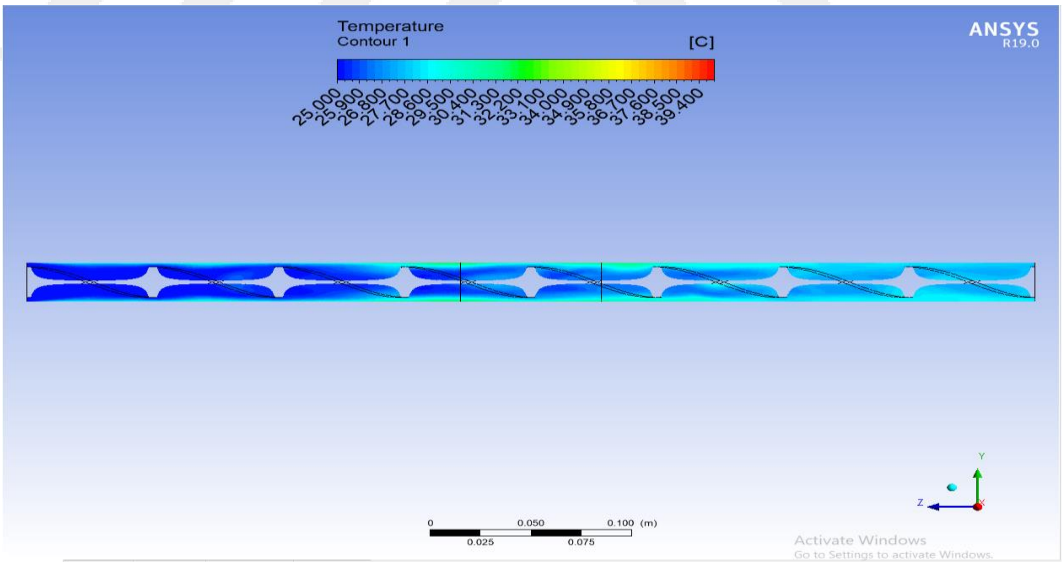

Figure 4.48: Effect Of Concentration Of Ferro-Nanofluid On Temperature Of Fluid At 4 Cycles, 0.3 Wt% Concentration Of Ferro-Nanofluid, And 4 Tesla Intensity Of Magnetic Field With 70 Width Of Magnetic Field.

Likewise temperature, velocity of fluid grows at constant level whether at 30 or 50 or 70 width of field. Velocity of fluid increase from 0.027 to 0.435 m/s with 0.3 wt% concentration of ferro-nanofluid, 4 cycles of rotation, 4 Tesla intensity of magnetic field as presented in Figures (4.49 to 4.51).

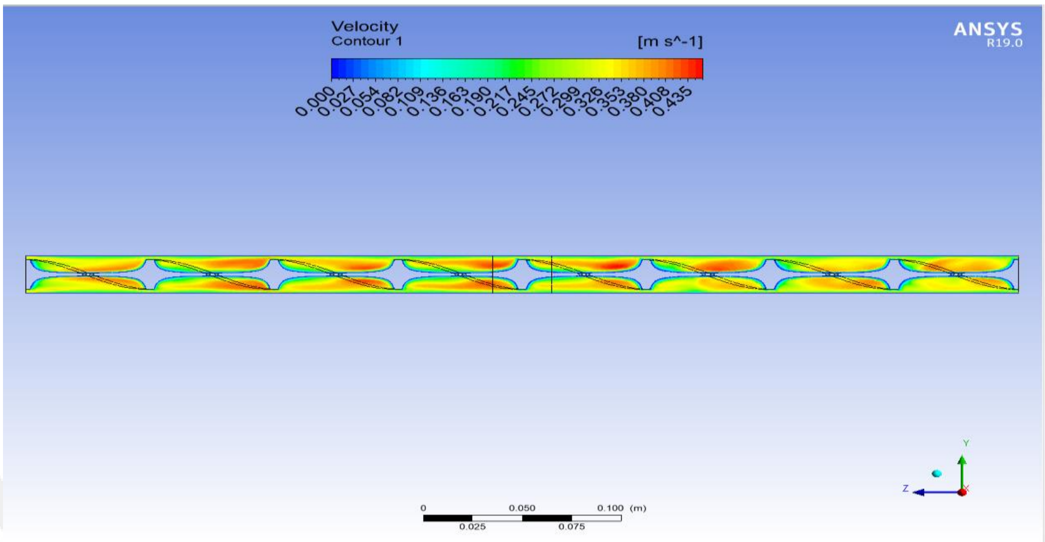

Figure 4.49: Effect Of Concentration Of Ferro-Nanofluid On Velocity Of Fluid At 4 Cycles, 0.3 Wt% Concentration Of Ferro-Nanofluid, And 4 Tesla Intensity Of Magnetic Field With 30 Width Of Magnetic Field.

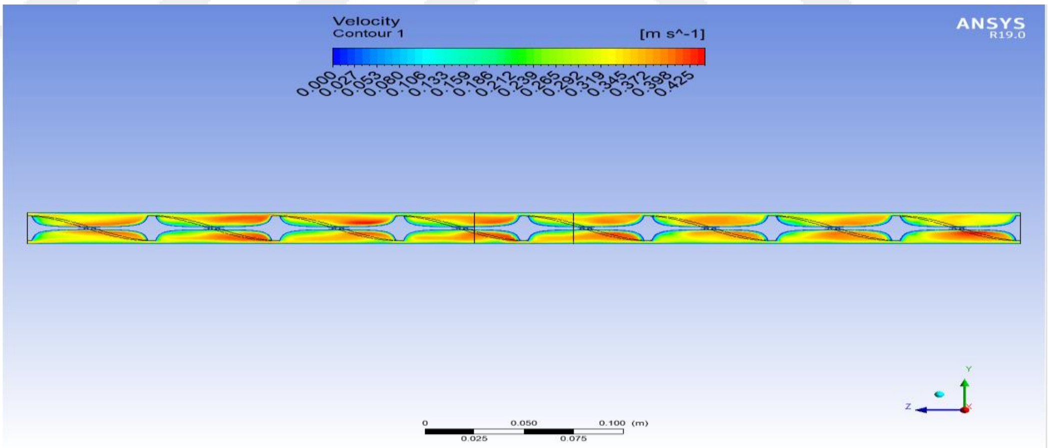

Figure 4.50: Effect Of Concentration Of Ferro-Nanofluid On Velocity Of Fluid At 4 Cycles, 0.3 Wt% Concentration Of Ferro-Nanofluid, And 4 Tesla Intensity Of Magnetic Field With 50 Width Of Magnetic Field.

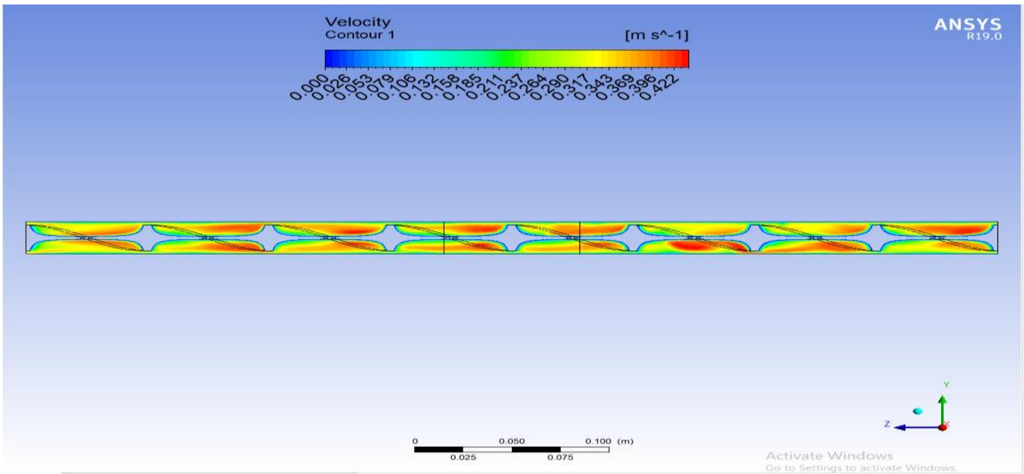

Figure 4.51: Effect Of Concentration Of Ferro-Nanofluid On Velocity Of Fluid At 4 Cycles, 0.3 Wt% Concentration Of Ferro-Nanofluid, And 4 Tesla Intensity Of Magnetic Field With 70 Width Of Magnetic Field.

0.5 wt% of concentration of ferro-nanofluid is the last value which has been taken to show the effect on pressure, temperature, and velocity of fluid. The pressure reduce from 378.909 to -40.412 pa with 30 width of magnetic field, while at 50 with of magnetic field, the pressure suffer extraordinary dropping from 1638.172 to -86.292 pa. at last, pressure continue to decrease from 372.834 to -38.361 pa at 0.5% concentration of ferro-nanofluid , 4 Tesla intensity of magnetic field, and 4 cycles of rotation. See Figures (4.52 to 4.54).

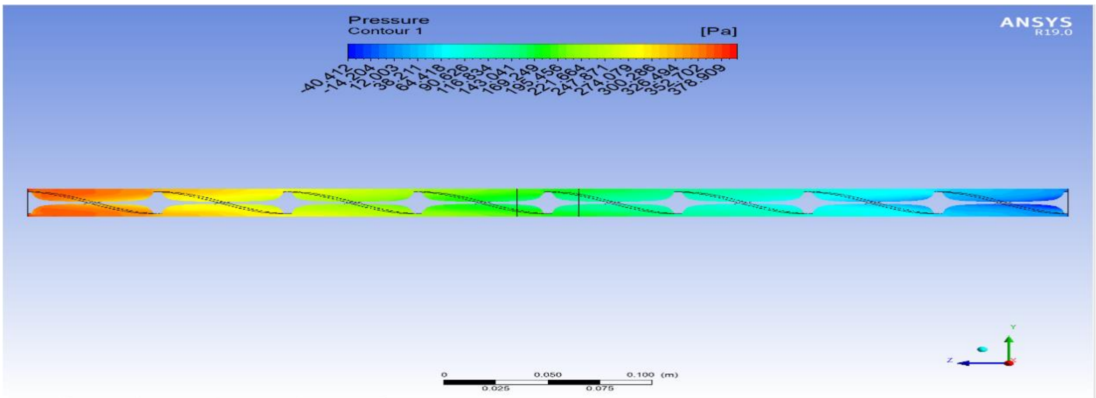

Figure 4.52: Effect Of Concentration Of Ferro-Nanofluid On Pressure Of Fluid At 4 Cycles, 0.5 Wt% Concentration Of Ferro-Nanofluid, And 4 Tesla Intensity Of Magnetic Field With 30 Width Of Magnetic Field.

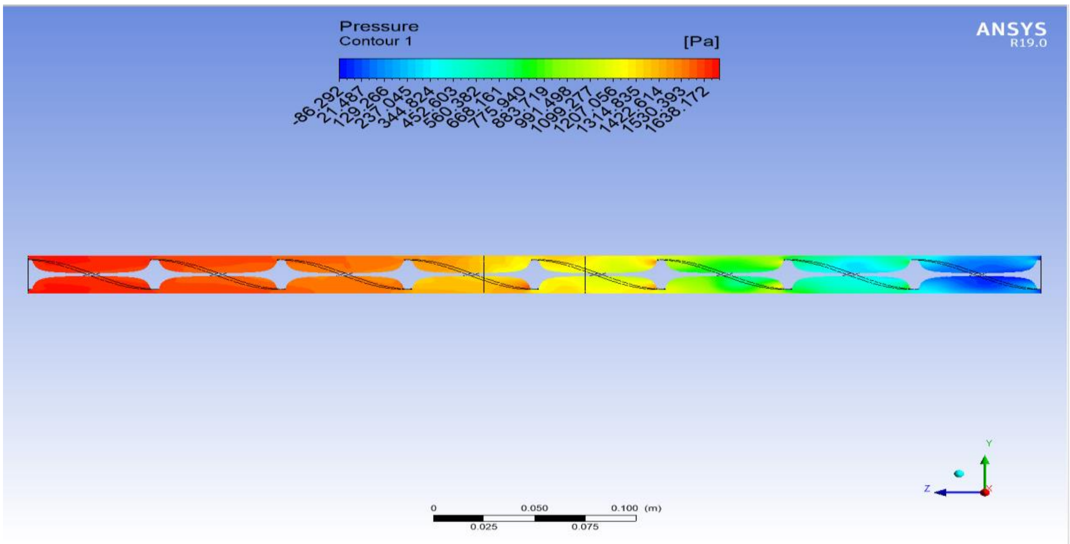

Figure 4.53: Effect Of Concentration Of Ferro-Nanofluid On Pressure Of Fluid At 4 Cycles, 0.5 Wt% Concentration Of Ferro-Nanofluid, And 4 Tesla Intensity Of Magnetic Field With 50 Width Of Magnetic Field.

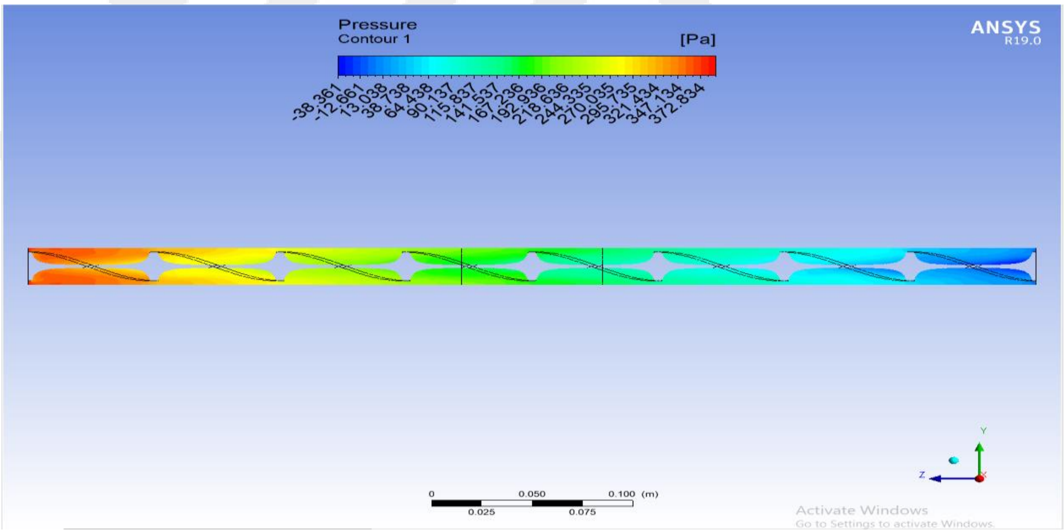

Figure 4.54: Effect Of Concentration Of Ferro-Nanofluid On Pressure Of Fluid At 4 Cycles, 0.5 Wt% Concentration Of Ferro-Nanofluid, And 4 Tesla Intensity Of Magnetic Field With 70 Width Of Magnetic Field.

as previously mentioned, temperature of fluid increased from 25 to 39.4 C with 30, 50, and 70 width of magnetic field at 0.5 wt% of concentration of ferro-nanofluid , 4 cycles of rotation, and 4 Tesla intensity of magnetic field as shown in Figures (4.55 to 4.57).

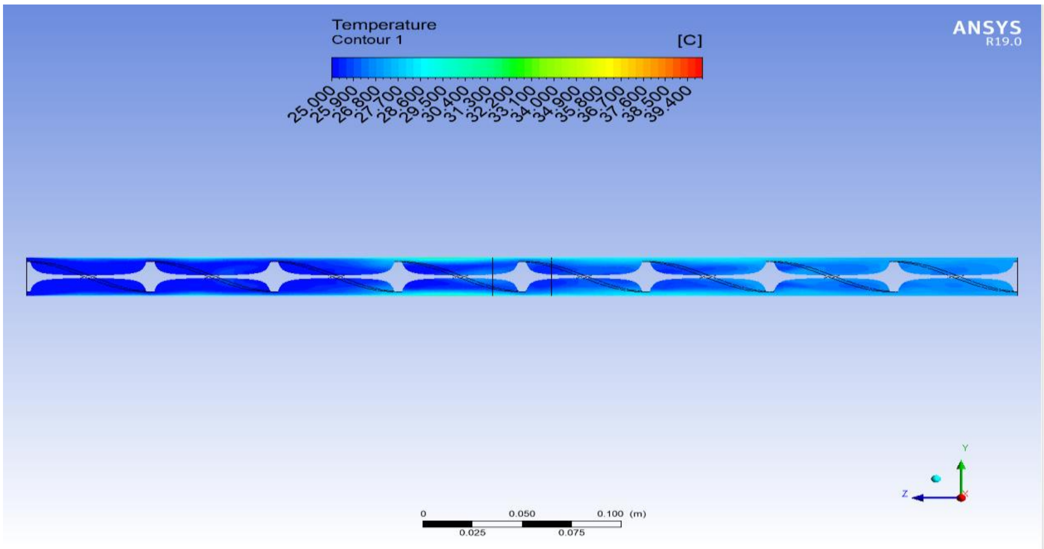

Figure 4.55: Effect Of Concentration Of Ferro-Nanofluid On Temperature Of Fluid At 4 Cycles Of Rotation, 0.5 Wt% Concentration Of Ferro-Nanofluid, And 4 Tesla Intensity Of Magnetic Field With 30 Width Of Magnetic Field.

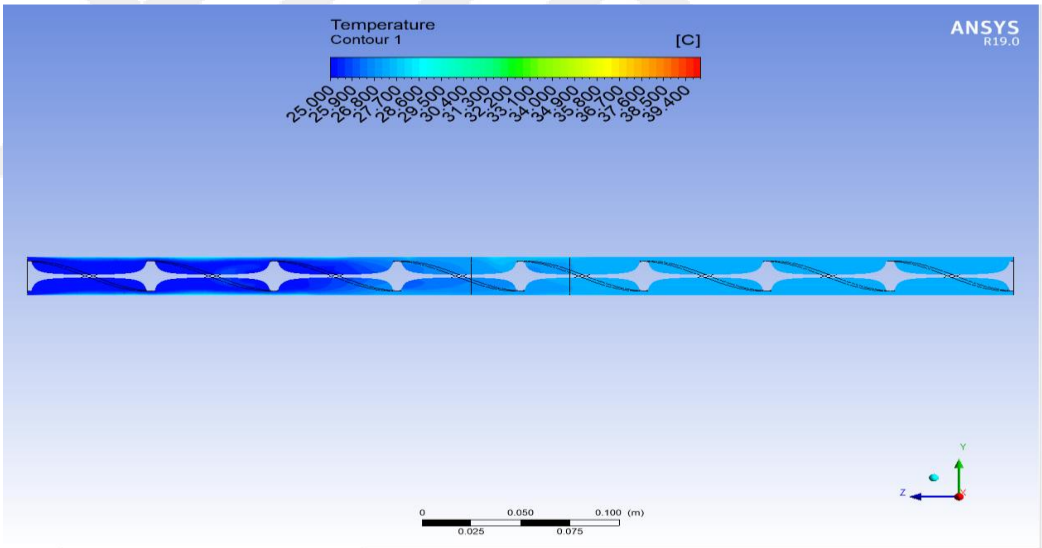

Figure 4.56: Effect Of Concentration Of Ferro-Nanofluid On Temperature Of Fluid At 4 Cycles Of Rotation, 0.5 Wt% Concentration Of Ferro-Nanofluid, And 4 Tesla Intensity Of Magnetic Field With 50 Width Of Magnetic Field.

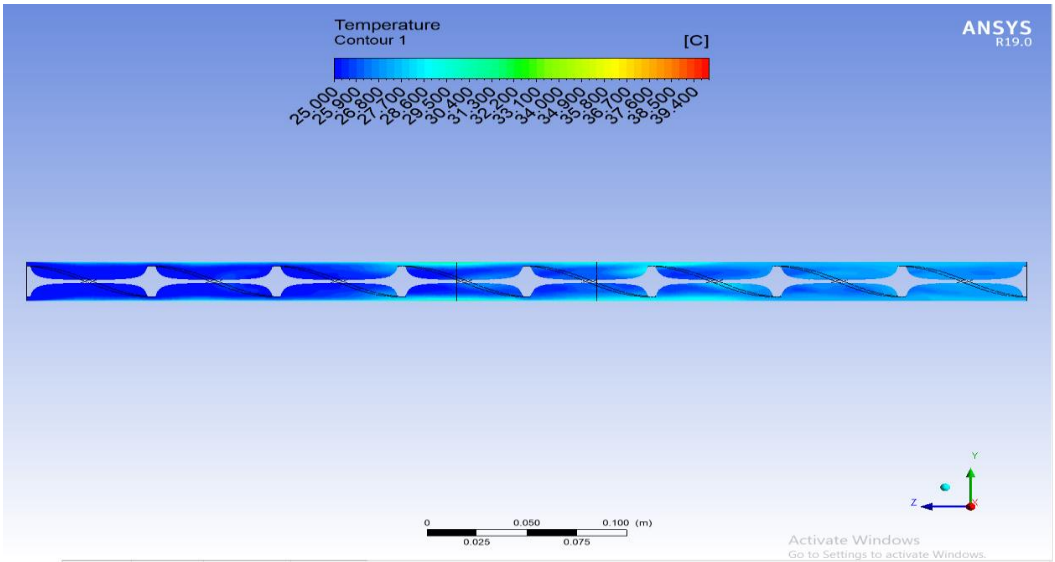

Figure 4.57: Effect Of Concentration Of Ferro-Nanofluid On Temperature Of Fluid At 4 Cycles Of Rotation, 0.5 Wt% Concentration Of Ferro-Nanofluid, And 4 Tesla Intensity Of Magnetic Field With 70 Width Of Magnetic Field.

The concentration of ferro-nanofluid has much effect on the velocity of fluid. It is rise from 0.064 to 1.027 m/s at 50 width of magnetic field, 4 cycles of rotation, 4 Tesla intensity of magnetic field. See figures (4.58 to 4.60).

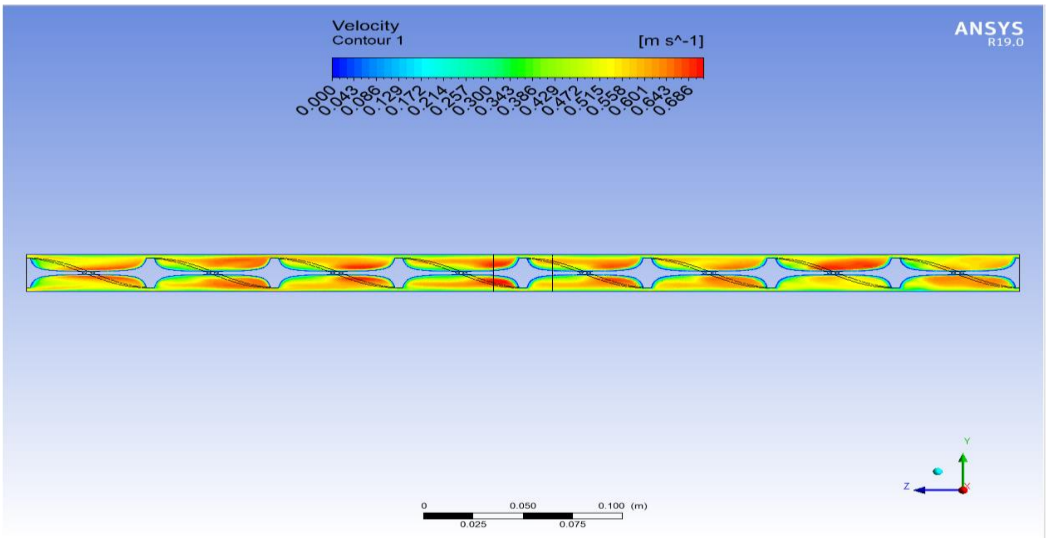

Figure 4.58: Effect Of Concentration Of Ferro-Nanofluid On Velocity Of Fluid At 4 Cycles Of Rotation, 0.5 Wt% Concentration Of Ferro-Nanofluid, And 4 Tesla Intensity Of Magnetic Field With 30 Width Of Magnetic Field.

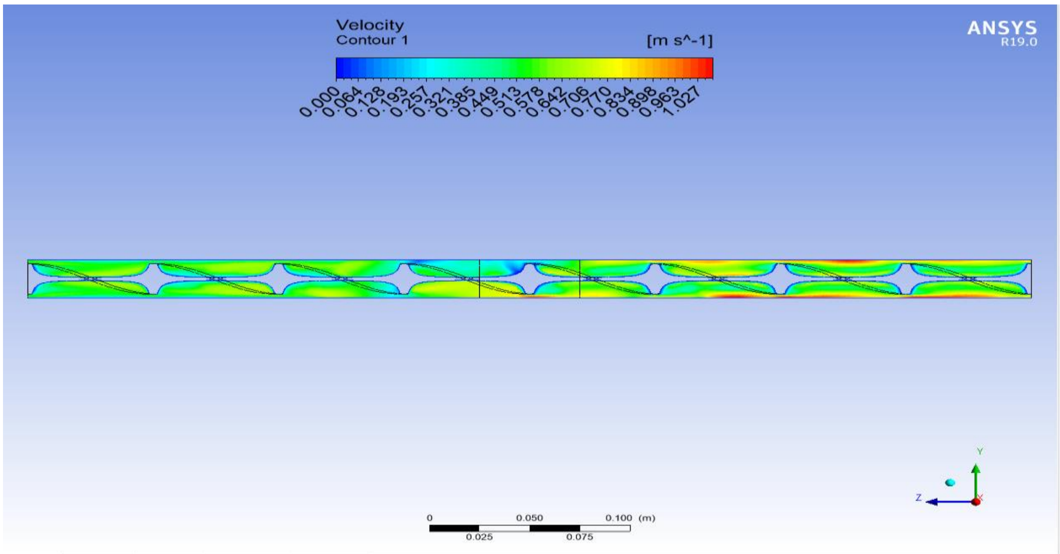

Figure 4.59: Effect Of Concentration Of Ferro-Nanofluid On Velocity Of Fluid At 4 Cycles Of Rotation, 0.5 Wt% Concentration Of Ferro-Nanofluid, And 4 Tesla Intensity Of Magnetic Field With 50 Width Of Magnetic Field.

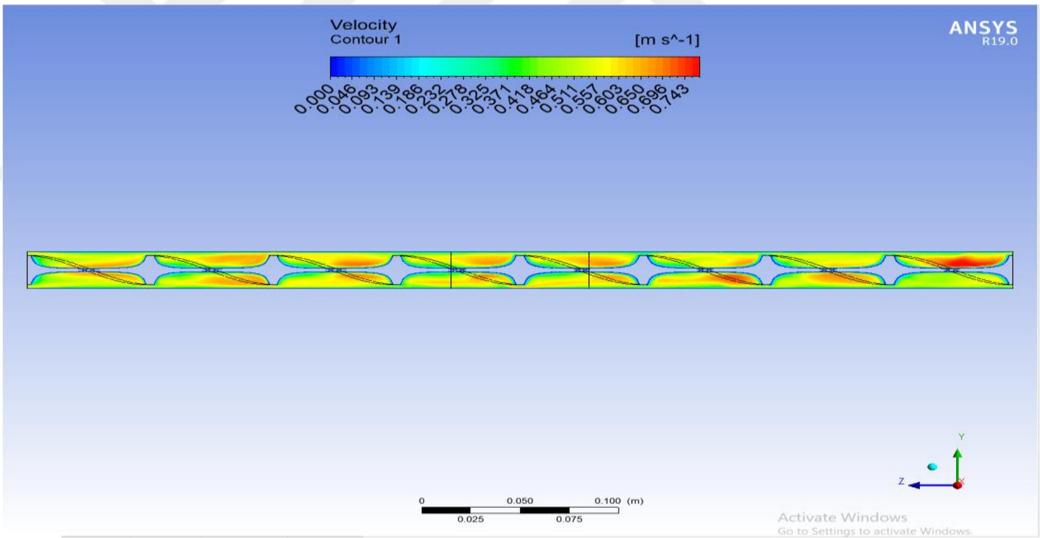

Figure 4.60: Effect Of Concentration Of Ferro-Nanofluid On Velocity Of Fluid At 4 Cycles Of Rotation, 0.5 Wt% Concentration Of Ferro-Nanofluid, And 4 Tesla Intensity Of Magnetic Field With 70 Width Of Magnetic Field.

The magnetic dipoles of the ferromagnetic particles are aligned with the magnetic field's lines and are magnetized particles. Due to the strong Kelvin force present, ferrofluid particles that are rotating close to the magnetic source deviate as a result. The magnetization of nanoparticles, which decreases at the bottom wall at high temperatures, can be used to explain this rotating action. Due to the thermomigration phenomena, the warm ferrofluid near the bottom wall travels to the colder areas where its magnetization rises. Therefore, the creation of the recirculation zone is caused by the non-uniformity of the magnetization of nanoparticles. This behaviour becomes more noticeable and the recirculation zone gets hotter as the magnetic field strength rises. The related temperature fields show the presence of a thermal boundary layer close to the heated wall, where parallel isotherms show that conduction heat transfer is the dominant mechanism of heat transfer. Applying and enhancing the magnetic field disturbs this property of the thermal layer. In fact, due to the movement of ferrofluid under the influence of the thermodiffusion phenomena, the isotherms become distorted in the recirculation zone and demonstrate the dominance of the convective heat transfer mode. By raising the magnetic number, the isotherms downstream of recirculation become narrower. This is because the heated wall was affected by the downward main flow distortion following recirculation. Due to this fact, the local heat transfer rate and temperature gradient both rise.

It is challenging to establish the changes in velocity together with the changes in nanoparticle concentration since the density and viscosity rise with increasing nanoparticle concentration. Numbers are used to study the connection between speed and nanoparticle concentration. Maxwell's theory states that as the Reynolds number (flow rate) and nanoparticle concentration increase, the pressure drop in the tube also rises, increasing energy consumption and decreasing experiment efficiency. Studying how the resistance coefficient varies with Reynolds number and nanoparticle mass percentage is essential. In fluid mechanics, the resistance coefficient is a dimensionless quantity. It is used to show that the resistance of nanofluids in a tube is mostly influenced by the shape of the tube (twisted tape) and the properties of the nanofluids. The resistance coefficients of nanofluids at various Reynolds numbers are shown in Figure. The 0%+rotating values coincide with the 0.5%+static values for laminar flow and the 0.3%+static values for turbulent flow. At laminar and turbulent flow, it is discovered that the resistance coefficient exhibits a decreasing tendency with the Reynolds number, which may be explained by the resistance coefficient. Resistance coefficient and Reynolds number have an inversely proportional connection. In addition, it can be seen that resistance coefficient increases with nanoparticle, which is due to the high viscosity caused by the increasing nanoparticle concentration.

4.2.3 Effect of Intensity of Magnetic Field

The factor of intensity of magnetic field has been investigated to explain the effect of magnetic field on pressure, temperature, and velocity of fluid. The pressure is going to drop at 2 Tesla intensity of magnetic field, 2 cycles of rotation, and 0.1 wt% concentration of ferro-nanofluid. Figures (4.61 to 4.63) show the pressure decrease from 35.044 to -0.094 Pa, 31.977 to -0.038 Pa, and 32.789 to -0.105 Pa at 30, 50, and 70 width of magnetic field respectively.

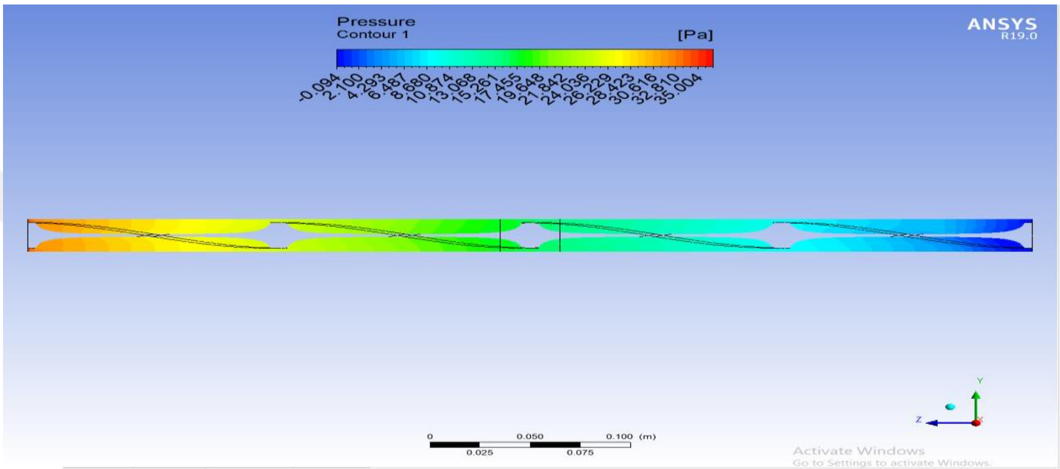

Figure 4.61: Effect Of Intensity Of Magnetic Field On Pressure Of Fluid At 2 Cycles Of Rotation, 0.1 Wt% Concentration Of Ferro-Nanofluid, And 2 Tesla Intensity Of Magnetic Field With 30 Width Of Magnetic Field.

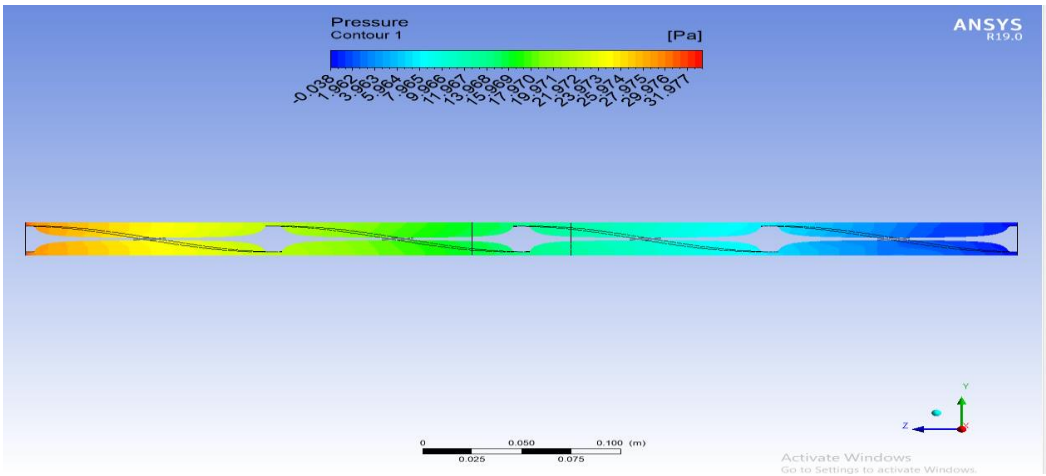

Figure 4.62: Effect Of Intensity Of Magnetic Field On Pressure Of Fluid At 2 Cycles Of Rotation, 0.1 Wt% Concentration Of Ferro-Nanofluid, And 2 Tesla Intensity Of Magnetic Field With 50 Width Of Magnetic Field.

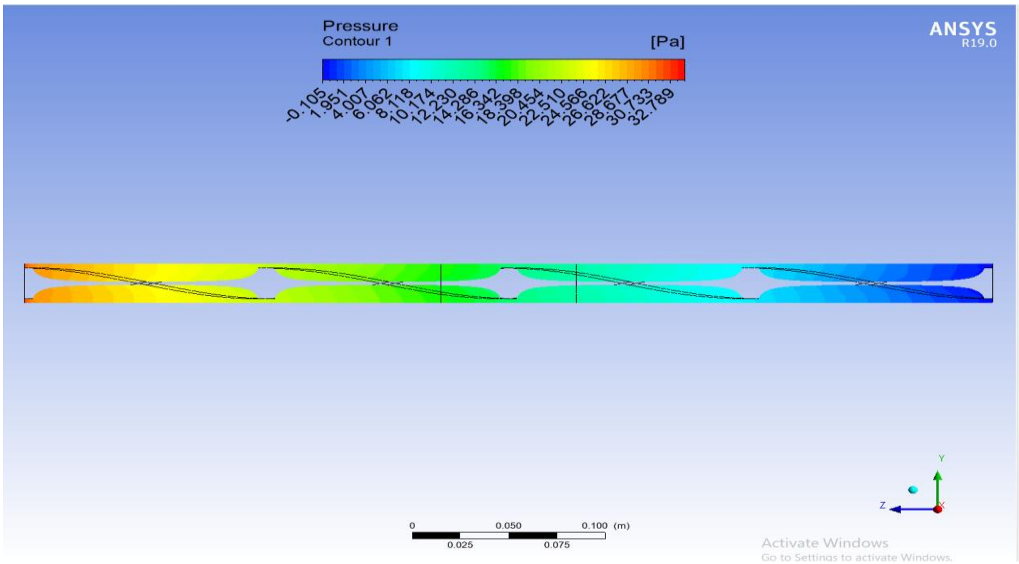

Figure 4.63: Effect Of Intensity Of Magnetic Field On Pressure Of Fluid At 2 Cycles Of Rotation, 0.1 Wt% Concentration Of Ferro-Nanofluid, And 2 Tesla Intensity Of Magnetic Field With 70 Width Of Magnetic Field.

The same rising of temperature has been obtained for all widths of magnetic field with 2cycles of rotation, 2 Tesla intensity of magnetic field, and 0.1 wt% concentration of ferro-nanofluid. See Figures (4.64 to 4.66).

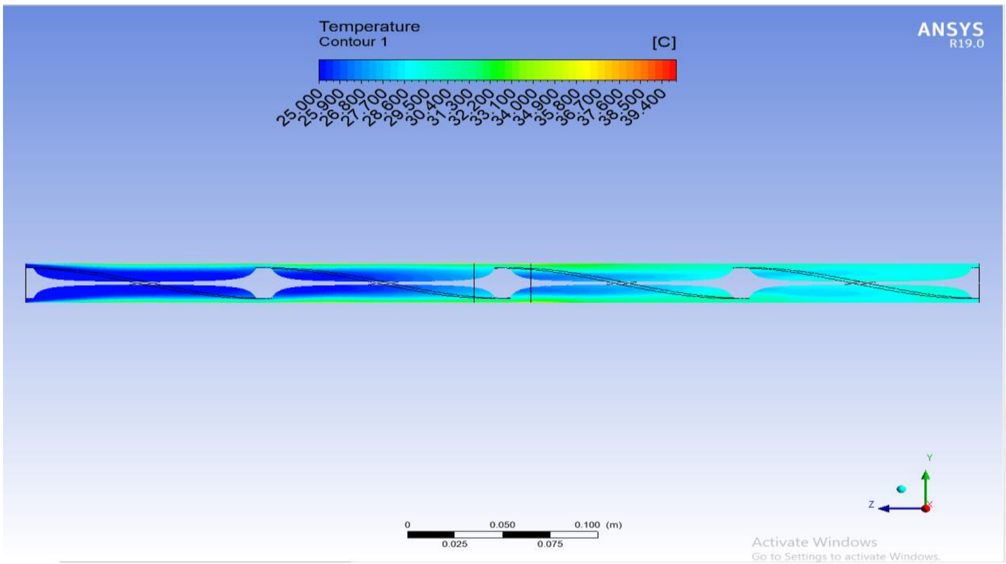

Figure 4.64: Effect Of Intensity Of Magnetic Field On Temperature Of Fluid At 2 Cycles Of Rotation, 0.1 Wt% Concentration Of Ferro-Nanofluid, And 2 Tesla Intensity Of Magnetic Field With 30 Width Of Magnetic Field.

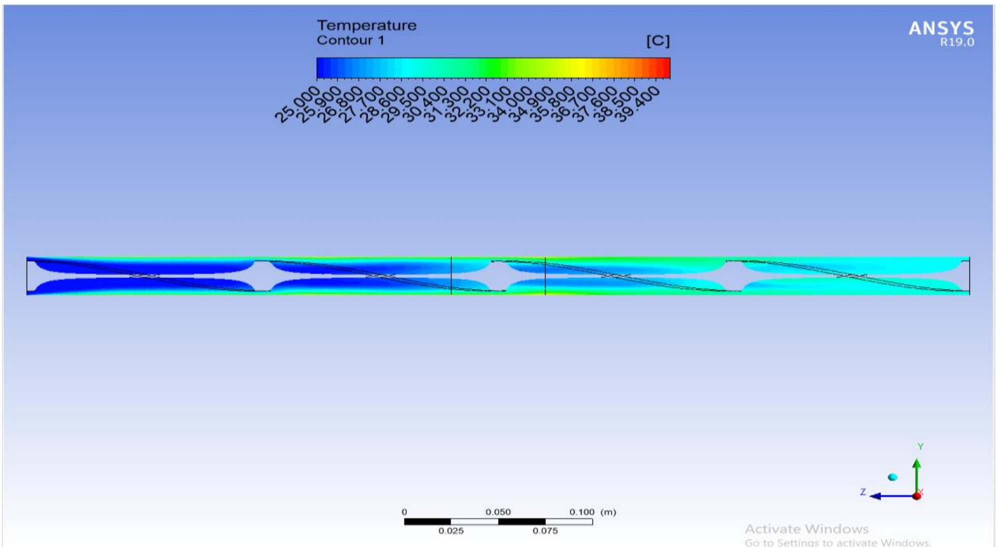

Figure 4.65: Effect Of Intensity Of Magnetic Field On Temperature Of Fluid At 2 Cycles Of Rotation, 0.1 Wt% Concentration Of Ferro-Nanofluid, And 2 Tesla Intensity Of Magnetic Field With 50 Width Of Magnetic Field.

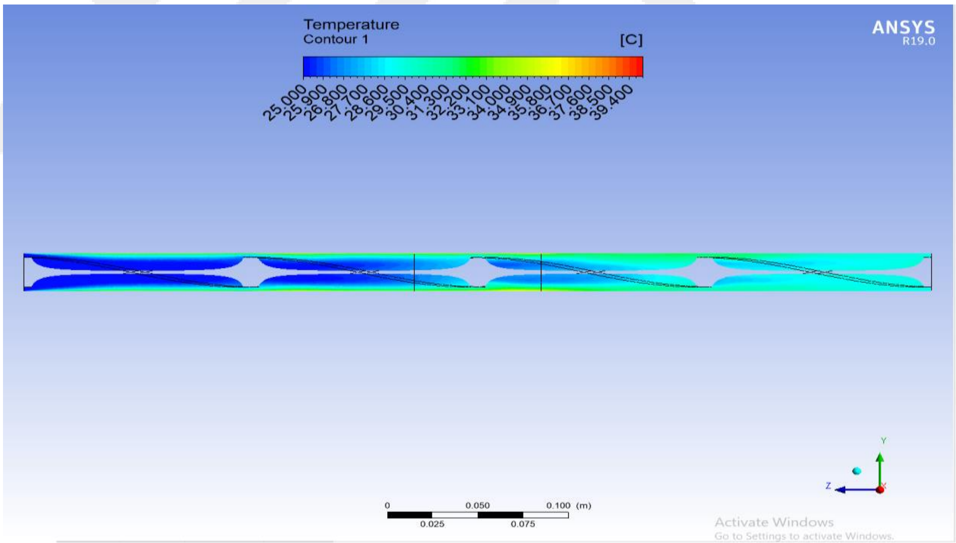

Figure 4.66: Effect Of Intensity Of Magnetic Field On Temperature Of Fluid At 2 Cycles Of Rotation, 0.1 Wt% Concentration Of Ferro-Nanofluid, And 2 Tesla Intensity Of Magnetic Field With 70 Width Of Magnetic Field.

Figures (4.67 to 4.69) present the effect of intensity of magnetic field on velocity of fluid. It is clear that the velocity grows from 0.009 to 0.148 m/s with 30 width of magnetic field, and continues to increase with 50, and 70 width of magnetic field at 2 cycles of rotation, 2 Tesla intensity of magnetic field, and 0.1 wt% concentration of nano-ferrofluid.

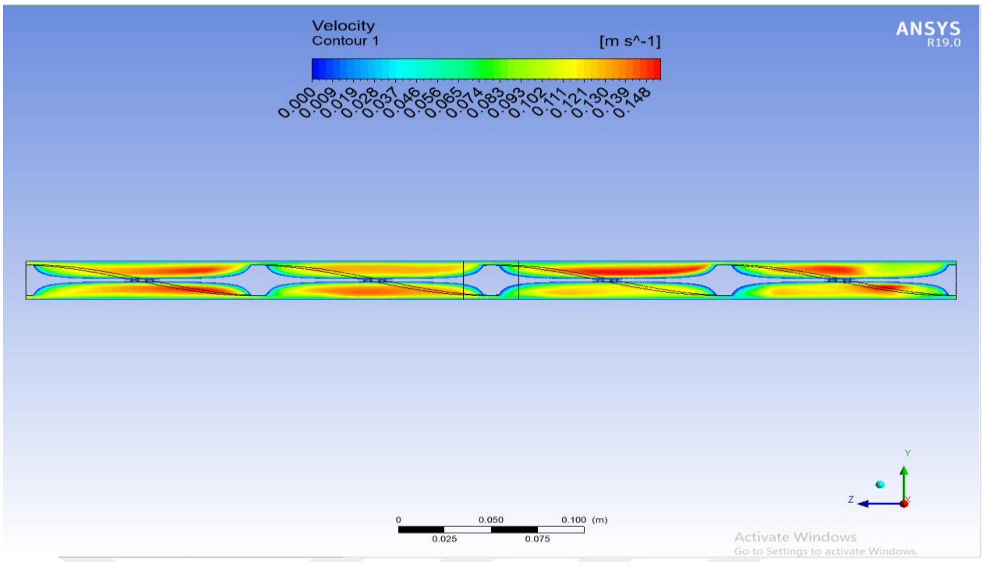

Figure 4.67: Effect Of Intensity Of Magnetic Field On Velocity Of Fluid At 2 Cycles Of Rotation, 0.1 Wt% Concentration Of Ferro-Nanofluid, And 2 Tesla Intensity Of Magnetic Field With 30 Width Of Magnetic Field.

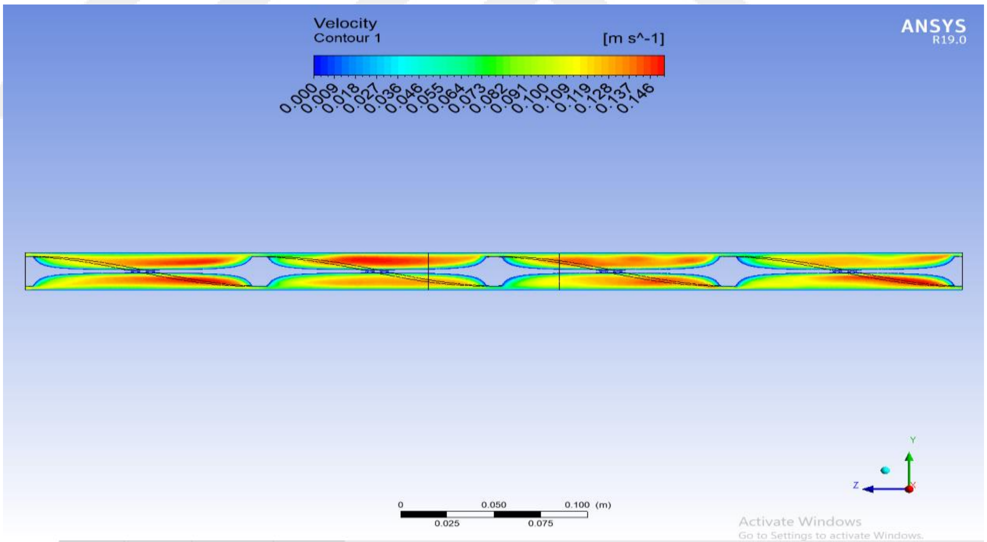

Figure 4.68: Effect Of Intensity Of Magnetic Field On Velocity Of Fluid At 2 Cycles Of Rotation, 0.1 Wt% Concentration Of Ferro-Nanofluid, And 2 Tesla Intensity Of Magnetic Field With 50 Width Of Magnetic Field.

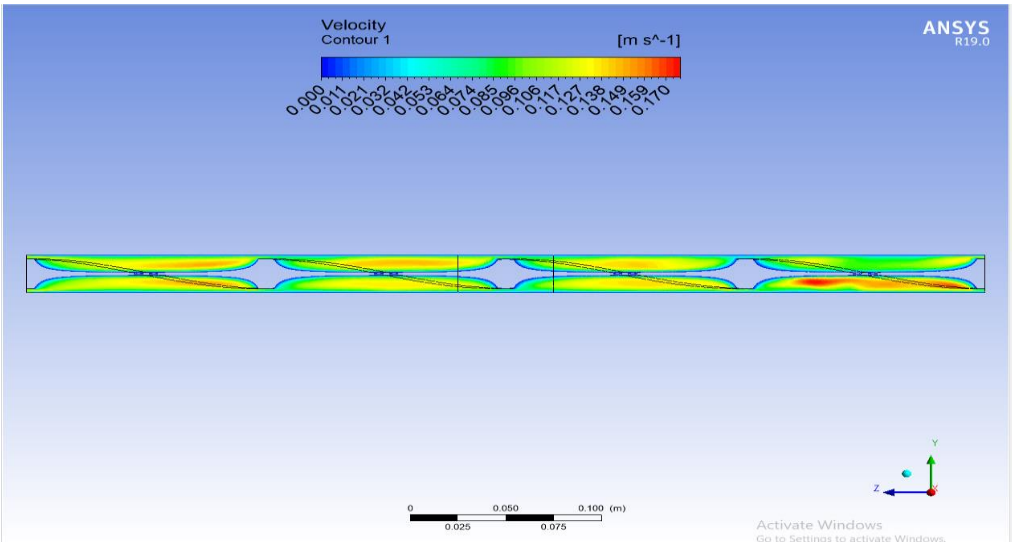

Figure 4.69: Effect Of Intensity Of Magnetic Field On Velocity Of Fluid At 2 Cycles Of Rotation, 0.1 Wt% Concentration Of Ferro-Nanofluid, And 2 Tesla Intensity Of Magnetic Field With 70 Width Of Magnetic Field.

The behavior of pressure drop still the same as mentioned above, ΔP increase to 44.9, 44.8, and 44.9 Pa at 2, 4, and 6 Tesla intensity of magnetic field respectively. Figures (4-70 to 4-72) display the growing of pressure drop at 2, 4, and 6 cycles of rotation respectively, with 70 mm thickness of magnetic.

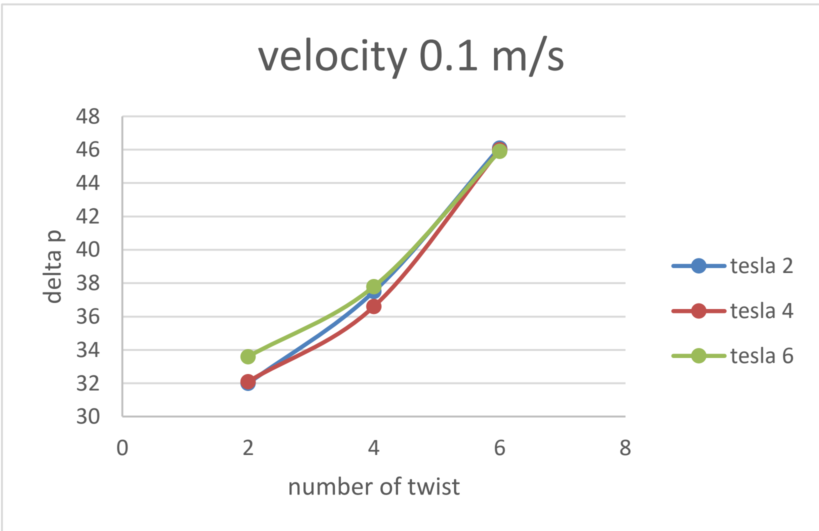

Figure 4.70: Effect Of Cycles Of Rotation And Intensity Of Magnetic Field On Pressure Drop At Velocity 0.1 M/S And Thickness Of Magnetic 70 Mm.

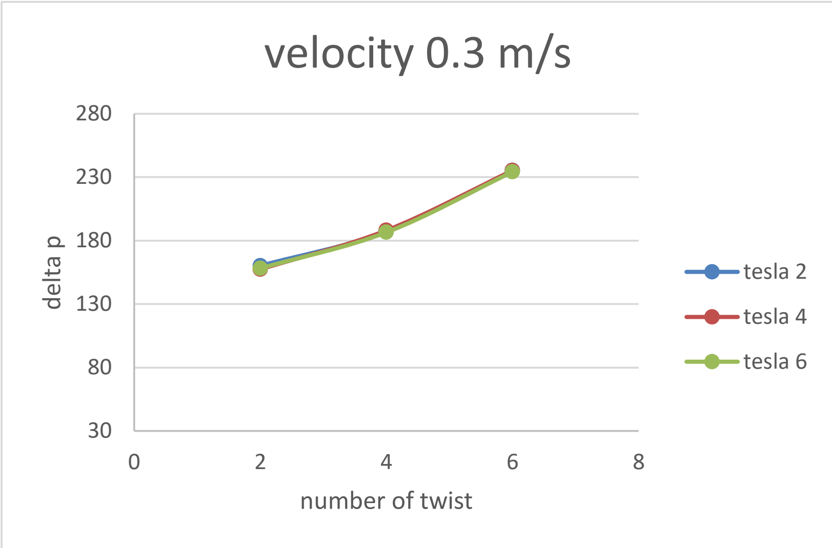

Figure 4.71: Effect Of Cycles Of Rotation And Intensity Of Magnetic Field On Pressure Drop At Velocity 0.5 M/S And Thickness Of Magnetic 50 Mm.

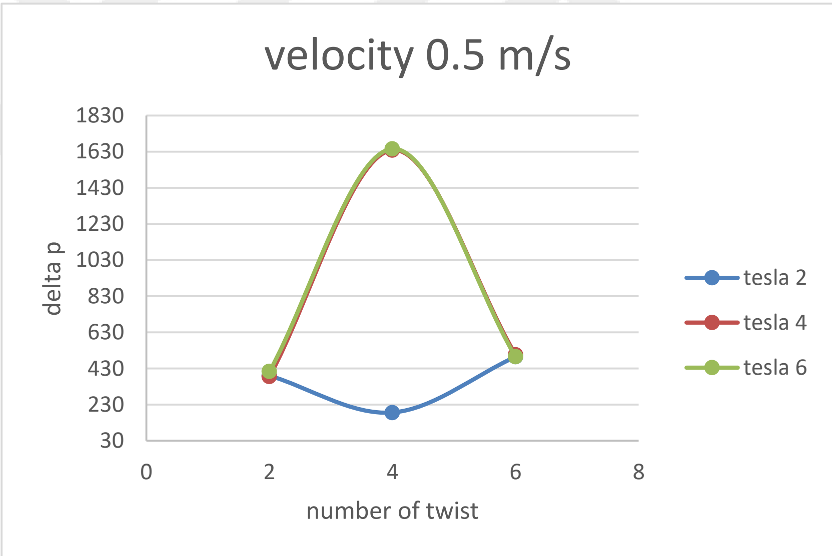

Figure 4.72: Effect Of Cycles Of Rotation And Intensity Of Magnetic Field On Pressure Drop At Velocity 0.5 M/S And Thickness Of Magnetic 70 Mm.

At intensity of magnetic field 4 Tesla, 2 cycles of rotations, and 0.1 wt% concentration of nano0ferrofluid, the pressure dropped as shown in Figures from (4.73 to 4.75). With width of magnetic field equal to 70, the pressure decreased from 32.668 to -0.095 Pa.

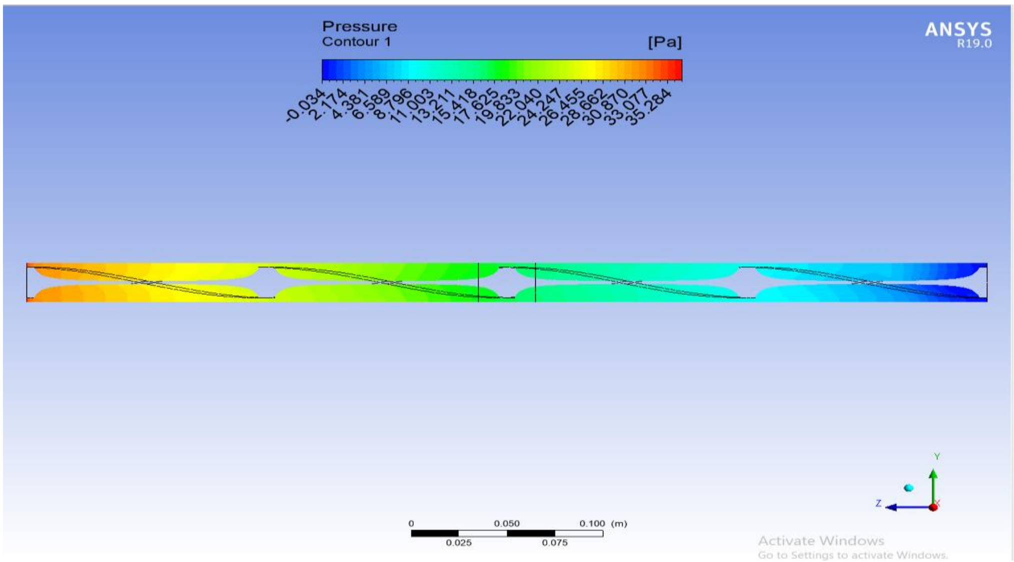

Figure 4.73: Effect Of Intensity Of Magnetic Field On Pressure Of Fluid At 2 Cycles Of Rotation, 0.1 Wt% Concentration Of Ferro-Nanofluid, And 4 Tesla Intensity Of Magnetic Field With 30 Width Of Magnetic Field.

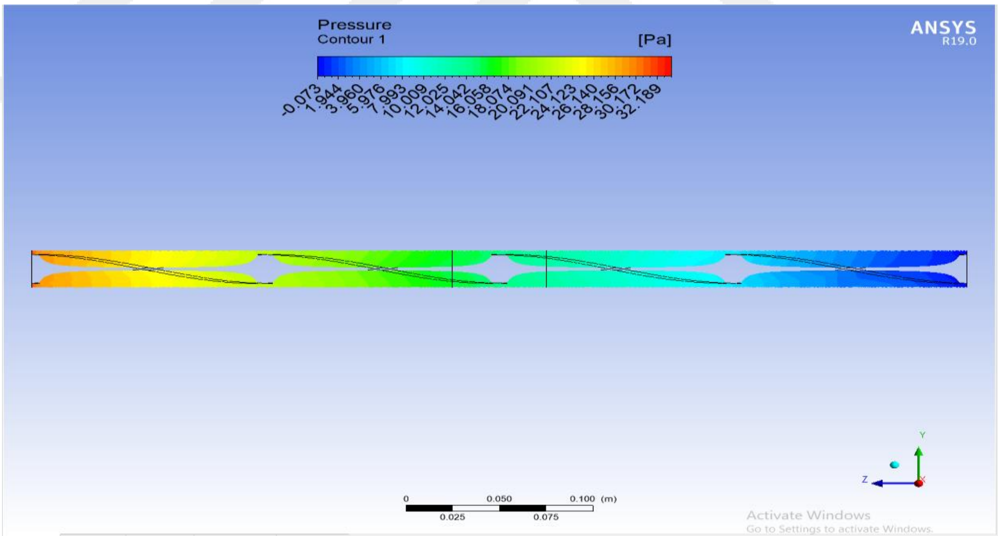

Figure 4.74: Effect Of Intensity Of Magnetic Field On Pressure Of Fluid At 2 Cycles Of Rotation, 0.1 Wt% Concentration Of Ferro-Nanofluid, And 4 Tesla Intensity Of Magnetic Field With 50 Width Of Magnetic Field.

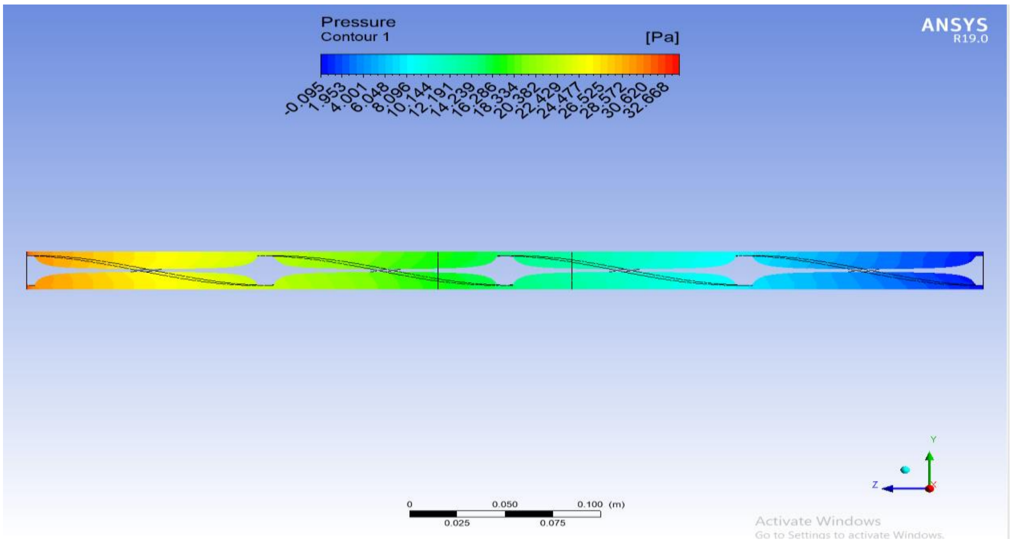

Figure 4.75: Effect Of Intensity Of Magnetic Field On Pressure Of Fluid At 2 Cycles Of Rotation, 0.1 Wt% Concentration Of Ferro-Nanofluid, And 4 Tesla Intensity Of Magnetic Field With 70 Width Of Magnetic Field.

The temperature of fluid rose as the same with 0.1 wt% concentration of ferro-nanofluid, 2 cycles of rotations, and intensity of magnetic field 4 Tesla with 30, 50, and 70 width of magnetic field. See Figures from (4.76 to 4.78).

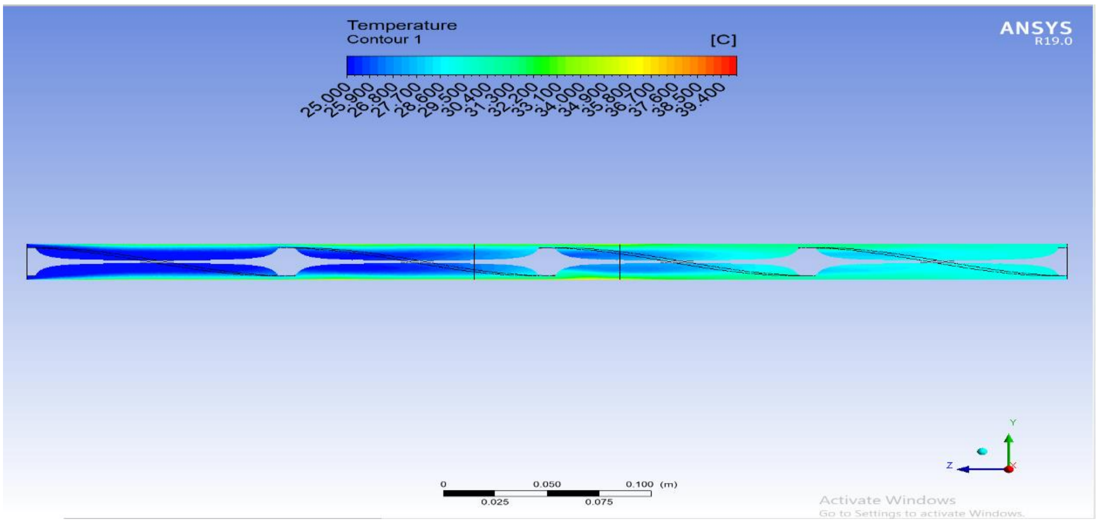

Figure 4.76: Effect Of Intensity Of Magnetic Field On Temperature Of Fluid At 2 Cycles Of Rotation, 0.1 Wt% Concentration Of Ferro-Nanofluid, And 4 Tesla Intensity Of Magnetic Field With 30 Width Of Magnetic Field.

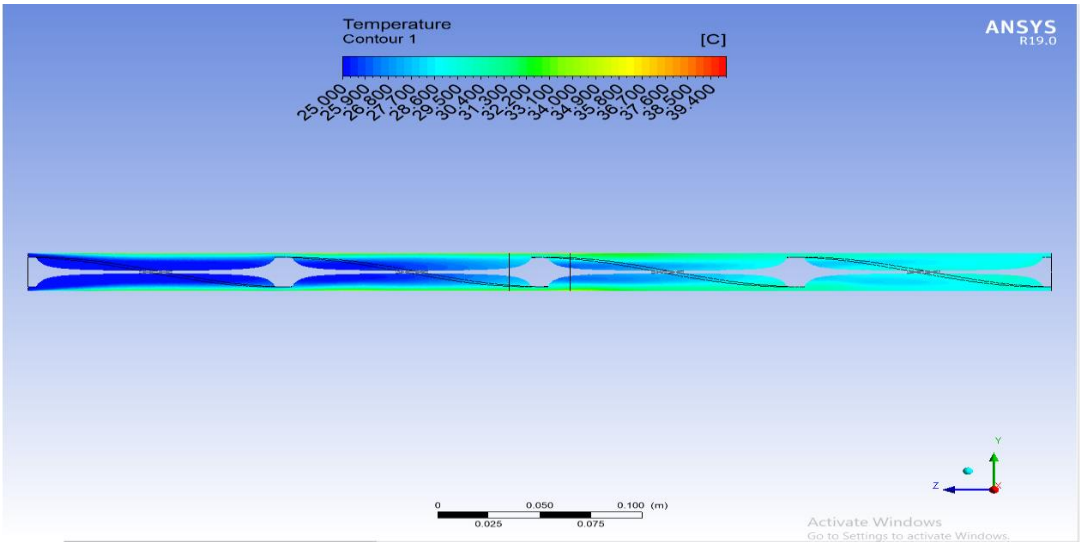

Figure 4.77: Effect Of Intensity Of Magnetic Field On Temperature Of Fluid At 2 Cycles Of Rotation, 0.1 Wt% Concentration Of Ferro-Nanofluid, And 4 Tesla Intensity Of Magnetic Field With 50 Width Of Magnetic Field.

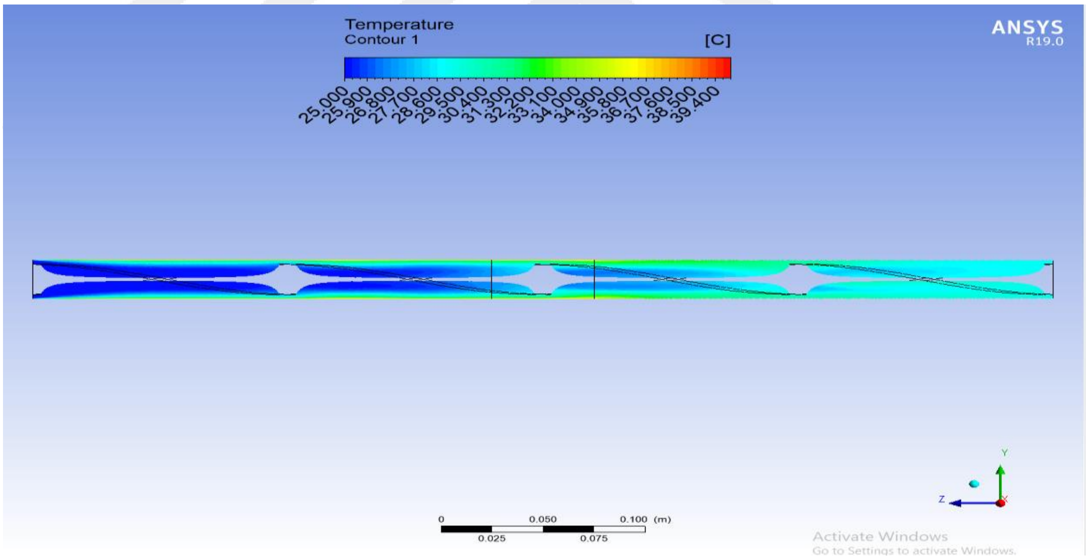

Figure 4.78: Effect Of Intensity Of Magnetic Field On Temperature Of Fluid At 2 Cycles Of Rotation, 0.1 Wt% Concentration Of Ferro-Nanofluid, And 4 Tesla Intensity Of Magnetic Field With 70 Width Of Magnetic Field.

Behaves as the same, the velocity of fluid increased once the intensity of magnetic field increased. At 2 cycles of rations, intensity of magnetic field 4 Tesla, and 0.1 wt%

concentration of ferro-nanofluid, the velocity grows from 0.01 to 0.159 m/s with 30 width of magnetic field as shown in Figures below.

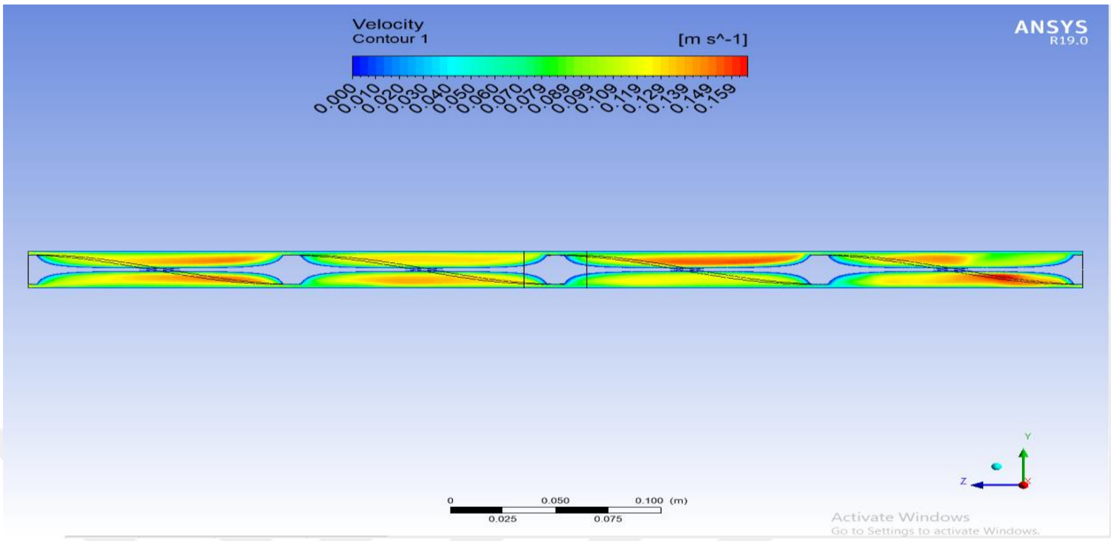

Figure 4.79: Effect Of Intensity Of Magnetic Field On Velocity Of Fluid At 2 Cycles Of Rotation, 0.1 Wt% Concentration Of Ferro-Nanofluid, And 4 Tesla Intensity Of Magnetic Field With 30 Width Of Magnetic Field.

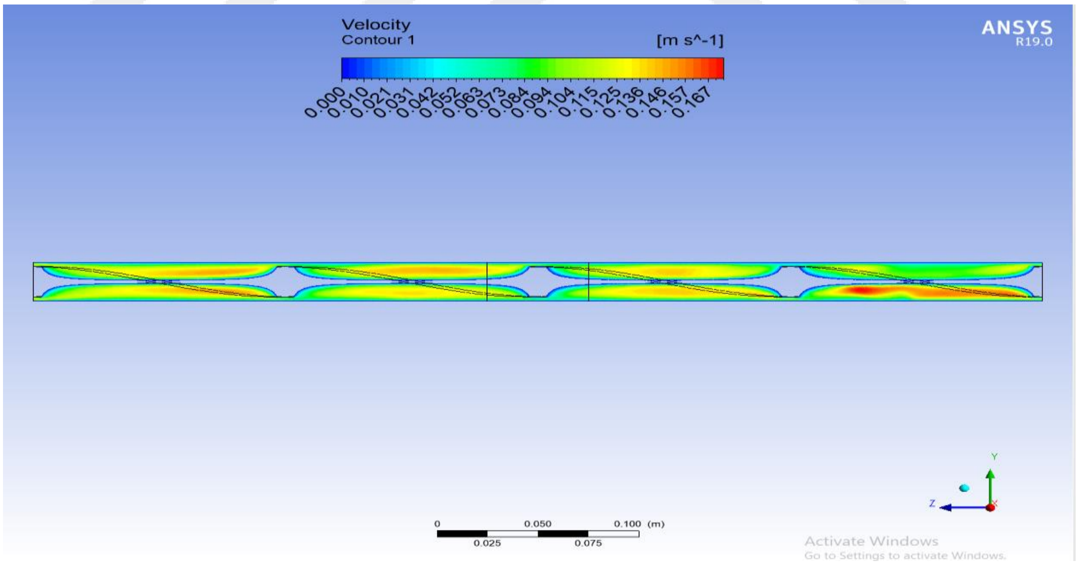

Figure 4.80: Effect Of Intensity Of Magnetic Field On Velocity Of Fluid At 2 Cycles Of Rotation, 0.1 Wt% Concentration Of Ferro-Nanofluid, And 4 Tesla Intensity Of Magnetic Field With 50 Width Of Magnetic Field.

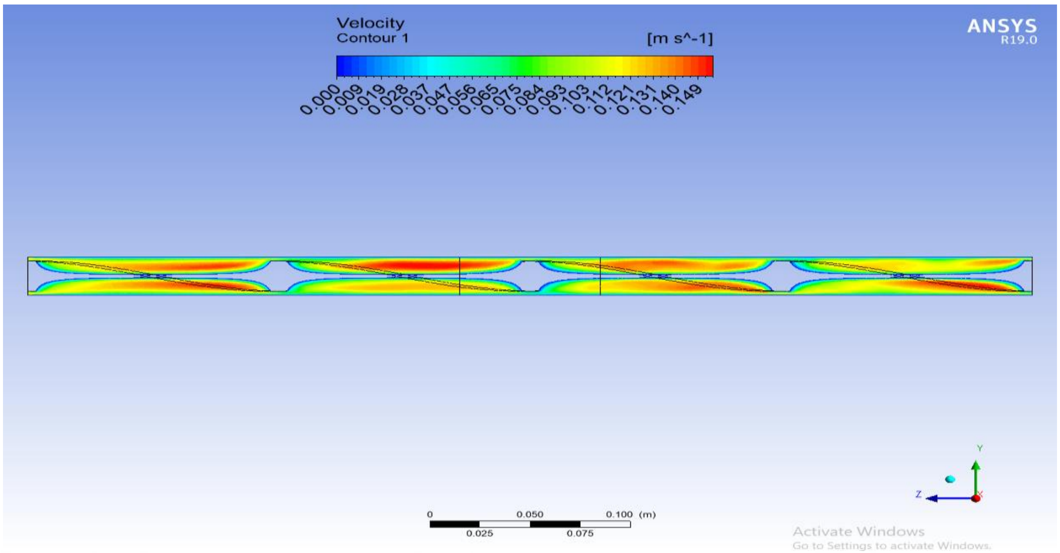

Figure 4.81: Effect Of Intensity Of Magnetic Field On Velocity Of Fluid At 2 Cycles Of Rotation, 0.1 Wt% Concentration Of Ferro-Nanofluid, And 4 Tesla Intensity Of Magnetic Field With 70 Width Of Magnetic Field.

The pressure of fluid dropped at 2 cycles of rotations, 6 Tesla intensity of magnetic field, and 0.1 wt% concentration of ferro-nanofluid with 30, 50, and 70 width if magnetic field as shown in Figures (4.82 to 4.84). Temperature of fluid rise from 25 to 39.4 ºC, see Figures (4.85 to 4.87) at the mentioned conditions. Finally, the velocity of fluid continue to grow with 30, 50, and 70 width of magnetic field, whereas velocity from 0.01 to 0.155 m/s as displayed in Figure (4.88 to 4.90).

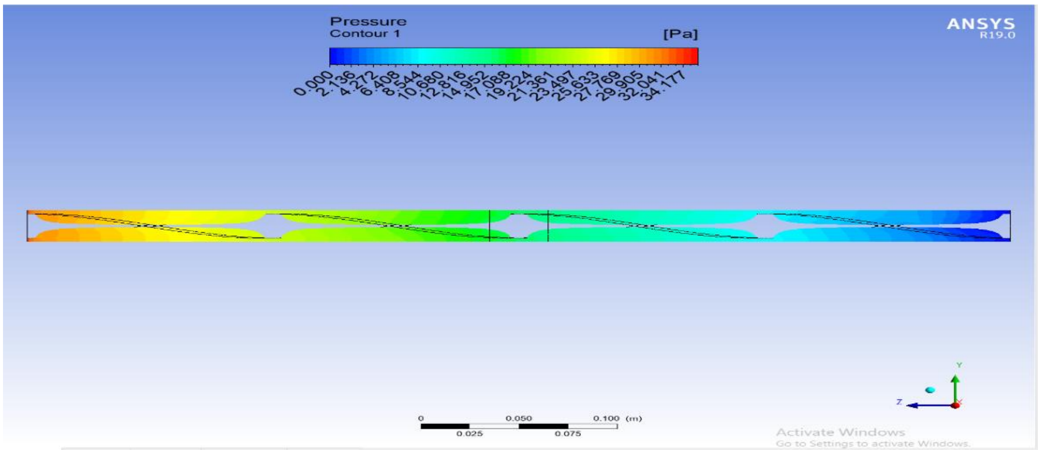

Figure 4.82: Effect Of Intensity Of Magnetic Field On Pressure Of Fluid At 2 Cycles Of Rotation, 0.1 Wt% Concentration Of Ferro-Nanofluid, And 6 Tesla Intensity Of Magnetic Field With 30 Width Of Magnetic Field.

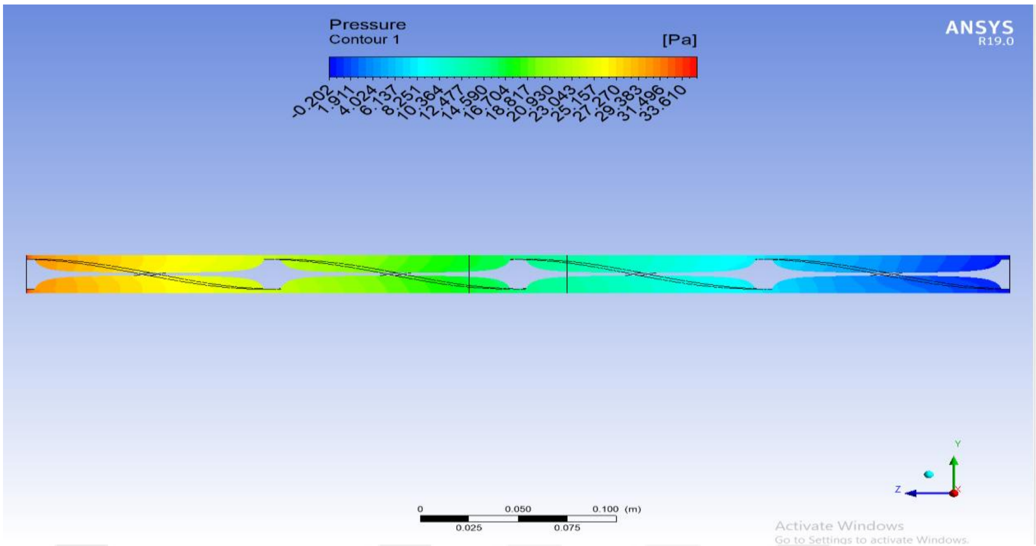

Figure 4.83: Effect Of Intensity Of Magnetic Field On Pressure Of Fluid At 2 Cycles Of Rotation, 0.1 Wt% Concentration Of Ferro-Nanofluid, And 6 Tesla Intensity Of Magnetic Field With 50 Width Of Magnetic Field.

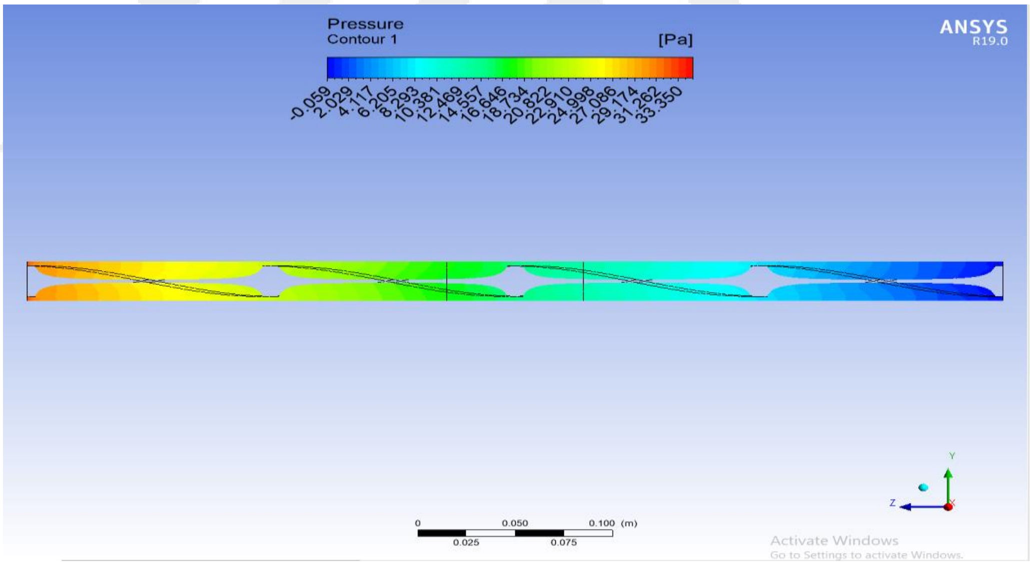

Figure 4.84: Effect Of Intensity Of Magnetic Field On Pressure Of Fluid At 2 Cycles Of Rotation, 0.1 Wt% Concentration Of Ferro-Nanofluid, And 6 Tesla Intensity Of Magnetic Field With 70 Width Of Magnetic Field.

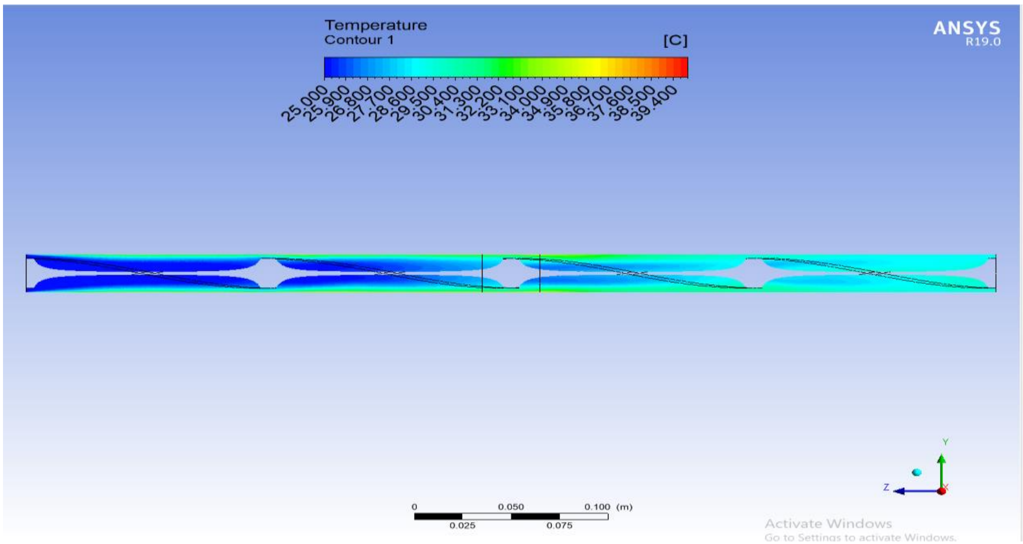

Figure 4.85: Effect Of Intensity Of Magnetic Field On Temperature Of Fluid At 2 Cycles Of Rotation, 0.1 Wt% Concentration Of Ferro-Nanofluid, And 6 Tesla Intensity Of Magnetic Field With 30 Width Of Magnetic Field.

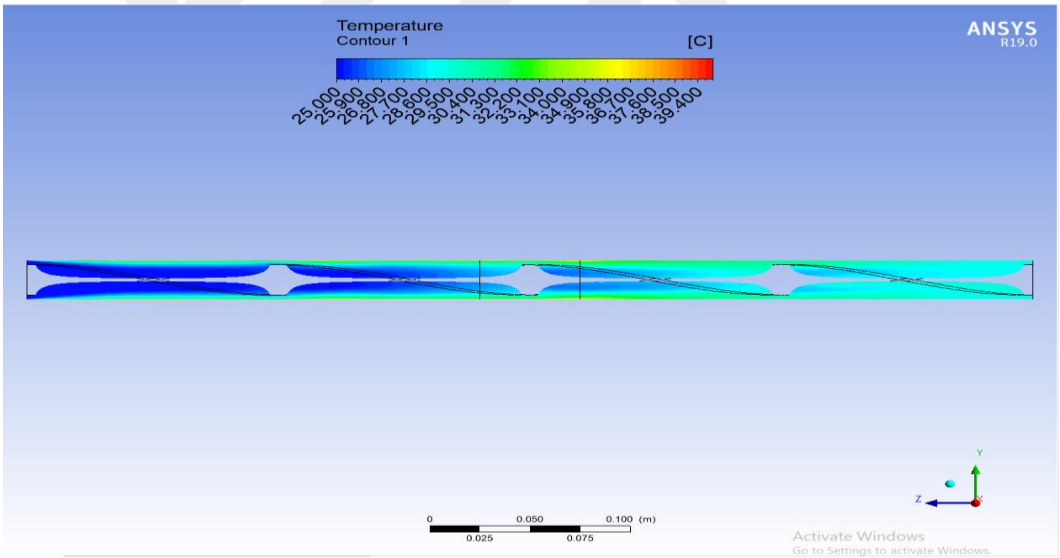

Figure 4.86: Effect Of Intensity Of Magnetic Field On Temperature Of Fluid At 2 Cycles Of Rotation, 0.1 Wt% Concentration Of Ferro-Nanofluid, And 6 Tesla Intensity Of Magnetic Field With 50 Width Of Magnetic Field.

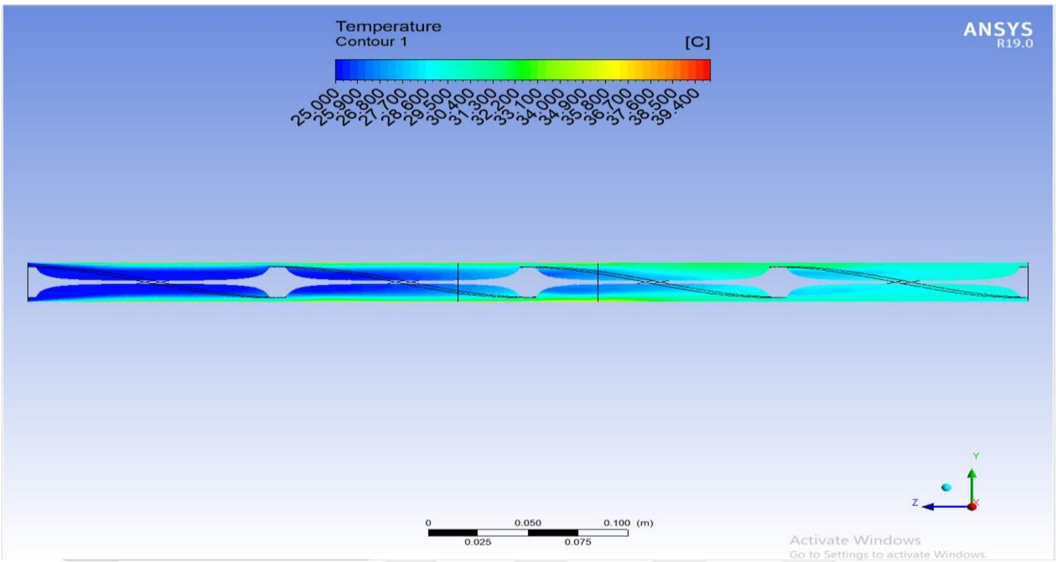

Figure 4.87: Effect Of Intensity Of Magnetic Field On Temperature Of Fluid At 2 Cycles Of Rotation, 0.1 Wt% Concentration Of Ferro-Nanofluid, And 6 Tesla Intensity Of Magnetic Field With 70 Width Of Magnetic Field.

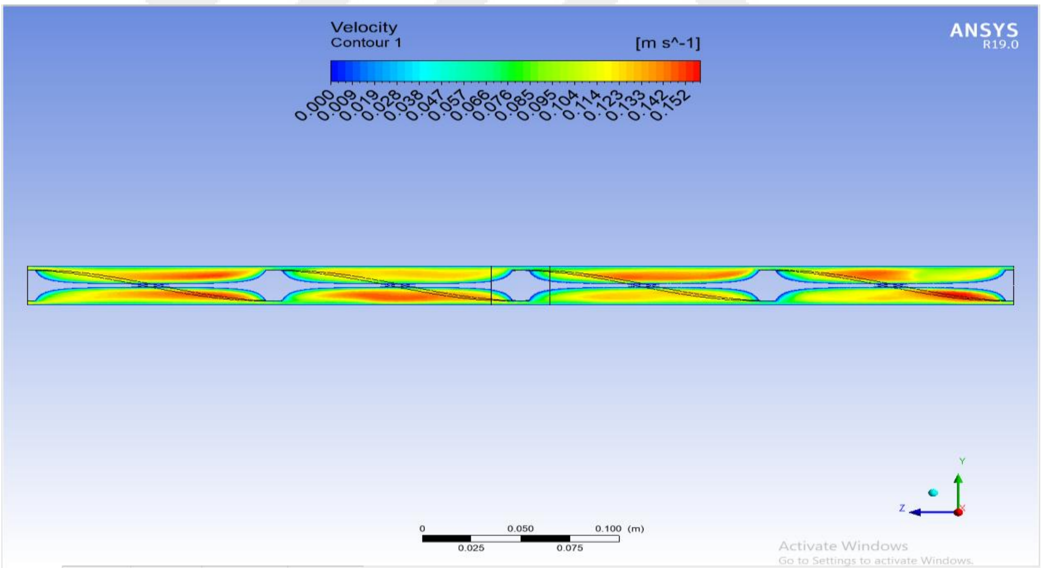

Figure 4.88: Effect Of Intensity Of Magnetic Field On Velocity Of Fluid At 2 Cycles Of Rotation, 0.1 Wt% Concentration Of Ferro-Nanofluid, And 6 Tesla Intensity Of Magnetic Field With 30 Width Of Magnetic Field.

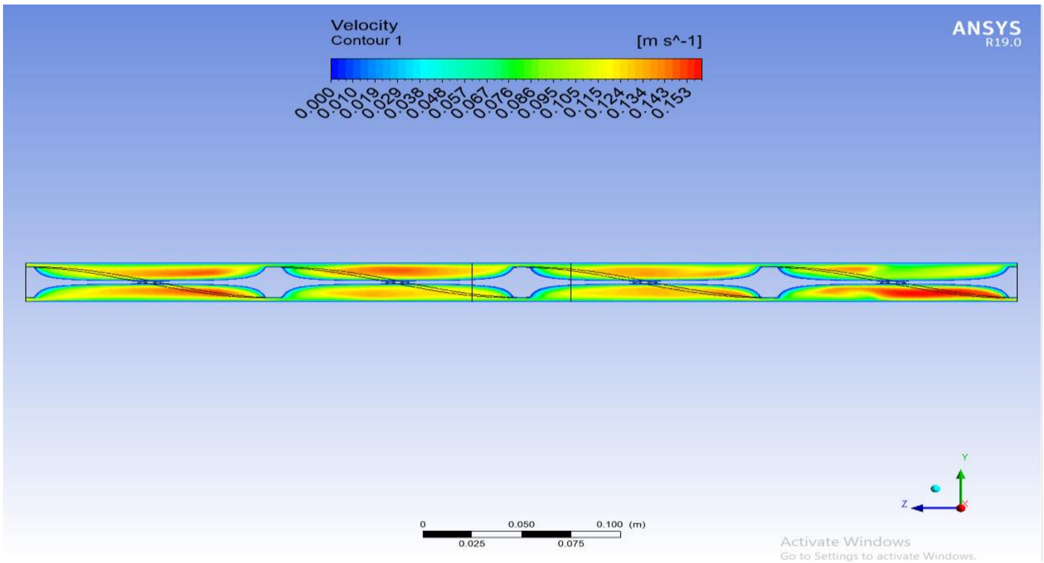

Figure 4.89: Effect Of Intensity Of Magnetic Field On Velocity Of Fluid At 2 Cycles Of Rotation, 0.1 Wt% Concentration Of Ferro-Nanofluid, And 6 Tesla Intensity Of Magnetic Field With 50 Width Of Magnetic Field.

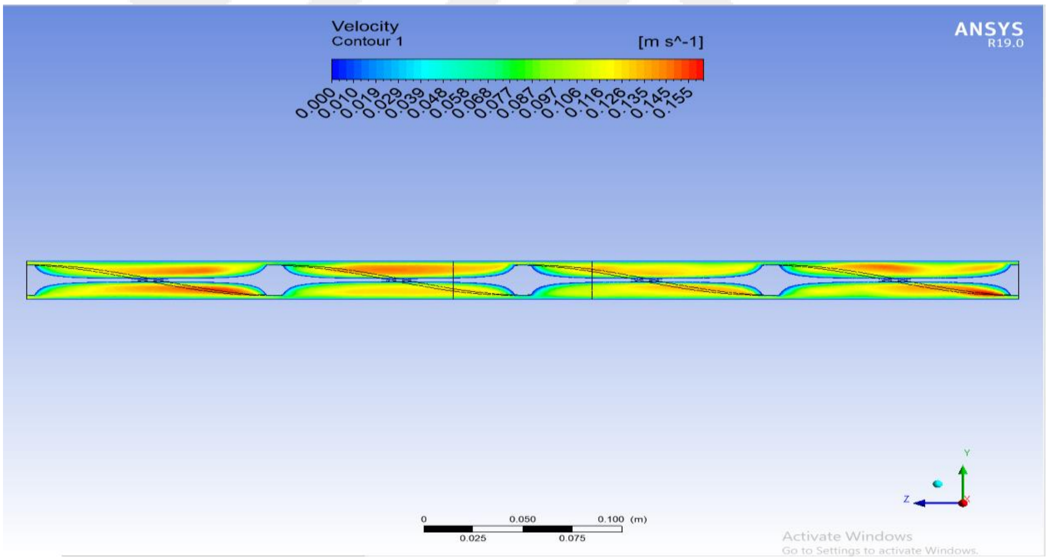

Figure 4.90: Effect Of Intensity Of Magnetic Field On Velocity Of Fluid At 2 Cycles Of Rotation, 0.1 Wt% Concentration Of Ferro-Nanofluid, And 6 Tesla Intensity Of Magnetic Field With 70 Width Of Magnetic Field.

It can be seen that the Nusselt number, which represents heat transfer rate, exhibits similar patterns and rises with increasing magnetic field strength at each constant centration. Additionally, a significant increase in the Nusselt number is shown in the presence of a magnetic field compared to both the absence of a magnetic field and water as the base fluid, respectively. This could be as a result of the chain-like structures that were created in the magnetic fields that were applied, which enhanced the convective heat transfer coefficient and, as a result, the Nusselt number Nu. Magnetic moments tended to line up with the applied magnetic field when there was an applied magnetic field present. When magnetic nanoparticles were mostly influenced by magnetic force as opposed to thermal motion. The nanoparticles produced chains that were orientated in the same direction as the applied field and stuck together. As a result, the chains connecting the flow of nanofluids and the pipe wall function as thermal tunnels, improving heat transfer. With the use of a steady magnetic field without any pumping power, the enhancement of heat transfer improves. This is due to the fact that when a steady magnetic field is supplied, the ferrofluid's dipoles align in the same direction as the magnetic field's applied externally, leading to a higher rate of heat transfer than would otherwise occur in the absence of a magnetic field.

The behavior of pressure drop still the same as mentioned above, ΔP increase to 44.9, 44.8, and 44.9 Pa at 2, 4, and 6 Tesla intensity of magnetic field respectively. Figure 4.91 display the growing of pressure drop at 2, 4, and 6 cycles of rotation respectively, with 70 mm thickness of magnetic.

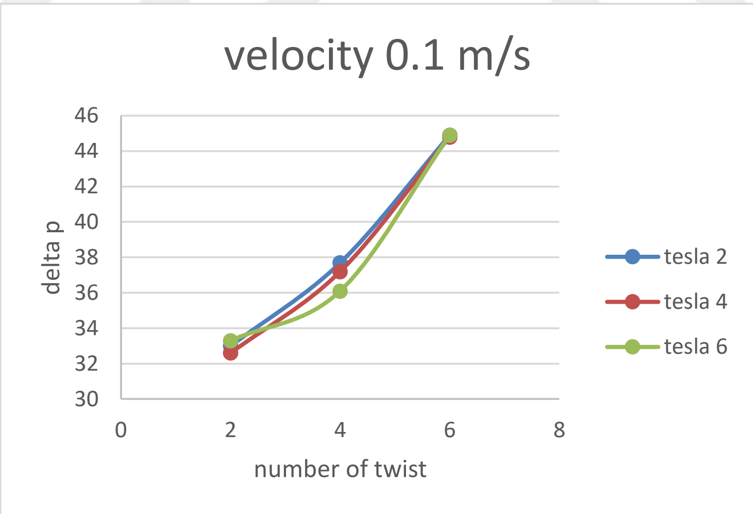

Figure 4.91: Effect Of Cycles Of Rotation And Intensity Of Magnetic Field On Pressure Drop At Velocity 0.1 M/S And Thickness Of Magnetic 70 Mm.

5. CONCLUSIONS AND RECOMMENDATIONS

5.1 CONCLUSIONS

From the current research, the following findings may be drawn:

a. Fe_2O_3 nanofluid was employed in the current investigation to examine heat transmission. In the end, it is true that heat transfer (whether of water or nanofluid, with or without the twisted tape) significantly rises with Reynolds number. The base fluid's heat transport is partially improved by the addition of nanoparticles.

b. Based on the results, the using of ferro-nanofluid and magnetic field to enhance the rate of heat transfer was successful and very efficient applied.

c. Computational Fluid Dynamics (CFD) studies are performed to grow a more profound knowledge into the field of the stream. To explain the impact of the disturbance model which includes the arrangement of two vehicle condition, (k-ε) model is utilized.

d. Water and Fe_3O_4 is considered as the running nanofluid and the characteristics of flow are assumed (Steady flow, three dimensional, Newtonian, Incompressible, Turbulent).

e. Ferrofluid's secondary magnetoconvective flow in the direction of the permanent magnet results in a reduction in convective heat transfer. The detrimental impact of the produced secondary flow is lessened when the flow rate is increased. As a result, at larger flow rates, convective heat transfer and Nu number are enhanced.

f. The phenomenon was fully simulated, taking into account the movement of mass, heat, and momentum in the system. The observed behavior is clearly depicted by simulation findings, which are in good agreement with the experimental data. Designing heat transfer devices for many uses, such as cooling electronics and micro reactors, may benefit from using this simulation for a variety of geometries and operating circumstances.

g. The parameters of concentration of ferro-nanofluid, intensity of magnetic field, and cycles of rotation have been taken in account to explain the effect on pressure, temperature, and velocity of fluid.

h. The pressure of fluid tends to decrease while temperature and velocity of fluid rises with increase intensity of magnetic field, concentration of ferro-nanofluid, and cycles of rotations.

5.2 RECOMMENDATIONS

Recommendations for the future work are:

i. Different types of nano-fluids materials can be used in this process such as: TiO_2, Cu, Ag and Al_2O_3

ii. Future projects will include investigate pressure drop experiments and two-phase liquid-liquid ferrofluidic plug flow. Future research will also look into the possibility of utilizing a non-uniform magnetic field to improve mixing.

iii. Study the heat transfer enhancement and flow characteristic of ferrofluid in a pipe for laminar flow regime with electric magnetic field.

iv. Experimentally study to estimate the influence of magnetic field on transfer of heat for different size of nanoparticle.

Experimentally Study to estimate the influence of magnetic field on the variation of thermal conductivity of oxide and metal oxide nanofluids.

REFERENCES

[1] Abbas, F., Ali, B., Hasan, Q., Ali, K., Karrar, A., Ammar, M., Ihab, O., & Mujtaba, A. (2022). Improvement of Heat Transfer by Using Porous Media, Nanofluid, and Fins: A Review. International Journal of Heat and Technology, 40, 497-521.

[2] Ramin, M., Hossein, A., Pouyan, T., Apurv, K., Morteza, H., & Alireza, R. (2021). Heat Transfer Enhancement of Nanofluid Flow in a Tube Equipped with Rotating Twisted Tape Inserts: A Two-Phase Approach. Heat Transfer Engineering Journal.

[3] Saadah, A., Shahrir, A. & Kamaruzzaman, S. (2020). A review on the thermal performance of nanofluid inside circular tube with twisted tape inserts, Advances in Mechanical Engineering, 12, 1-26.

[4] Matin, G., Omid, H., Erfan, E., & Ebrahim, B.(2021). Experimental investigation on laminar convective heat transfer of nano ferrofluids under constant and alternating magnetic field. AUT Journal of Mechanical Engineering, 5, 10-10.

[5] Budi, K., Agung, T., Koji, E., Takahiko, M., & Muhammad, A. (2019). Heat Transfer Enhancement of TiO_2/Water Nanofluids Flowing Inside a Square Minichannel with a Microfin Structure: A Numerical Investigation. Energies, 12, 3041.

[6] Suvanjan, B., Devendra, K., Sanghati, R., Kunal, D., Ali, C., Rachid, B., Akshoy, R., & Huan, Z. (2021). Computational investigation on heat transfer augmentation of a circular tube with novel hybrid ribe. E3S Web of Conferences, 321, 04012.

[7] Jiawang, Y., Xian, Y., Jin, W., Hon, H., & Bengt, S. (2022). Review on Thermal Performance of Nanofluids With and Without Magnetic Fields in Heat Exchange Devices. Frontiers in Energy, 10.

[8] Ellahi, R., Tariqb, M., Hassanc, M., & Vaf, K. (2016). On boundary layer nano-ferroliquid flow under the influence of low oscillating stretchable rotating disk. Journal of Molecular Liquids.

[9] Yahya, S., Reza, H., & Majid, S. (2016). Experimental study on heat transfer enhancement of laminar ferrofluid flow in horizontal tube partially filled porous media under fixed parallel magnet bars. Journal of Magnetism and Magnetic Materials, 2016.

[10] Budi, K., Budi, S., Agung, T., Muhammad, A., & Takahiko, M. (2018). Heat Transfer Enhancement of TiO_2/Water Nanofluid at Laminar and Turbulent Flows: A Numerical Approach for Evaluating the Effect of Nanoparticle Loadings. Energies, 11, 1584.

[11] Budi, K., Agung, T., Koji, E., Takahiko, M., & Muhammad, M. (2019). Heat Transfer Enhancement of TiO_2/Water Nanofluids Flowing Inside a Square Minichannel with a Microfin Structure: A Numerical Investigation. Energies, 12, 3041.

[12] Mansour, T., & Mehran, T. (2022). Magnetic Field Effect on Ferro-Nanofluid Heat Transfer in a Shell and Tube Heat Exchanger with Seven Twisted Oval Tubes. Advanced Design and Manufacturing Technology, 15.

[13] Gary, R., Nicolette, G., & Cameron, S. (2019). Heat Transfer Enhancement Using Ferrofluids. Proceedings of the 6th International Conference of Fluid Flow, Heat and Mass Transfer, 2019.

[14] Cherepanov, H., & Krauzin, P. (2019). On the Thermodynamic Theory of Colloidal Suspensions," Physica A.

[15] Khan, W., Khan, Z., & Haq, R. (2015). Flow and Heat transfer of Ferrofluids Over a Flat Plate with Uniform Heat Flux. Eur. Phys. J. Plus, 130, 86.

[16] Qi, L., Saad, F., Mohammed, F., & Gang, L. (2017). A Ferrofluid Based Energy Harvester: Computational Modeling, Analysis, and Experimental Validation. Journal of Magnetism and Magnetic Materials.

[17] Mojtaba, B., & Mohammad, G. (2019). Effect of Magnetic Field on the Hydrodynamic and Heat Transfer of Magnetite Ferrofluid Flow in a Porous Fin Heat Sink. Journal of Magnetism and Magnetic Materials.

[18] Saadah, A., Shahrir, A., & Kamaruzzaman. S. (2020). A review on the thermal performance of nanofluid inside circular tube with twisted tape inserts. Advances in Mechanical Engineering, 12, 1–26.

[19] Sompol, S., Chinaruk, T., Nuthvipa, J., & Pongjet, P.(2019). Experimental and numerical heat transfer investigation in turbulent square-duct flow through oblique horseshoe baffles. Chemical Engineering and Processing, 90, 58–71.

[20] Sagar, P., Sakshum, K., Vishrut, M., Abhijit, R., Parth, P., and Indrajit, M." Comparative study of heat transfer characteristics of a tube equipped with X-shaped and twisted tape insert," Materials Today: Proceedings, 2020.

[21] Promvonge, P., & Eiamsa-ard, S. (2007). Heat transfer behaviors in a tube with combined conical-ring and twisted-tape insert. International Communications in Heat and Mass Transfer, 34, 849–859.

[22] Sonal, N., & Vijay, P. (2014). Nanofluid heat transfer enhancement with twisted tape insert—A Review International Journal of Mechanical Engineering and Robotics Research, 3, 2.

[23] Eiamsa-ard, S., Kiatkittipong, K., & Jedsadaratanachai, W.(2015). Heat transfer enhancement of TiO_2/water nanofluid in a heat exchanger tube equipped with overlapped dual twisted-tapes. Engineering Science and Technology, 1-15.

[24] Aghayari, R., Maddah, H., Baghbani, J., Mohammadiun, H., & Nikpanje, E.(2015). An experimental investigation of heat transfer of Fe_2O_3 /Water nanofluid in a double pipe heat exchanger. International Journal of Nano Dimensions, 6, 517-524.

[25] Abdulhassan, A., & Nabeel, S. (2016). Experimental Investigation of Heat Transfer Enhancement with Nanofluid and Twisted Tape Inserts in a Circular Tube. Engineering and Technology Journal, 34, Part (A), 3.

[26] Syam, L., Manoj, K., Punnaiah, V., & Antonio, C. (2017). Experimental investigation of Al_2O_3/water nanofluids on the effectiveness of solar flatplate collectors with and without twisted tape inserts. Renewable Energy.

[27] Varma, K., Kishore, P., & Prasad, P. (2017). Enhancement of Heat Transfer Using Fe_3O_4 / Water Nanofluid with Varying Cut-Radius Twisted Tape Inserts. International Journal of Applied Engineering Research, 12, (18), 7088-7095.

[28] Qi, C., Guiqing, W., Yuying, Y., Siyuan, M., and Tao, L. (2018). Effect of rotating twisted tape on thermo-hydraulic performances of nanofluids in heat-exchanger systems. Energy Conversion and Management, 166, 744-757.

[29] Kanthimathi, T., Bhramara, P., & Ayub, S. (2019). Heat Transfer Performance of EG-Water Based Fe_3O_4 and its Hybrid Nanofluids in a Double Pipe Heat Exchanger. International Journal of Recent Technology and Engineering, 8, (4).

[30] Sheikholeslami, M., Jafaryar, M., Mohammadali, H., Ahmad, S., Zhixiong, L., Truong, K., & Mohsen, B.(2019). Heat transfer and turbulent simulation of nanomaterial due to compound turbulator including irreversibility analysis. International Journal of Heat and Mass Transfer, 137, 1290-1300.

[31] Palanisamy, K., & Mukesh, K. (2019). Experimental investigation on convective heat transfer and pressure drop of cone helically coiled tube heat exchanger using carbon nanotubes/ water nanofluids. Heliyon, 5, e01705.

[32] Arash, R., & Azadeh, S. (2019). Heat transfer enhancement in a curved tube by using twisted tape insert and turbulent nanofluid flow. Journal of Thermal Analysis and Calorimetry, 2019.

[33] Gangtao, L., & Issam, M. (2019). Review of single-phase and two-phase nanofluid heat transfer in macro-channels and micro-channels. International Journal of Heat and Mass Transfer, 136, 324–354, 2019.

[34] Mowafaq, S., Jinan, M., Laith, H., & Humam, K. (2020). Study the effect of Nano fluid on Heat Transfer in Finned Pipe with Internal V-Cut Twisted Tape. Journal of Mechanical Engineering Research and Developments, 43, (5), 161-177.

[35] Saadah, A., Shahrir, A., & Kamaruzzaman, S. (2020). A review on the thermal performance of nanofluid inside circular tube with twisted tape inserts. Advances in Mechanical Engineering, 12, (6), 1–26.

[36] Suvanjan, B., Devendra, K., Shramona, C., Rahul, R., Alibek, I., & Mohsen, S. (2021). Turbulent Flow Heat Transfer through a Circular Tube with Novel Hybrid Grooved Tape Inserts: Thermohydraulic Analysis and Prediction by Applying Machine Learning Model. Sustainability, 13, 3068.

[37] Morteza, B., & Nader, A. (2020). Forced Convective Heat Transfer of Non-Newtonian CMCbased CuO Nanofluid in a Tube. Journal of Heat and Mass Transfer Research, 7, 155-163.

[38] Reza, F., & Ashkan, G. (2020). Numerical study on heat transfer and nanofuid flow in pipes fitted with different dimpled spiral centre plate. SN Applied Sciences, 2:298.

[39] Mehdi, G., Ramin, M., Hossein, A., Hafiz, A., Pouyan, T., & Wahiba, Y. (2020). Thermo-Hydraulic Performance Analysis on the Effects of Truncated Twisted Tape Inserts in a Tube Heat Exchanger. Symmetry, 12, 1652.

[40] Muhammad, R., Nosheen, G., Jae, D., Seifedine, K., & Yu-Ming, C. (2020). Numerical treatment of radiative Nickel–Zinc ferrite-Ethylene glycol nanofluid flow past a curved surface with thermal stratification and slip conditions. Scientific Reports, 10:16832.

[41] Nakhchia, M., & Rahmati, M. (2021). Entropy Generation of Turbulent Cu-Water Nanofluid Flows inside Thermal Systems Equipped by Transverse-Cut Twisted turbulators. Journal of Thermal Analysis and Calorimetry, 143, 2475–2484.

[42] Muhammad, S., Ilyas, K., Sharidan, S., & Ahmad, Q. (2021). Shape effect on MHD flow of time fractional Ferro-Brinkman type nanofuid with ramped heating. Scientific Reports. 11:3725, 2021.

[43] Muhammad, I., Ebrahem, A., Tareq, S., Abdallah, S., Yu-Ming, C., & Goshtasp, C. (2021). Assessment of economic, thermal and hydraulic performances a corrugated helical heat exchanger filled with non-Newtonian nanofuid. Scientifc Reports, 11:11568.

[44] Alireza, A., Suvanjan, B., Amin, D., Goldanlou, A., Rostami, S., & Mohsen, S. (2021). Heat transfer and fluid flow analysis using nanofluids in diamond-shaped cavities with novel obstacles. Engineering Applications of Computational Fluid Mechanics, 15(1), 1034–1056.

[45] A., Olabia, Tabbi, W., Enas, T., Khaled, E., Atiqure, R., & Mohammad, A. (2021). Geometrical effect coupled with nanofluid on heat transfer enhancement in heat exchangers, International Journal of Thermofluids, International Journal of Thermofluids, 10, 100072.

[46] Abbas, F., Ali, B., Hasan, Q., Ali, K., Karrar, A., Ammar, M., Ihab, O., & Mujtaba, A.(2022). Improvement of Heat Transfer by Using Porous Media, Nanofluid, and Fins: A Review. International Journal of Heat and Technology, 40, (2), 497-521.

[47] Li, Y., Shaghayegh, B., Wanich, S., Pouya, B., Sandhir, S., Alla, D., & El-Shafay, A. (2022). Numerical assessment of the influence of helical baffle on the hydrothermal aspects of nanofuid turbulent forced convection inside a heat exchanger. Scientifc Reports, 12:2245.

[48] Yuvraj, D., Arjun, S., Ganesh, P., Aditya, A., & Tushar, T. (2022). Thermal Analysis of a Ferro Fluid Interrupted and Continuously Twisted Tape Heat Exchanger. International Journal of Advanced Research in Science, Communication and Technology (IJARSCT), 2(7).

[49] Majid, H., & Nam-Trung, N. (2017). Magnetofluidics for Manipulation of Convective Heat Transfer. International Communications in Heat and Mass Transfer, 81, 149-154.

[50] Ehsan, F., Musa, M., & Ahmed, S. (2018). Experimental and Numerical Study of Heat Transfer Enhancement in a Shell and Tube Heat Exchanger using Helical Coiled Wire Inserts. Tikrit Journal of Engineering Sciences, 25(2), 74 – 79.

[51] Gan, N., Stanley, C., Nguyen, N., & Rosengarten, G. (2018). Ferrofluids for heat transfer enhancement under an external magnetic field. International Journal of Heat and Mass Transfer, 123,110-121.

[52] Barzegar, M., Mohsen, S., Valiallah, M., Ganji, D., & Rasoul, M. (2018). Heat transfer enhancement of ferrofluid inside an 90° elbow channel by non-uniform magnetic field. Journal of Magnetism and Magnetic Materials, 2018.

[53] Morteza, M., Mohit, B., Ali, R., Mousa, F., Hamid, H., & Davood, T.(2019). Heat transfer enhancement of ferrofluid flow within a wavy channel by applying a non-uniform magnetic field. Journal of Thermal Analysis and Calorimetry, 2019.

[54] Mojtaba, B., & Mohammad, G. (2019). Effect of magnetic field on the hydrodynamic and heat transfer of magnetite ferrofluid flow in a porous fin heat sink. Journal of Magnetism and Magnetic Materials, 2019.

[55] Yeping, P., Ali, S., Masoud, A., & Moradi, R.(2019). A numerical simulation for magnetohydrodynamic nanofluid flow and heat transfer in rotating horizontal annulus with thermal radiation. Royal Society of Chemistry Advances, 9, 22185–22197.

[56] Mousavi, S., Jamshidi, N., & Rabienataj-Darzi, A. (2019). Numerical investigation of the magnetic field effect on the heat transfer and fluid flow of ferrofluid inside helical tube. Journal of Thermal Analysis and Calorimetry, 137, 1591-1601.

[57] Amira, J., Zouhaier, M., & EL-Cafsi, A. (2019). Effect of magnetic field on the mixed convection Fe_3O_4/water ferrofluid flow in a horizontal porous channel. Pramana–J. Phys., 94:156.

[58] Humam, K., Ali, H., & Mahir, F.(2020). Improvement of Heat Transfer by Nanofluid and Magnetic Field at Constant Heat Flux on Tube. International Journal of Mechanical & Mechatronics Engineering, 20, (03).

[59] Snehal, V., & Dilip, R. (2020). Convective Heat Transfer Enhancement of Fe_3O_4-Water Nanofluid under the effect of External Magnetic Field and Twisted Tape Insert. International Journal of Current Engineering and Technology, 10(3).

[60] Areum, L., Chinnasamy, V., & Honghyun, V. (2021). Effect of Magnetic Field on the Forced Convective Heat Transfer of Water–Ethylene Glycol-Based Fe_3O_4 and Fe_3O_4–MWCNT Nanofluids. Appl. Sci. 11, 4683.

[61] Yun-Seok, C., & Youn-Jea, K. (2021). Effect of Magnetic Nanofluids on the Performance of a Fin-Tube Heat Exchanger. Appl. Sci., 11, 9261.

[62] Saba, Y.(2021). Evaluation of water-based Fe_3O_4 ferrofluid heat transfer in the presence of external electromagnetic field: A review. Journal of Mechanical Research and Application, 10(4), 1-25.

[63] Munzer, S., Ayoup, M., & Al-busoul, M. (2022). Investigation of heat transfer enhancement using ferro-nanofluids (Fe_3O_4/water) in a heated pipe under the application of magnetic field. Advances in Mechanical Engineering, 14(6), 1–17.

[64] Hyun-Su, K., Yun-Seok, C., Hyeon-Seok, S., & Youn-Jea, K.(2022). Experimental Study on the Heat Transfer Performance of Various Magnet Arrangements in a Closed Space Filled with Ferrofluid, Appl. Sci., 12, 8666.

[65] Jiawang, Y., Xian, Y., Jin, W., Hon Huin, C., & Bengt, S.(2022). Review on Thermal Performance of Nanofluids With and Without Magnetic Fields in Heat Exchange Devices. Frontiers in Energy Research, 10.

[66] Basma, S., Suvanjan, B., Najib, H., Fayçal, H., Essam, Y., Suresh, K., Mir, W., Alsheddi, T., and Al Nuwairan, M. (2022). Effect of Magnetic Baffles and Magnetic Nanofluid on Thermo-Hydraulic Characteristics of Dimple Mini Channel for Thermal Energy Applications. Sustainability, 14, 10419.